8-24-2011

Stromatolitic Knobs in Storrs Lake, San Salvador, Bahamas: Insights into Organomineralization

Alexandre J. Fowler
Alexandre.Fowler@UConn.edu

Stromatolitic Knobs in Storrs Lake, San Salvador, Bahamas: Insights into Organomineralization

Alexandré J. Fowler

B.A., Hartwick College, 2009

A Thesis

Submitted in Partial Fulfillment of the

Requirements for the Degree of

Masters of Science

at the

University of Connecticut

2011

APPROVAL PAGE

Master of Science Thesis

Stromatolitic Knobs in Storrs Lake, San Salvador, Bahamas: Insights into Organomineralization

Presented by

Alexandré J. Fowler, B.A.

Major Advisor _____
Dr. Christophe Dupraz

Associate Advisor _____
Dr. Pieter Visscher

Associate Advisor _____
Andrew Bush

University of Connecticut

2011

ACKNOWLEDGMENTS

I would like to thank all of those who supported me throughout the duration of my masters research. Acknowledgment is made to the Donors of the American Chemical Society Petroleum Research Fund (Grant 635169) for support of this research.

I offer my sincerest thanks to my advisor, Christophe Dupraz, for supporting me with unfailing patience, friendship, and sense of humor. I would also like to thank Pieter Visscher, my secondary advisor, for expanding my scientific horizons beyond geology. Thanks to them, I can now say with absolute certainty, that I do know a thing or two about microbiology.

Special thanks to Andrew Bush for joining my committee and for exhaustive proofreading of my thesis.

Thanks to Marie Cantino for teaching me how to use a Scanning Electron Microscope.

My deepest gratitude to David Griffing and Lisa Park for selflessly sacrificing their valuable time during the 15th Symposium on the Geology of the Bahamas and other Carbonate Regions to assist me with my field work.

I would also like to thank the Gerace Research Centre for hosting the 15th Symposium on the Geology of the Bahamas and other Carbonate Regions, providing me with the

opportunity to present previous research, perform new research, and learn about the current research of others in my field, all in a week's time.

Special thanks to all off my colleagues at the University of Connecticut Center for Integrative Geosciences.

I can never fully express my gratitude to my family, who have always believed in me without fail, and never let me give up.

Finally, I thank Matthew Daigneault, the world's most supportive partner, for all of the late nights, listening to my rants, providing hugs, hot chocolate, and assistance when needed, and for helping me see things through to the end. I couldn't have done it without you.

TABLE OF CONTENTS

LIST OF TABLES

LIST OF FIGURES

LIST OF EQUATIONS

ABSTRACT

Storrs Lake, a hypersaline lake on the east coast of San Salvador Island, Bahamas, contains well-developed microbial mats, some of which have developed calcified structures called microbialites. Many of these microbialites are laminated, and therefore classified as stromatolites. This study focuses on small stromatolitic knobs located in the southern portion of Storrs lake, which are still actively forming, to gain insights into the early stages of stromatolite formation. These knobs appear to be forming as the result of *in situ* micritic precipitation mediated by both photosynthetic and heterotrophic microbial metabolisms. By comparing these small stromatolitic knobs to larger stromatolitic heads in deeper portions of the same lake, as well as other modern closed-system and open-marine stromatolites, a mechanism for organomineralization and laminae formation can begin to be determined. The mechanism for *in situ* precipitation is relatively comparable in each of these systems, though the mechanism of laminae formation varies from microbial to more extrinsic controls. This project can be used to inform future studies of fine-grained stromatolites in the fossil record, providing crucial knowledge about the history of Earth's carbon cycle.

INTRODUCTION

THE CARBON CYCLE

In the modern world where terms like “climate change,” “global warming,” “greenhouse gases,” and “carbon footprint,” are used in the mainstream media like never before, it has become increasingly important for people to understand the carbon cycle and how it affects our planet. The carbon cycle is a complex system that has a profound influence on the lithosphere, hydrosphere, atmosphere, and biosphere. In order to better understand this important system, the carbon cycle can be simplified by breaking it down into two major cycles that influence each other: the “short-term,” or biologic carbon cycle (Figure #1), and the “long-term,” or geologic carbon cycle (Figure #2).

The short-term, or biologic carbon cycle, and the long-term, or geologic carbon cycle, are linked in many ways. For example, respiration by animals and other organisms in the short-term carbon cycle is an output of the atmospheric CO_2 needed for the alteration of silicate minerals in the long-term carbon cycle. Another example is shown by the carbonate buffering equation (Stumm & Morgan, 1996):

$$CaCO_3 + \underbrace{H_2O + CO_2}_{\text{Carbonic Acid } (H_2CO_3)} \longrightarrow 2HCO_3^- + Ca^{2+} \qquad (1)$$

Any uptake in CO_2, such as through photosynthesis by plants or cyanobacteria in the biological carbon cycle, would push the equation to the left to achieve equilibrium, favoring $CaCO_3$ precipitation, creating carbonate rocks in the geologic carbon cycle.

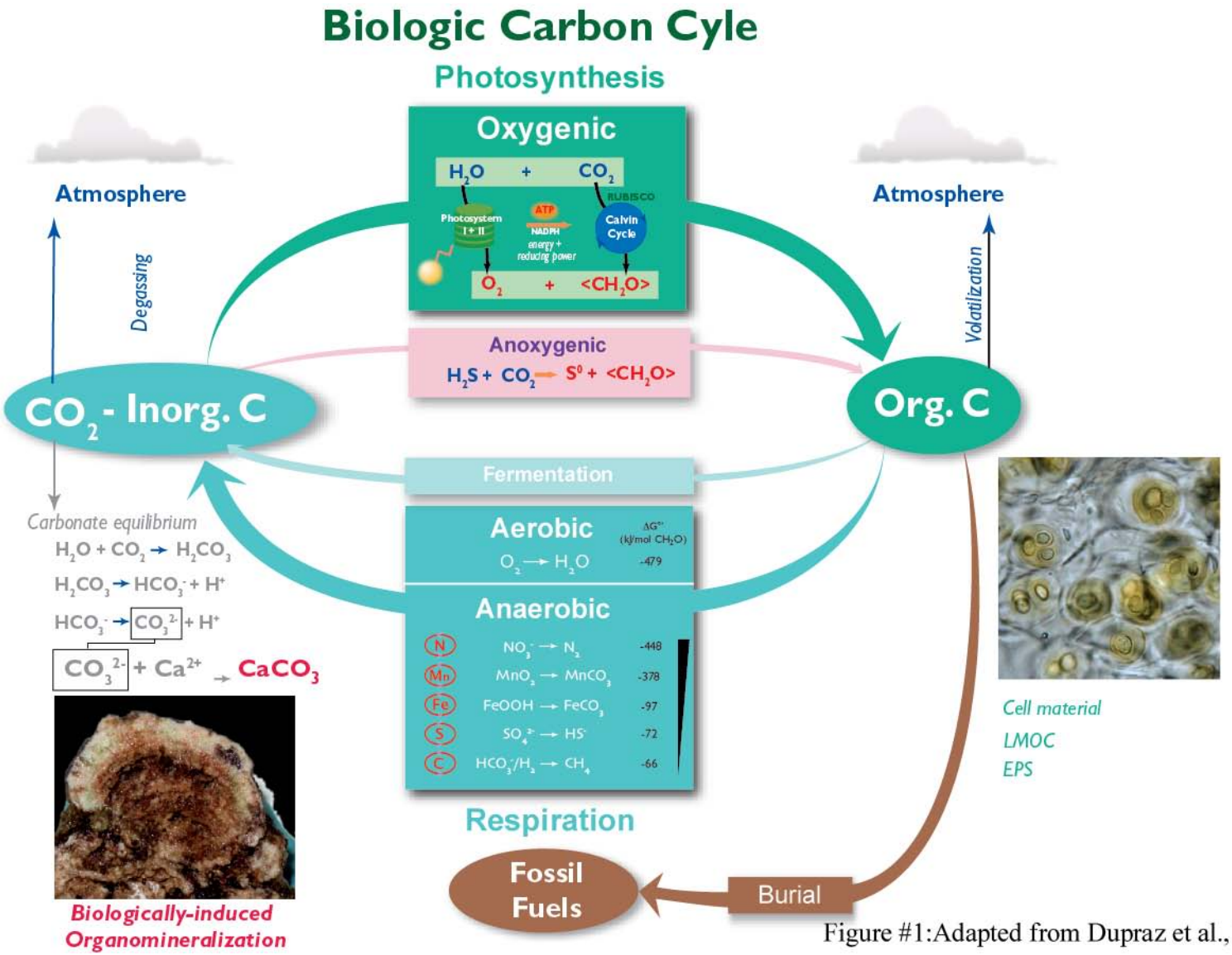

Figure #1:Adapted from Dupraz et al., 2009

Geologic Carbon Cycle

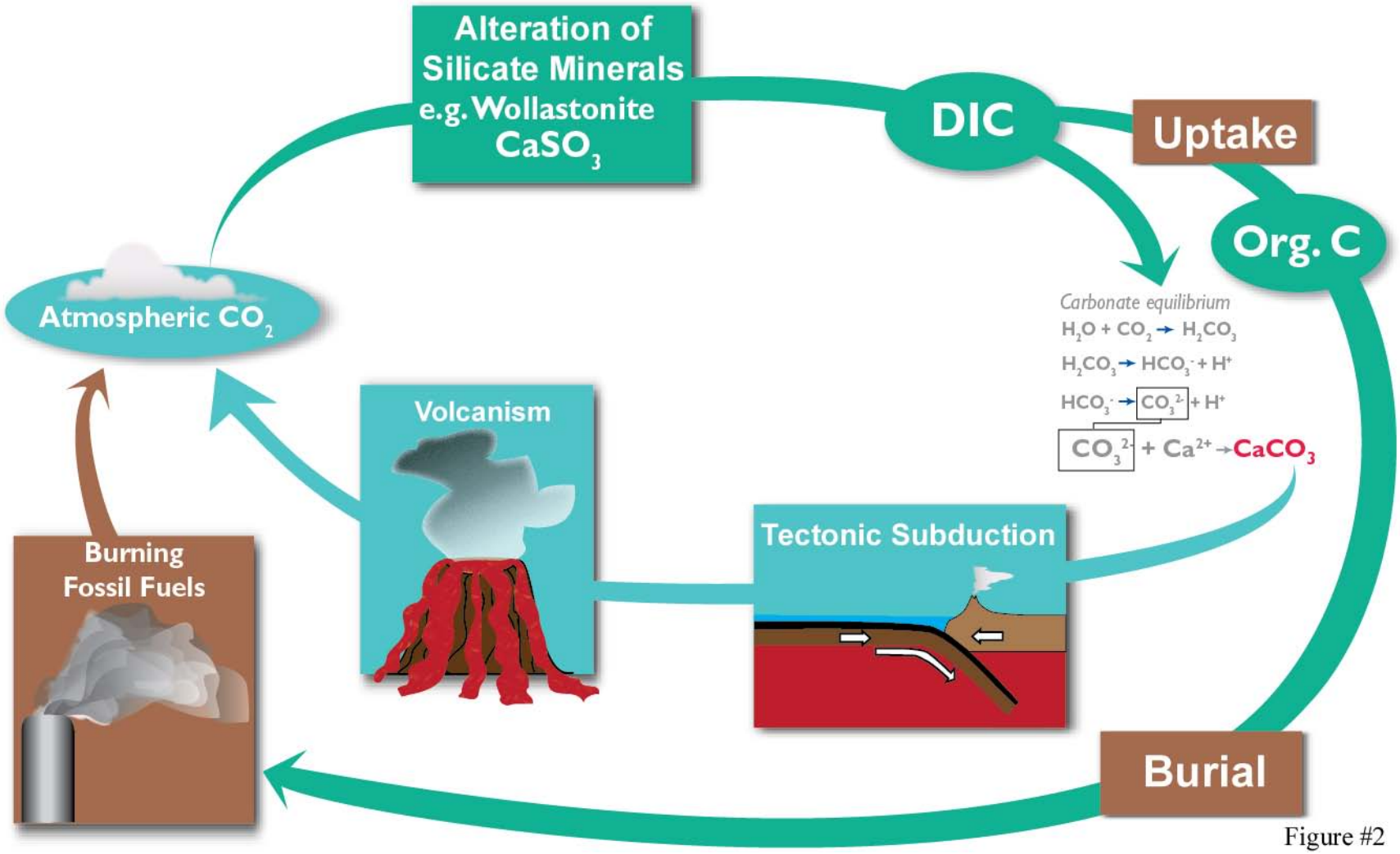

Figure #2

Likewise, any output of CO_2, such as an increase in volcanism or burning of fossil fuels in the geologic carbon cycle, would increase acidification of the hydrosphere, favoring $CaCO_3$ dissolution, and making it difficult for coral, clams, and other organisms to create their carbonate skeletons and shells in the biologic carbon cycle (Stumm & Morgan, 1996).

BIOMINERALIZATION VS. ORGANOMINERALIZATION

The role of organisms in driving calcium carbonate precipitation is a quintessential example of the relationship between the biologic carbon cycle and the geologic carbon cycle and is the fundamental background of this study. Organisms influence calcium carbonate precipitation via two major mechanisms: biomineralization and organomineralization (Dupraz et al., 2009). Biomineralization is induced calcium carbonate precipitation, where the morphology of the mineral is genetically controlled by organisms such as found in coral or clams. For example, although there is some room for small variations, a certain species of coral will always construct the same basic skeletal structure according to its genetic code (Dupraz et al., 2009). Organomineralization, on the other hand, is not genetically controlled. Organomineralization is calcium carbonate precipitation that is influenced by microbial metabolisms, but the morphology of the mineral is mainly controlled by environmental conditions (Dupraz et al., 2009). One microbial community can produce an infinite number of morphologies depending on the conditions, and the same community can produce different morphologies as conditions

change, due to seasonal variation, storm events, changes in salinity or sedimentation rates, etc.

MICROBIALITES

When microbial communities drive organomineralization to form calcium carbonate structures, the structure is known as a *microbialite* (Burne & Moore, 1987). A *microbialite*, as defined by Burne & Moore (1987), is an "organosedimentary deposit formed from interaction between benthic microbial communities and detrital or chemical sediments (in calcareous microbialites, processes include trapping and binding, inorganic calcification (tufa), and biologically influenced calcification)." Because the morphology is not genetically controlled, it is difficult, if not impossible, to look at a structure in the rock record and definitively say that the structure is a microbialite, as opposed to a structure that formed abiotically. Likewise, it is not fully understood why modern microbialites form certain morphologies, or form at all, in certain places on Earth, and form different morphologies, or don't form at all, in other places with similar conditions (Dupraz et al., 2009).

MICROBIALITE FORMATION

Microbialite formation begins with the colonization of sediment by cyanobacteria. Cyanobacteria are most active ~0.5-2 millimeters below the sediment surface, where they are protected from harsh solar radiation but will still have plenty of access to photosynthetically active radiation (PAR) for photosynthesis. Because cyanobacteria are so active in this subsurface zone, there will be a large flux of oxygen a few millimeters

below the sediment. These active cyanobacteria display high rates of photosynthesis and have enough energy to fix nitrogen in addition to creating organic carbon and oxygen through oxygenic photosynthesis. Using sticky extracellular polymeric substances (EPS), filamentous and coccoidal cyanobacteria may also begin to stabilize the sediment through trapping and binding of grains (Visscher & Stolz, 2005).

Shortly after colonization by cyanobacteria, aerobic (chemoorgano)heterotrophs will move in as well. They will gain energy from the organic carbon, fixed nitrogen, and oxygen created by the cyanobacteria according to the following reaction:

$<CH_2O> + O_2 \rightarrow CO_2 + H_2O + \text{energy}$ (Visscher & Stolz, 2005) (2)

Since the oxygen that is produced by the cyanobacteria is now being consumed by the aerobic chemoorganoheterotrophs, chemical reactions, and diffusing out of the system, anaerobic heterotrophs, specifically sulfate reducing bacteria (SRBs) in marine and hypersaline environments, can now colonize as well. They gain energy from the organic carbon created by the cyanobacteria along with the high sulfate concentrations in sea water according to the following reaction:

$<2CH_2O> + SO_4^{2-} \rightarrow 2HCO_3^- + 2H_2S$ (Patterson & Walter, 1994) (3)

Chemolithoautotrophs can then colonize and gain energy from the sulfide and create biomass from the carbon dioxide created by the SRBs according to the following reactions: a) $H_2S + 2O_2 \rightarrow SO_4^{2-} + 2H^+$ b) $CO_2 \rightarrow <CH_2O>$ (4) (Visscher & Stolz, 2005)

The sulfate created by the chemolithoautotrophs will also feed the metabolisms of the SRBs, which will in turn create more sulfide that can be used by the chemolithoautotrophs. Other chemolithoautotrophs, such as purple and green sulfur bacteria, can also use this sulfide and carbon dioxide to create biomass, and will also produce elemental sulfur according to the following reaction:

$CO_2 + 2H_2S \rightarrow <CH_2O> + 2S^0 + H_2O$ (Visscher & Stolz, 2005) (5)

All of these different types of bacteria will create a mature, metabolically diverse microbial mat with complex element cycling. Through "a type of bacterial cell-to-cell communication that depends upon exchanges of molecular signals between neighboring cells," called quorum sensing (Decho et al., 2010), the bacterial community in this mat coordinate physiological activities and work together to create EPS to protect itself and help stabilize the sediment. If precipitation and/or the trapping and binding of sediment occurs within the mat, the mat can become a microbialite (sedimentary structure) (Visscher & Stolz, 2005).

MICROBIALITE CLASSIFICATION

Although an infinite number of varying morphologies can be formed through microbial organomineralization, microbialites can be classified into three main types of structures based on their internal morphologies (Figure #3): *stromatolites*, which have a laminated internal fabric, *thrombolites*, which have a clotted internal fabric, and *leiolites*, or *cryptic microbial crust*, which are structureless with no defined internal fabric (e.g., Aitken, 1967; Kennard & James, 1986; Braga et al., 1995; Dupraz & Strasser, 1999, 2002; Turner

et al., 2000; Shapiro, 2000; Riding, 2000). Of the three, stromatolites have received the most attention by the scientific community. This is due, in part, to the fact that stromatolites are believed to be among the oldest traces of life in the rock record (Hofman et al., 1999; Allwood et al., 2006, 2007). This, however, is controversial due to the fact that few fossil stromatolites preserve remains of the microbial communities that are supposed to be responsible for their formation, so it is difficult to prove that they are not simply abiotic sedimentary structures (Grotzinger & Knoll, 1999).

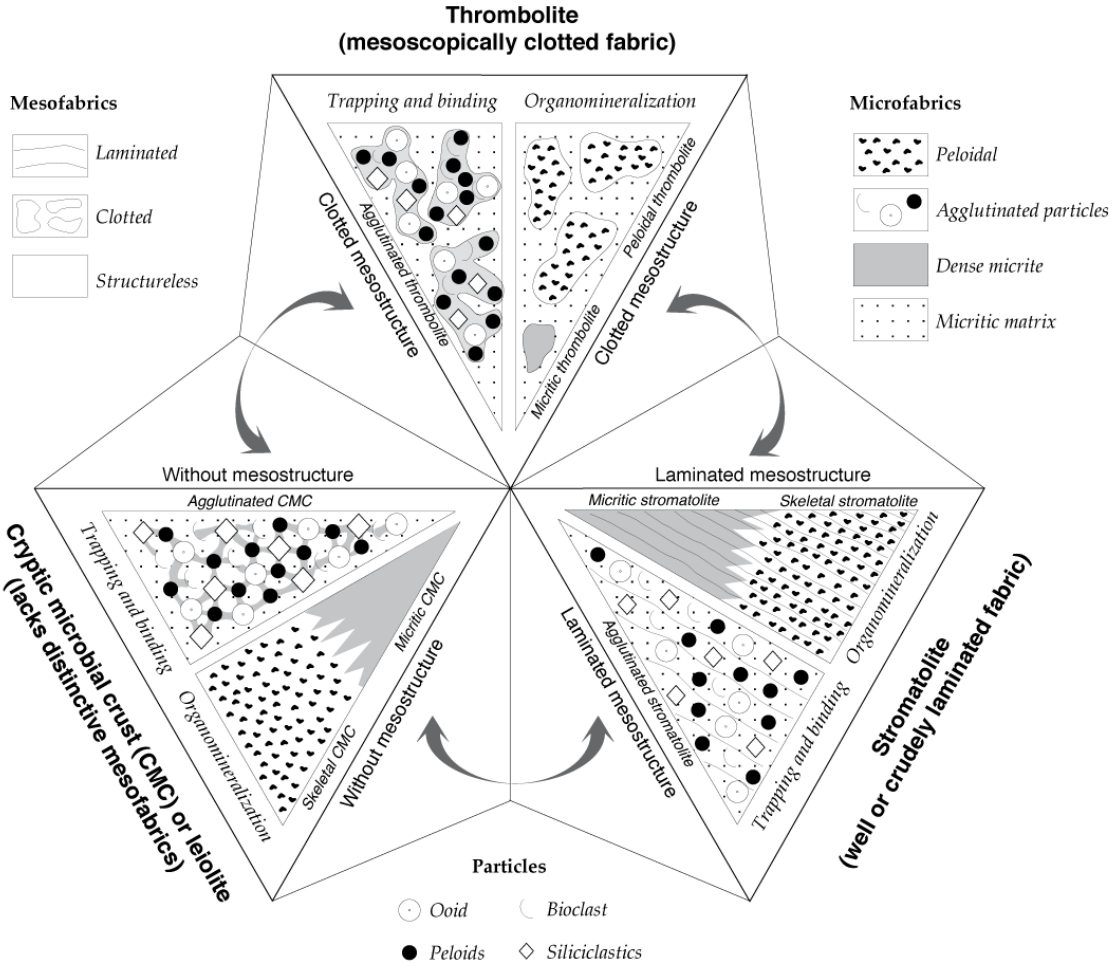

Figure #3: Microbialite Classification Diagram:
Classification of Jurassic microbolites based on the meso and microstructure (adapted from Christophe Dupraz, based on Kennard and James, 1986 and own observations)

HISTORY OF THE TERM "STROMATOLITE"

Kalkowsky (1908) introduced the term *Stromatolith* – layered stone – to describe columns and domes of well layered carbonate, and suggested that they were formed by "simply organized plant-like organisms," what we would refer to today as *microbes* (Riding, 2011). This definition remains controversial, as scientists debate between descriptive, purely geological definitions and genetic definitions (e.g. Ginsburg 1991; Grotzinger & Knoll, 1999). This is due to the difficulty in proving the biological origin, or lack thereof, of fossil "stromatolites" (Grotzinger & Knoll, 1999). For this reason, many authors are using the descriptive definition of Semikhatov et al. (1979) that emphasizes the laminated features and the specific growth pattern (initiation from a point or a limited surface) without referencing the possible biogenicity (see Grotzinger & Knoll, 1999).

MODERN STROMATOLITES

Although the descriptive definition is used to describe fossil "stromatolites," no recent abiotically-produced laminated deposits are referred to as *stromatolites* (Riding, 2000). Recent stromatolites are built through benthic microbial activity or at least organically mediated processes (e.g., Golubic et al., 1976; Riding, 1991, 2000; Riding et al., 1991; Verrecchia et al., 1995; Freytet & Verrecchia, 1999; Seong-Joo et al., 2000; Reid et al., 2000, 2003b). Thus, recent stromatolites can be considered as a form of microbialite, as defined by Burne & Moore (1987); equivalent to 'microbolite' (Riding,1991), which display lamination as their specific mesostructure (see Riding, 1991, 2000; Dupraz & Strasser, 1999). Riding (2011) proposed the definition, "macroscopically layered

authigenic microbial sediments with or without interlayered abiogenic precipitates," meaning that *stromatolites* can refer to either "Fine-grained Crust (typically unevenly layered and with complex clotted and peloidal microfabrics)," or "Hybrid Crust (thin alternations of Sparry and Fine-grained crust)." "Stromatolites therefore include microbial and hybrid types; they can form domes and columns, but also commonly occur as sheet-like masses. In the definition, *with* abiogenic precipitates can refer to Hybrid Crust, and *without* abiogenic precipitates can refer to Fine-grained Crust" (Riding, 2011). Modern stromatolites can be seen today in places such as Shark Bay, Australia (e.g. Reid et al., 2003a); Highborne Cay (Reid et al., 2000), Exuma Islands, Bahamas (Dupraz et al., 2004; Glunk et al., 2011); and in Storrs Lake, San Salvador Island, Bahamas, the field site for this study.

STROMATOLITE FORMATION

Stromatolite formation is traditionally attributed to the process of trapping and binding of sediment and/or $CaCO_3$ precipitation associated with the photosynthetic uptake of CO_2 and HCO_3^- by cyanobacterial mats (e.g., Monty, 1977; Pentecost & Riding, 1986; Merz-Preiß & Riding, 1999). This view is now enlarged as detailed studies introduce many other pathways leading to carbonate precipitation in microbialites, including numerous bacterial metabolisms, extracellular polymeric substances (EPS) turn-over and organomineralization (e.g., Trichet & Défarge, 1995; Arp et al., 1999; Visscher et al., 2000; Reid et al., 2000; Trichet et al., 2001; Zavarzin, 2002; Dupraz et al., 2004, Dupraz & Visscher, 2005).

The open marine stromatolites found in Highborne Cay in the Exuma Islands of the Bahamas have been studied extensively, and the mechanism for their formation is the most well-understood of any modern stromatolites (Reid et al., 2000). There are three major types of microbial mats that are responsible for the creation of the Highborne Cay stromatolites, which cycle back and forth with changing extrinsic factors. The first of these three mat types is formed by a "Pioneer Community," which involves cyanobacteria that trap and bind sediment grains (especially ooids), using EPS created by the bacteria as a sticky "glue" to stabilize the sediment. This type occurs when a lot of sedimentation is taking place, such as periods of high wave energy, or during storm events. When enough sediment is trapped, the bacterial community will recolonize closer to the surface in order to have access to sunlight for photosynthesis (Reid et al., 2000).

The second mat type is formed by a so-called "Bacterial Biofilm Community." This type occurs when there is a "quiet," lower-energy period with less sedimentation occurring. Because there is less wave action occurring to wash it away, a thick microbial biofilm can develop at the surface of the stromatolite. If the environment has a constant supply of calcium, calcium carbonate will be precipitated in the form of a micritic crust through organomineralization. The maximum production of calcium carbonate precipitation will be found near the top of the stromatolite, where the bacterial community is most active (Reid et al., 2000).

The third mat type is made up by an "Endolith Community." This mat type is found during longer quiet periods when coccoidal cyanobacteria degrade the trapped grains

within the stromatolite, and heterotrophic bacteria replace organics within the bore holes with micritic aragonite. This results in a very stable sediment layer, as the grains become fused together with micritic aragonite (Reid et al., 2000).

As extrinsic environmental factors change, the stromatolites will cycle between these three types of microbial mats. This will create layers of trapped and bound grains, micritic crust, and degraded fused grains (Figure #4). This cycling results in the characteristic laminated structure which comprises the Highborne Cay stromatolites (Reid et al., 2000).

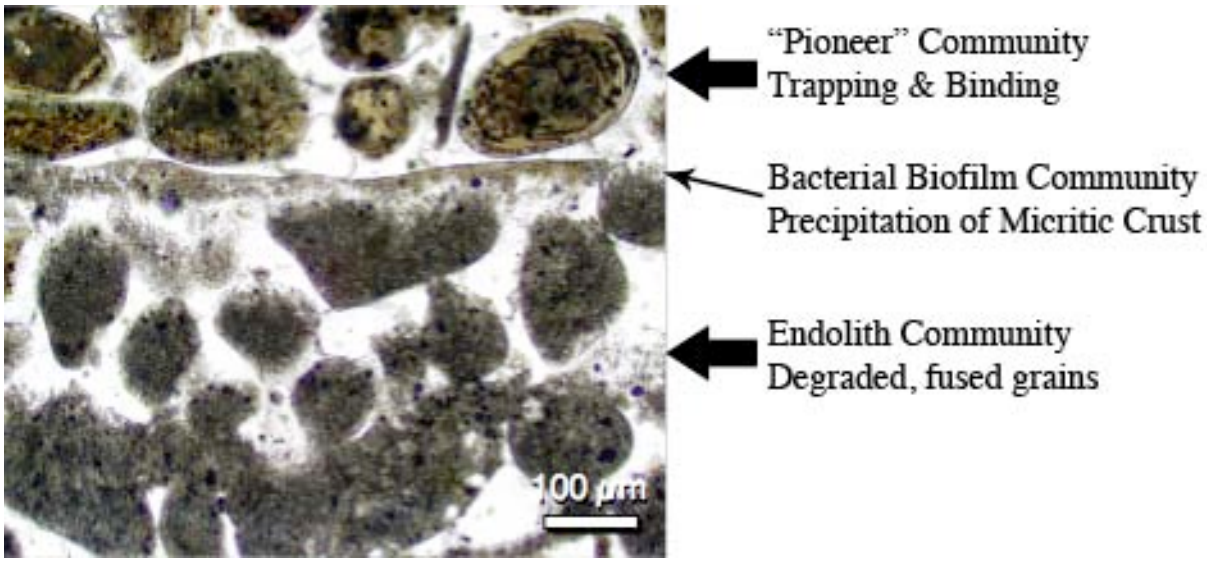

Figure #4: Three major microbial mat types in Highborne Cay stromatolites. Viewed in thin section. Adapted from Reid et al., 2000.

FOSSIL STROMATOLITES

Fossil stromatolites display a wide range of macroscopic morphologies, but all definitions include a laminated mesostructure for fossil stromatolites (Riding, 2000; Riding et al., 1991). While the Highborne Cay stromatolites are largely coarse-grained, with the exception of thin layers of precipitated micrite, most fossil stromatolites that have been

discovered have a fine-grained, micritic microstructure (Riding, 2011; Riding et al., 1991). This makes it difficult to make direct comparisons between the open-marine, Highborne Cay stromatolites, and the fossil stromatolites. Modern, fine-grained, micritic stromatolites would provide a better basis for comparison. Although modern stromatolites do not have a profound impact on today's global carbon cycle, they provide a gateway to understanding stromatolites of the fossil record. In an early Earth, before the advent of plants, animals, and other eukaryotes, stromatolites would have dominated the global carbon cycle, having significant impacts on the planet's climate and atmosphere. Thus, understanding ancient stromatolites is critical to understanding Earth's history.

THROMBOLITE FORMATION

Thrombolites, mesoscopically clotted microbialites, are not thought to be quite as ancient as stromatolites, becoming more important since the end of the Precambrian (Konhauser, 2007, pp. 163), with definitive fossil evidence dated at 1.92 Ga (Myshrall et al., 2010; Kah & Grotzinger, 1992). Their formation is not well understood (Myshrall et al., 2010; Thompson et al., 1990; Moore & Burne, 1994), but it "appears as though a gradual change from stromatolite to thrombolite might be explained simply on the basis of rising sealevel" (Feldmann & McKenzie, 1998). Several alternative hypotheses exist about thrombolite formation. "Their formation has been attributed to rapid rates of calcification by coccoid cyanobacteria" (Konhauser, 2007, pp. 163). "Thrombolites can also be formed by green algae in subtidal marine environments. The deepening water, decrease in salinity, and increase in energy and nutrient supply favor algal growth over

cyanobacterially dominated shallow water stromatolites that form with them a laterally gradational biofacies" (Feldmann & McKenzie, 1998). Open marine thrombolites in Highborne Cay, Exuma, Bahamas have been attributed to calcified filamentous cyanobacteria, identified as *Dichothrix* sp. (Myshrall et al., 2010). More study is needed to understand how the clotted mesostructure of thrombolites is formed.

GOALS OF THIS STUDY

Although the mechanism for stromatolite formation at Highborne Cay is relatively well understood and has been studied extensively (Reid et al., 2000; Dupraz et al., 2011), as coarse-grained microbialites, they do not provide a direct, morphological analog to the micritic, fine-grained stromatolites found within the fossil record. In order to develop a better understanding of the formation of ancient fossil stromatolites, it would make sense to study modern fine-grained, micritic stromatolites. The first step would be to compare the recent coarse- and fine-grained stromatolites to determine if similarities in the mechanisms responsible for organomineralization exist between the two types, followed by a determination of what creates the laminated structure characteristic of stromatolites. If similarities do exist, a model for stromatolite formation can then be formulated, and potentially used to test fine-grained fossil stromatolites, despite differences in microbial communities between modern and ancient forms.

Storrs Lake, a hypersaline lake located on San Salvador Island, Bahamas, contains modern, fine-grained stromatolites, first described by Hattin in 1982 (see detailed description below). Although a significant amount of data has been collected on these

stromatolites, particularly in the northern portion of the lake (e.g. Mann & Hoffman, 1984; McNeese, 1988; Neumann et al., 1989; Mann & Nelson, 1989; Pentecost, 1989; Zabielski, 1991), the mechanisms of calcium carbonate precipitation and laminae formation are not well understood.

In addition to the existence of large, 'sub-fossil' stromatolites, Storrs Lake also contains smaller, younger, fine-grained stromatolitic knobs (Dupraz et al., 2006), which are the main focus of this project. The goals of this study include thoroughly describing the small stromatolitic knobs, determining the mechanisms for organomineralization and laminae formation in these knobs, and comparing Storrs Lake stromatolites with other closed-system and open marine stromatolites in order to create a model of stromatolite formation that may inform future studies of fossil stromatolites.

GEOGRAPHIC AND GEOLOGIC SETTING OF SAN SALVADOR BAHAMAS

(Fowler, 2009)

The Bahama Archipelago contains many hypersaline lakes, and is an ideal setting to study microbialites. The ~1400 km long archipelago is located to the southeast of the North American continental margin, and consists of 700 islands and 2,500 smaller islets and cays (Curran, 1997; Curran & White, 1995). These islands are surrounded by shallow-water banks or platforms above thick sequences of carbonate rock (Curran, 1997). The Bahamas Platform is comprised of Pleistocene limestone overlying Tertiary

and Cretaceous limestone (Bathurst, 1975). The plateau is submerged to an average depth of >7-10 m, and is covered with recent carbonate sediment deposits (Bathurst, 1975). The platform drops steeply at the edge to a depth of 200 m in a distance of 2 km or less (Bathurst, 1975). Most of the platform's islands consist of a sequence of subtidal, intertidal, and eolian carbonate rocks from the late Pleistocene and Holocene Epochs (Curran & White, 1995). The Pleistocene and Holocene units are separated by a disconformity that is marked by karst and soil features, including terra rossa paleosols, and caliche crusts. (Curran & White, 1995). The banks of the platform are tectonically stable. Some isostatic subsidence does occur, but has been at equilibrium with carbonate sedimentation since the Early Jurassic (Mullins & Lynts, 1977; Curran, 1997). The development of sedimentary facies are mainly controlled by a gradual, eustatic sea level rise (Curran & White, 1995).

San Salvador Island, the field location of this study, is the easternmost island on the Bahamas Platform. It is located on a small, isolated bank at the eastern edge of the Bahamas (Curran, 1997). The island is ~11 km wide by 21 km long, and is surrounded by a narrow platform with a steep, abrupt shelf-edge break on its eastern side (Curran, 1997). This drop-off occurs at 36 to

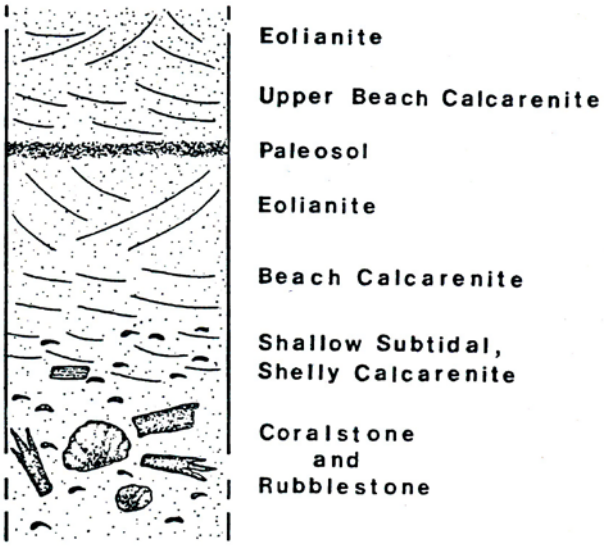

Figure #5: Shallowing upward sequence of the Bahamas (Curran, 1997)

185 m and breaks into a steep continental slope to about 4700 m (Adams, 1983). The western edge of the platform does not have a steep drop-off, and is submerged to a depth of about 15 to 20 m (Adams, 1983). Successive stages of carbonate eolian accretion are represented by arcuate ridges along the island (Curran, 1997). The shorelines of San Salvador Island are comprised of eroded eolianite headlands, beaches of fine- to medium-grained skeletal carbonate sands, and Holocene beachrock (Curran, 1997). San Salvador displays the same shallowing upward sequences (Figure #5) that are recognized throughout the Bahamas (Curran, 1997).

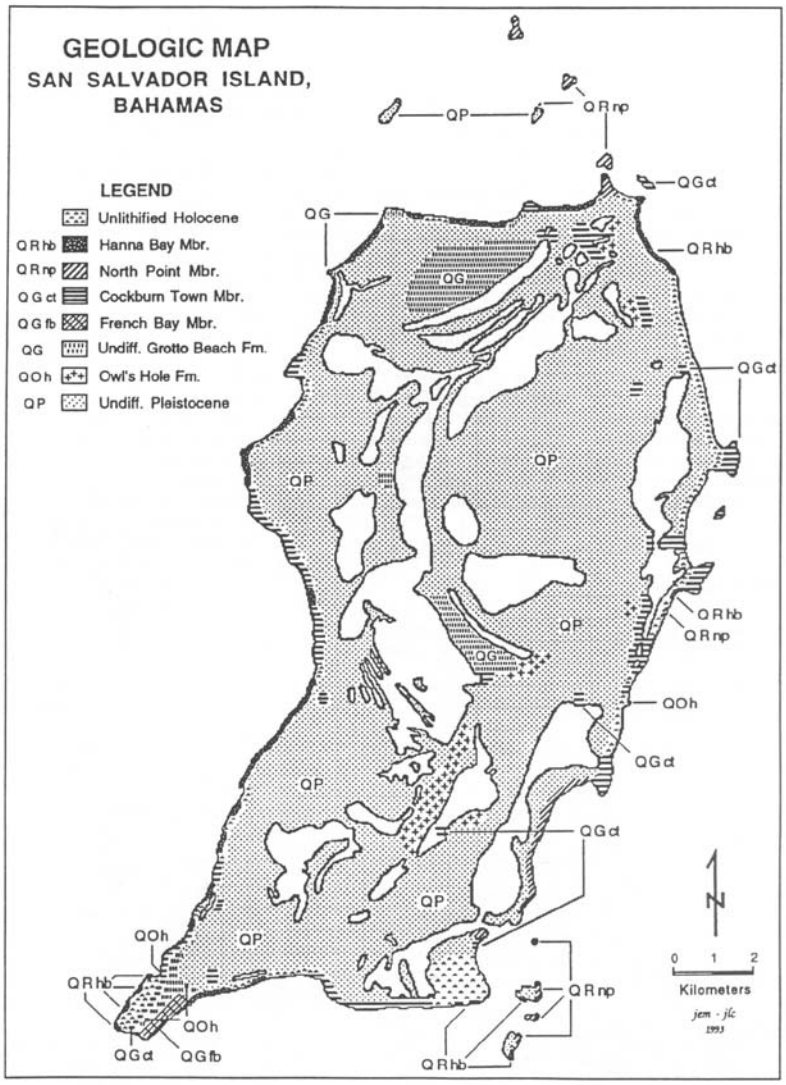

Figure #6: Geologic map of San Salvador (Carew & Mylroie, 1995)

GEOGRAPHIC AND GEOLOGIC SETTING OF STORRS LAKE

Storrs Lake is a hypersaline lake located on the northeastern, windward coast of San Salvador island, which is home to several other hypersaline lakes as well. The lake is located between the Queen's Highway to the west and Green Bay to the east, and it runs between the Polly Hill Settlement to the north and the Fortune Hill Settlement to the south.

Figure #7: Location map of Storrs Lake on San Salvador Island

Storrs Lake is comprised of a large northern sector and a smaller, shallower southern sector, with a small zone called "the narrows" separating the two (Zabielski, 1991). The lake once comprised three distinct depositional basins separated by two bedrock sills running east to west. The three basins were open to the ocean 4,300 ±70 years ago (Zabielski, 1991). The three basins were subsequently closed off from the ocean by the southern progradation of a spit running north-south (Zabielski, 1991). The northern basin was closed off first 3,100 ±70 years ago, followed by the central and southern basins (Zabielski, 1991). The three basins became one lake after being flooded during continued Holocene sea-level rise (Zabielski, 1991). After being closed off, evaporation led to a concentration of the salt in the seawater that filled the lake, causing the lake to become hypersaline (Zabielski, 1991).

Being a fairly shallow lake, Storrs Lake only reaches a maximum depth of two meters, and water levels fluctuate throughout the year. During the dry season (December-April), evaporation reduces the water level, which recovers during the wet season (May-November) as the result of increased rainfall and groundwater recharge (Mann & Nelson, 1989). Although some tidal influx and outflow of seawater does occur through five known conduits at the northernmost end of the lake and through a small seep in a barrier dune at the southeast margin, these effects are negligible, and daily tidal fluctuation of lake water levels has never been observed (Mann & Nelson, 1989). Storrs Lake is hypersaline and density-stratified, but salinity levels fluctuate dramatically in response to water level. During dry periods, the salinity of the lake can increase to as high as 93.5

PSU as salt is concentrated due to evaporation, and salinity will decrease again to as low as 38 PSU as the salt is diluted by recharge and rainfall during wet periods (Mann & Nelson, 1989).

NORTHERN SECTOR

The northern sector of Storrs Lake has been the focus of more research than the southern sector. This is due to the extensive carbonate deposits that have been developing in the northern sector for the last 3000 years (first described by Hattin, 1982). Transects taken from the shoreline of this northern sector toward the center of the lake in previous studies have shown the evolution of carbonate deposits from laminated crust near the shoreline, to bulbous crust further into the water, to larger mushroom and club-shaped heads in the deeper regions toward the center of the lake (Figure #8) (Neumann et al., 1989; Mann & Nelson, 1989; Paull et al., 1992).

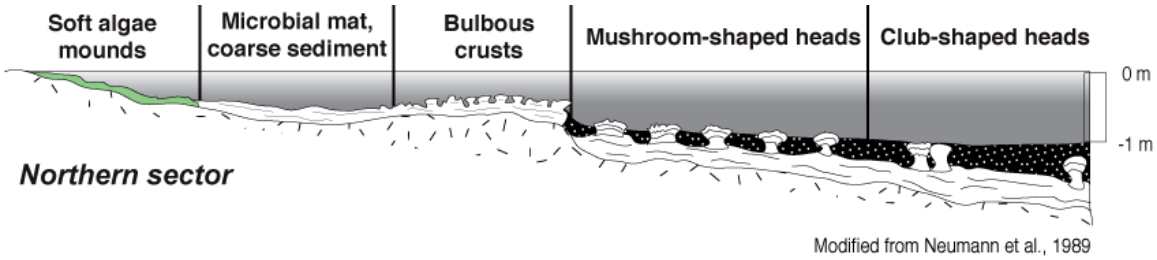

Figure #8: Storrs Lake Northern Sector zones. Zones and depth are shown to scale.

PREVIOUS WORKS ON STROMATOLITES IN STORRS LAKE'S NORTHERN SECTOR

Hattin, 1982

Hattin first described the stromatolites of Storrs Lake in 1982 in the Proceedings of the First Symposium on the Geology of the Bahamas. He described the 'algal' (now known

to be *microbial*) mats in general throughout the lake as "lumpy or mammilated surfaces" that develop when the mats are exposed during times of low water levels. The general underlying sediment was described as "unconsolidated, and laminations are at best poorly developed." However, "true columnar stromatolites," were only found by Hattin in the northernmost part of Storrs Lake, composed of "crudely laminated, fine sand- to fine gravel-sized carbonate grains that are bound together to form crumbly limestone knobs that are as much as 15 to 20 cm in diameter and 12 to 15 cm tall." Hattin described the modern stromatolites as having an irregularly columnar shape, with "crust composed of nearly white, well-cemented, very fine-grained calcitic limestone," "which extends beneath the stromatolite and apparently formed a base on which the structure was constructed." Hattin also stated that the stromatolites were topped with 'algal' mats created by filamentous cyanobacteria resembling *Lyngbya*.

Mann and Nelson, 1989

Mann and Nelson described the northern sector of Storrs Lake as having several different microbialite structures separated into depth-controlled zones. They described the outer zone at the lake's margin as exposed during the dry season for weeks to months. Soft, thrombolitic microbialites without calcium carbonate laminations were observed in this exposed region, and their formation was attributed to *Phormidium hendersonii* and another unidentified species.

Headed towards the lake, Mann and Nelson described an adjacent zone of crumbly stromatolites with bumpy surface textures, measuring up to 15 cm in height, which were

sometimes partially exposed. These crumbly stromatolites displayed a green layer overlying a pink layer in the living 'algal' portion of the structures.

Continuing lakeward, the zone of crumbly stromatolites was followed by "a zone of flat-topped, irregular, hard stromatolitic microbialites developed on hard substrates of varying depth but whose tops are impressive in their uniform depth; these structures are apparently never emergent." Although the lake floor is irregular, the tops of these stromatolites were so uniform that they appear to form a plateau or "table-top," which Mann and Nelson inferred to mean that depth was the main control on the height of these structures.

In the deeper (50-120 cm) portion of the central-northern sector of the lake, Mann and Nelson observed large, columnar stromatolites ranging in height from 10 to 70 cm depending on depth, and ranging in diameter from 20 to 40 cm. These columnar stromatolites had rounded tops with vertical or slightly flared sides and a smoother surface texture than other the microbialites. These stromatolites are never emergent, and "are consistently 40-50 cm beneath the inferred minimum lake level." These structures are unevenly spaced, but were found closer together in shallower regions.

Thick, organic-rich ooze covered in a soft, 5 mm-thick, coherent alga layer was observed between the stromatolite structures, as well as covering much of the lake bottom. This ooze/algal mat layer was also covered with a layer of calcium carbonate crust, thicker than 5 mm, in some areas throughout the lake. "Anoxic conditions prevail beneath the

algal mat as indicated by organic-rich content, black color, strong odor, and slightly gaseous nature." The maximum depth from the water's surface to the sediment/mat surface observed by Mann and Nelson was 75-80 cm, with a maximum sediment/mat thickness of 90 cm.

Mann and Nelson believed the primary control on the zonation of the microbialite structures in the northern sector of Storrs Lake was water depth. They stated that depth may "be an indirect controlling factor operating through light levels and salinity rather than an inherent physical aspect of depth." They also believed that substrate strength could be another controlling factor, with "table-topped" stromatolites preferring exposed bedrock, and soft thrombolitic mounds preferring ooze substrate. Salinity stratification and wind agitation of the water surface could also be potential controls, but were not thoroughly understood by Mann and Nelson.

Neumann et al., 1989

Neumann and his colleagues observed the same distributional zones of microbialite structures with the same types of morphologies described by Mann and Nelson (1989) in the northern sector of Storrs Lake. Neumann et al. also observed the lake floor sediments, and described them as being up to 2 m thick, and "covered by a thick, tough, leathery, microbial mat which becomes less cohesive and more flocculant as water depth increases to 1.5 to 2 m." XRD analysis performed by Neumann et al. showed sharper peaks of Mg-calcite in sediments from individual layers on the lake bottom than those of the calcified stromatolite structures. Neumann et al. concluded from this that the

stromatolite “heads are composed of a broader spectrum of Mg-calcite phases deposited over a greater time span.” They also believed that the mat-bound lake bottom sediments were precipitated by the cyanobacteria in the mats, based on a lack of forams and ostracodes in the surface sediment, indicating that the sediment was not detrital. XRD analysis of stromatolite heads revealed a spectrum of 12-17 mole percent Mg-calcite, and no lo-Mg calcite or aragonite. Thin section analysis revealed the Mg-calcite to be comprised of 48% micrite (<5 microns), 38% spar/microspar (5-20 microns), 14% pore space, and trace amounts of rhombohedral crystals, foraminifera, ostracodes, and gastropod shells. The micrite was thought to be original precipitation, while the spar/microspar is thought to be the result of recrystallization.

Neumann et al. observed the same calcium carbonate crust on top of the sediment/mat layer described by Mann and Nelson (1989). They stated that the crust was laminated and began within 50 m of the lake shore line at depths of ~20 cm during the very wet season of December when their study occurred. This crust extended outward into the same zones of stromatolites observed by Mann and Nelson. Neumann et al. observed that in the zone of “table-top” stromatolites described by Mann and Nelson, “surficially blackened heads of radiating calcified elements occur.”

Neumann et al. described the microbial mats observed in Storrs Lake as “very complex assemblages of filamentous and coccoid cyanobacteria, bacteria, and diatoms,” and identified some of the micro-organisms within the mats as *Phormidium* (also identified by Mann & Nelson, 1989), *Beggiatoa* (colorless sulfur bacterium), *Navicula*

(*diatomacea*), *Microcoleus* (cyanobacterium), *Chromatium* (purple-sulfur bacterium), *Calothrix, Spirulina,* and *Scytonema* (cyanobacteria). The mats were described as having a bright green layer overlying a deep pink layer. Neumann et al. performed microelectrode analysis on the mats, and separated them into three types (1) clear, nearshore bulbous mats, (2) the laminated mat that overlies much of the lake bottom, and (3) the more cohesive "leathery" mat surrounding the stromatolites. Oxygen "profiles made in the afternoon, when photosynthesis has been active for some time, show remarkably high oxygen concentrations in the upper 5 to 10 mm of the mats. The most extreme case is the four fold increase of oxygen above atmospheric concentration in the leathery mat." "The oxygen concentration peaks at 400 percent of saturation at only 5 mm into the mat whereupon it rapidly goes to 0 and the mat becomes completely anaerobic. Post-respiration intervals reveal the reverse. They show no oxygen maxima, just a rapid decrease from saturation to anaerobiosis." Neumann et al. inferred these oxygen profiles to indicate highly active photosynthesis and carbon dioxide uptake. "This loss of carbon dioxide produces high pH levels [>9 at the oxygen maxima] during the day and should achieve the reverse at night. The suggestion is that the intensely photosynthesizing mats create the potential to precipitate calcium carbonate in daylight and dissolve it at night." Neumann et al. could not make any precise conclusions as to what factors caused this process to result in net accretion of calcium carbonate in the crust and microbialite structures. However, SEM imaging on the microbial mats revealed euhedral mineral material associated with cyanobacterial filaments, indicating that the mats are responsible for the precipitation of the Mg-calcite identified by XRD analysis.

According to Neumann et al., “The thin sections and the micro-oxygen/pH profiles both suggest that photosynthetically driven, mat-mediated, micro-environments are subject to short intervals alternately favoring precipitation and then dissolution. This might provide an explanation of net accretion at the photosynthetically active, mat-covered stromatolite head, but it doesn’t explain how the head-like forms are produced nor what modifications might follow in the anaerobic interior of the heads.”

Pentecost, 1989

Allan Pentecost studied microbial mats comprised mainly of the heterocystous filamentous cyanobacteria *Scytonema* in several areas of San Salvador island, as well as the Exuma islands in the Bahamas. He observed poorly laminated *Scytonema* heads comprised of “concretionary structures 5-20 cm in diameter and 2-30 cm tall” in some of the ponds on San Salvador island, and found similar algal heads just offshore of the ‘narrows’ of Storrs Lake.

“*Scytonema* was the dominant cyanobacterium in all profiles with greatest biomass in the upper 4 mm of mat. The biomass (cell volume excluding the sheath)” was 3 parts per thousand in mats found in the narrows of Storrs Lake. Healthy cells were found even at depths of 13 mm where there is minimal sunlight in the Storrs Lake narrows mats. The *Scytonema* in the mats of all the field sites included in Pentecost’s study were mainly found as empty sheaths, and were much more abundant than sheaths containing trichomes.

Although other cyanobacteria were found in the mats, they did not contribute much to the total biomass. These cyanobacteria were mostly aggregates of coccoid *Gloeocapsa* cells ranging from 1 to 8 microns in diameter, with translucent brown, or some violet-pigmented sheaths. Small numbers of large cells resembling *G. gigas* were also found in the Storrs Lake mats. However, Pentecost also stated that "*Gloeocapsa* is difficult, if not impossible to separate from poorly developed *Entophysalis*. Well-developed mats of *Entophysalis* were often associated locally with the *Scytonema* mats and much of the coccoid material sampled may in fact belong to this taxon." Other cyanobacteria found in small numbers in the mats throughout San Salvador include *Schizothrix calcicola* s. lato, *Johannesbaptista* with 3-6 micron-wide filaments, and *Nitzchia* diatoms (found in a thin slime only in Storrs Lake). "Although none of these cyanobacteria matched the biomass level of *Scytonema*, their distribution with depth followed a similar pattern. Diatoms were also found in all the Bahamian mats. Although Pentecost did not identify them, he did observe purple photosynthetic bacteria 2-10 mm below many of the mat surfaces.

"Polygonal mats at the edge of Storrs Lake were associated with uncemented micrite, but the top 2 mm of mat was virtually free of sediment. Petrological sections revealed irregular or tubular clumps of micrite attached to the *Scytonema* sheaths. Deeper within the mat the tubes coalesced, but there was no evidence of recrystallization immediately below the mat. The partially lithified heads from the same lake were similar consisting of fine, mostly anhedral crystals 1-6 μm in diameter. In all of these mats, the porosity was high and consequently the calcium carbonate content correspondingly low. Low

magnesian calcite was identified in all samples using X-ray diffraction and atomic absorption spectrophotometry."

Paull et al., 1992

Paull and colleagues performed isotope analysis on Storrs Lake samples, and concluded: "(1) The carbonate laminations of the stromatolites in Storrs Lake have developed over the last 2310 years.

(2) These stromatolites grow at an average rate of 160 mm per thousand years with one macroscopic-lamination preserved every 21 years on average.

(3) The macroscopic Mg-calcite laminations which comprise the stromatolite heads are themselves composed of yet finer scale, discontinuous laminae cut by many micro-unconformities.

(4) Correlating between the macroscopic-laminae in adjacent stromatolites is ill-advised, because the laminated record in these heads are incomplete and/or do not reflect conditions throughout the lake.

(5) The distinction between the range of $\delta^{18}O$ values for carbonates in the stromatolitic heads from those of the carbonate sediments within the lake is further evidence that these structures are not derived from trapping and binding lake sediments and suggests that they are precipitated locally.

(6) The lack of inter-head correlation may be explained by local microenvironmental changes under the mats within individual heads.

(7) Stromatolite calcification may be stimulated by organic matter degradation, including sulfate reduction, which produce alkalinity changes."

Bebout, 1992

Bebout studied Storrs Lake over five years as part of his doctoral dissertation at the University of North Carolina at Chapel Hill. He measured the rates of photosynthesis and nitrogen fixation in the Storrs Lake stromatolites, and determined that the stromatolites in the northern sector no longer show much biological activity. Biological activity by the *Scytonema* communities responsible for the stromatolites may be inhibited by the high salinity and low light levels characteristic of the turbid, hypersaline water of Storrs Lake. Bebout determined that the growth of stromatolites in the northern sector may be limited to "intermittent periods of lower salinity, and/or periods of reduced water column turbidity."

SOUTHERN SECTOR

Although Storrs Lake's northern sector has been the focus of several studies, little information has been published on the southern sector (south of the narrows). The southern sector is smaller and shallower than the northern sector, and was the last basin to be closed off from the open ocean (Figure #9) (Zabielski, 1991). Just like the northern sector, the water in the southern sector is hypersaline and fluctuates between ~40 and ~90 PSU (Mann & Nelson, 1989), with an average pH of 8.5 (this study). Although large stromatolitic heads exist in the southern sector (Dupraz et al., 2006), this study focuses on the southern sector's smaller stromatolitic knobs, as well as small, thrombolitic knobs along the southern sector's shoreline. Because the southern sector closed off from the ocean more recently than the northern sector (Zabielski, 1991), the stromatolites have not

had as much time to develop. By focusing on this 'younger' part of Storrs Lake, where active microbial mats are forming recent build-ups and crusts, this study investigates the initial stages of carbonate precipitation within the microbial mat, the processes leading to laminae formation, and the environmental conditions that may influence these processes. This study could provide insights into the origin of the larger stromatolitic heads found in within Storrs Lake, as well as recent stromatolites in other areas and potentially those found in the fossil record.

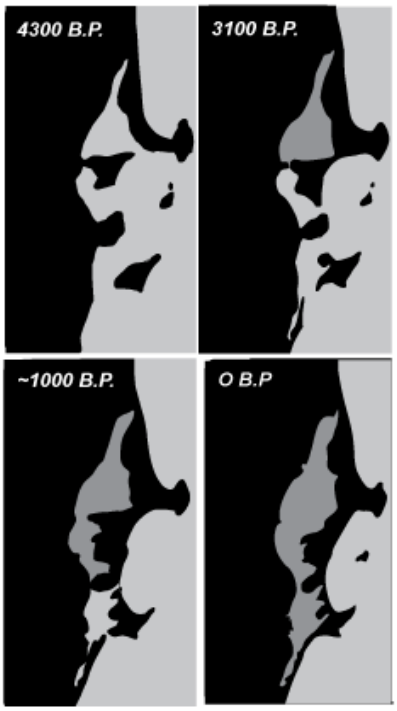

Figure #9: Stages of Storrs Lake basins closing (Zabielski, 1991)

METHODS

FIELD METHODS

Field work for this study occurred between June 18 and June 20, 2010, in Storrs Lake, located on the eastern (windward) side of San Salvador Island, Bahamas. This fieldwork included sampling, data collection, and field mapping along two transects near the southern end of the lake (Figure #10).

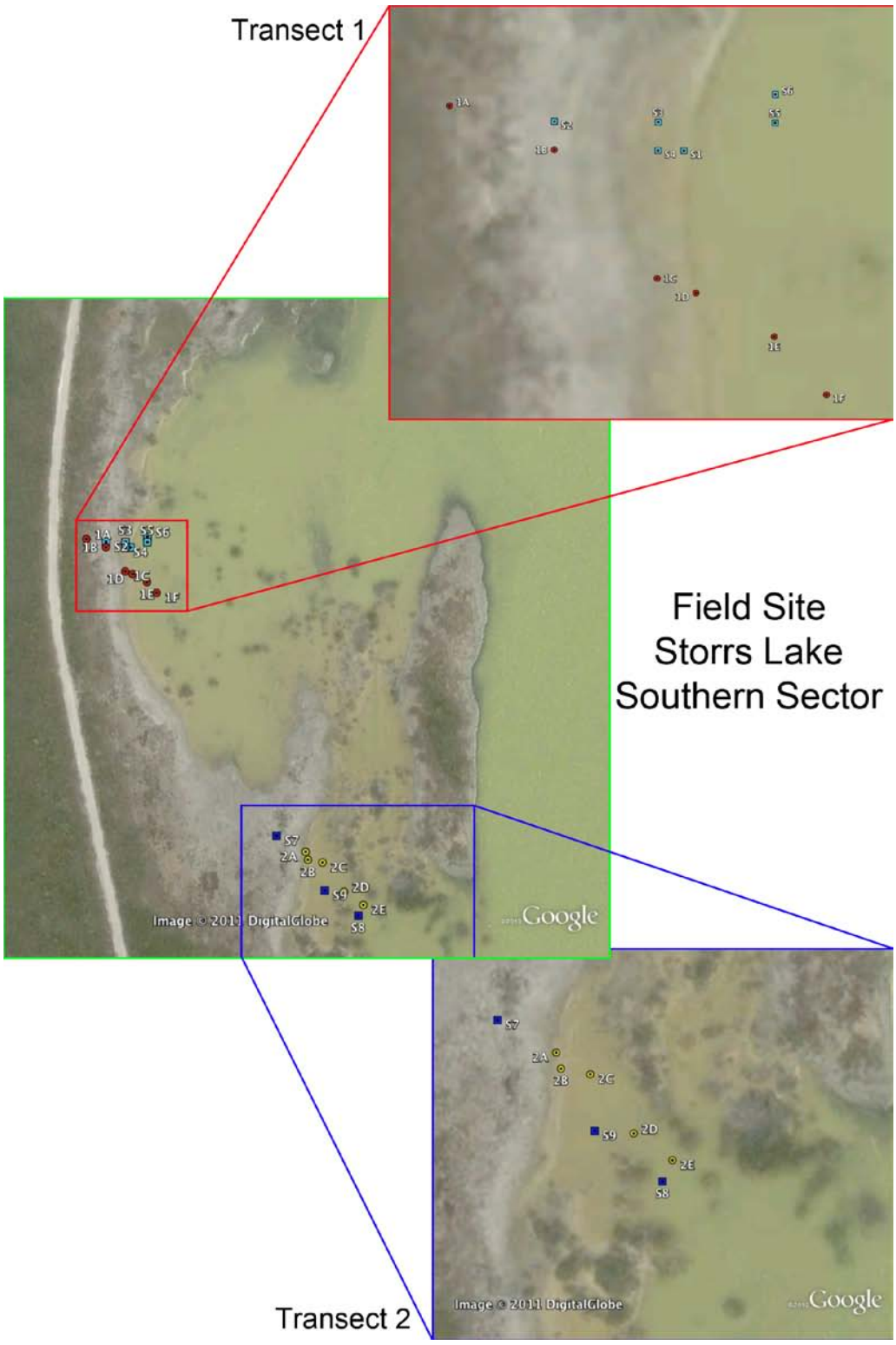

Figure #10: Satellite Images outlining the locations of the two mapped transects (1A-1F & 2A-2F) and sampling sites (S1-S9) for this field study. Courtesy of Google Earth.

Sampling Procedures (microbial samples)

Samples of *Dichothrix* knobs were taken from the dry, exposed region surrounding the lake using a knife to cut the knobs from the ground. Small rectangular samples of calcium carbonate crust were also cut from this exposed region. Small plastic containers were filled with samples of the thick EPS layer floating at the outermost margins of the lake. *Scytonema* knobs were cut and pulled up from the deeper (~18-20 cm) portion of the lake.

Most *Dichothrix* and *Scytonema* knobs were wrapped in plastic wrap, placed in plastic containers upon collection, and refrigerated for storage. Some smaller portions of *Dichothrix* and *Scytonema* knobs were fixed on the day of sampling in a 3% formalin solution with a salinity of 60 PSU to match the average salinity of Storrs Lake at the time of sampling. These fixed samples were stored in small glass containers and refrigerated.

Sampling Procedures (water samples)

Water samples were taken at the shallow and deep ends of both transects. Each sample was collected in a clean, half-liter plastic bottle. Each bottle was rinsed with lake water at the sampling site, then fully submerged and capped under water to ensure minimal head space. One 500 mL bottle of water from each of the two transects was wrapped in aluminum foil to prevent light penetration, and refrigerated for storage.

Water samples from the shallow and deep ends of each transect were filtered on the day of sampling. These samples were first poured through coffee filters to remove large

particulates, and were then filtered sequentially through 5, 1, and 0.22 μm syringe filters. This filtration resulted in two 10 mL subsamples from the shallow and deep ends of each transect, for a total of eight 0.22 μm filtered subsamples. These filtered samples were stored in 15 mL falcon tubes and refrigerated.

One 500 mL sample from each transect was used for titration analysis on the day of sampling (See Laboratory Methods: Titration Methods).

All microbial and water samples were kept refrigerated except during transport from the Gerace Research Center on San Salvador to the University of Connecticut and during analysis.

Field Data Collection

Field data were collected to determine the environmental parameters at each sampling location. A conductivity meter was used to determine the salinity, conductivity, and temperature of each sampling site. A GPS device was used to collect the latitude and longitude coordinates of each sampling location. A 1-inch diameter PVC pipe was marked at 2-centimeter intervals for use as a depth gauge. In the deeper portions of each transect, depth was measured to both the surface of the soft microbial mats, and to the surface of the Pleistocene rock below the soft mats. Photographs were taken of each sampling site, and were labeled with the corresponding GPS coordinates.

Due to the high temperatures of the lake at the time of sampling, pH data could not be obtained in the field. The pH of each transect was determined by taking the pH of water samples on the day of sampling after the samples had cooled to room temperature.

Field Mapping Techniques

Field mapping of each transect was conducted using a combination of measuring tape and GPS. Each transect was broken into zones based on the types of microbial features found in that section. The distance from one zone to the next was measured with measuring tape, and GPS waypoints were taken at both ends of each zone. Photographs were also taken along each transect to indicate the features of each zone, and depth was measured at the ends of each submerged zone.

LABORATORY METHODS

Titration Methods

Titrations were performed on water samples both on the day of sampling at the Gerace Research Center and several months later at the University of Connecticut.

Titrations done at the Gerace Research Center on the day of sampling were performed on unfiltered samples using a manual stir rod and a Mettler Toledo pH/conductivity meter. Acid titrations were done using 1 M HCl, followed by degassing, next, base titrations were done using 1 N NaOH. GRAN function calculations were done both in Microsoft Excel and using the web-based USGS Alkalinity Calculator (http://or.water.usgs.gov/alk/).

Titrations performed at the University of Connecticut several months later were done on unfiltered samples using a magnetic stir bar on a stir plate and a Mettler Toledo pH/conductivity meter. Acid titrations were done using 1 M HCl, followed by degassing, then base titrations were done using 1 N NaOH. GRAN function calculations were done both in Microsoft Excel and using the web-based USGS Alkalinity Calculator (http://or.water.usgs.gov/alk/).

Ion Chromatography

Ion Chromatography using the Dionex ICS-3000 model was used to determine the anion and cation concentrations of water samples from each transect. Water samples were filtered to .22 μm on the day of collection and kept refrigerated until analysis. Due to the high salinity of these samples (~60 PSU), they were diluted 500-2000 times prior to IC analysis. This dilution was high enough to prevent the analytical columns from becoming saturated with salt, but low enough that the ions could still be detected at a useable resolution. Dionex Seven Anion Standard II and Dionex Cation-II Standard were used for anion and cation analysis respectively. Each were diluted to 50, 25, 10, 5, and 1 ppm, and placed in that order ahead of the samples in the IC sample trays. A blank of deionized water was also placed in between each sample in the sample trays.

Calculation of Saturation Indices

After ion chromatography and titration analysis, WEB-PHREEQ, an online aqueous geochemical modeling program by the North Dakota State University Department of

Geosciences (based on the PHREEQC program created by David Parkhurst of the USGS) was used to calculate the saturation indices of the water samples with respect to calcite, aragonite, dolomite, and gypsum (See appendix). Saturation indices are calculated by the log of the ratio of a mineral's ion activity product (IAP), the product of the activities of dissolved ions (i.e. $\{Ca^{2+}\}X\{CO_3^{2-}\}$) to the mineral's solubility product (K_{sp}), in the equation $SI=\log(IAP/K_{sp})$ (Stumm & Morgan, 1996). (6)

If the saturation index is equal to 1, the water is saturated, or at equilibrium with the mineral. If the saturation index is greater than 1, the water is supersaturated with respect to the mineral, and precipitation is geochemically favorable. If the saturation index is less than 1, the water is undersaturated with respect to the mineral, and dissolution is geochemically favorable (Stumm & Morgan, 1996).

Isotopic Analyses

The stable carbon and oxygen isotope composition of carbonate samples from Storrs Lake were determined by Christophe Dupraz using a VG Micromass 602 mass spectrometer (Micromass UK Ltd, Altrincham) at the University Pierre and Marie Curie (Paris). The stable carbon and oxygen isotope ratios are reported in the delta notation as the per mil (‰) deviation relative to the Vienna PeeDee Belemnite (VPDB) standard: $\delta = (R_{sample} - R_{standard}) / R_{standard} \times 1000$ with $R = {}^{13}C/{}^{12}C$ or ${}^{18}O/{}^{16}O$. (7)

Laboratory standards were calibrated relative to the international standard NBS-19, where $\delta^{13}C = 1.95‰$ and $\delta^{18}O = -2.2‰$ VPDB. Analytical uncertainty, monitored by analyses of the laboratory standard Carrara marble, was no greater than ± 0.05‰ for carbon and ± 0.1‰ for oxygen.

X-ray Diffraction

Mineralogy of Storrs Lake samples was determined by Christophe Dupraz with X-ray diffraction (XRD) using a Scintag diffractometer. Deconvolution peaks (Pearson VII distribution functions) were used to calculate mole % of magnesium calcite following Kübler (1992).

Oxygen Profiles

O_2 profiles were built in soft mats, 'subcalcified *Scytonema* knobs', and 'jelly bombs' using microelectrodes. Depth profiles were determined using needle electrodes with an outer diameter of 0.8 mm (Visscher et al., 1991). Multiple profiles were measured on the same samples and averaged prior to plotting the depth distribution.

MICROSCOPY TECHNIQUES AND SAMPLE PREPARATION

Scanning Electron Microscopy

Samples were prepared for SEM analysis following four different protocols in order to determine the most effective method for these unique structures. The samples were cohesive, but still somewhat delicate, so the rotator was not employed during any part of the sample preparation process. The stromatolite samples were large, so small subsamples were taken for SEM preparation. This was done using a razor blade to section off portions that demonstrated strong lamination, which were then broken off from the larger samples.

Protocol 1: Three Subsamples

Two unfixed stromatolite samples SL10-1SAB2 (two subsamples) and SL10-2K2 (one subsample) were subsampled using the razor blade technique. These three subsamples were prepared for SEM analysis using Protocol 1. This protocol is outlined as follows:

Day 1 (10/4/10):

Place samples in 1.5% glutaraldehyde, 1.5% paraformaldehyde in 0.1 M HEPES buffer with 0.9 M NaCl and leave over night in refrigerator.

*pH of buffered aldehyde measures ~pH 8.0

Day 2 (10/5/10):

(1) Dilute the 2X buffer to 1X. (For two samples, made ~40 mL)
(2) Briefly rinse the samples in the diluted buffer.
(3) Submerge samples in fresh 1X diluted buffer for 20 minutes. (2:30 PM – 2:50 PM)
(4) Repeat step 3. (2:58 PM – 3:18 PM)
(5) Repeat step 3. (3:23 PM – 3:43 PM) *Do step 6 while waiting*
(6) Mix 5 mL of osmium from 4% vial with 5 mL of the 2X buffer to create 10 mL of 2% buffered osmium.
(7) After step 5 is done, pour off buffer solution and immediately replace with 2% buffered osmium solution, and leave over night in refrigerator.

Day 3 (10/6/10):

(1) Pour off osmium solution and immediately replace with cold (4°C from refrigerator) DI water.
(2) Return DI water and samples to refrigerator. Let stand for 10 minutes.
(3) Refresh cold DI water in sample containers. Repeat step 2.
(4) Repeat step 3.
(5) After samples have been submerged in cold DI water in the refrigerator three times (10 minutes each), pour off the DI water and immediately replace with cold (4°C from refrigerator) 30% ethanol solution.
(6) Return ethanol solution and samples to the refrigerator. Let stand for 30 minutes.
(7) After 30 minutes, pour off 30% ethanol solution and immediately replace with cold (4°C from refrigerator) 50% ethanol solution.
(8) Return ethanol solution and samples to the refrigerator. Let stand for 30 minutes.
(9) After 30 minutes, pour off 50% ethanol solution and immediately replace with cold (4°C from refrigerator) 70% ethanol solution.
(10) Return ethanol solution to the refrigerator. Leave samples out of refrigerator. Let stand for 30 minutes. Do not return samples to refrigerator at any time past this point.

(11) After 30 minutes, pour off 70% ethanol solution and immediately replace with room temperature 95% ethanol solution. Leave samples out of refrigerator. Let stand for 30 minutes.
(12) After 30 minutes, pour off 95% ethanol solution and immediately replace with room temperature 100% ethanol. Let stand at room temperature for 30 minutes.
(13) After 30 minutes, refresh 100% ethanol. Let stand at room temperature for another 30 minutes.
(14) After 30 minutes, refresh 100% ethanol. Let stand at room temperature over night.

Day 4 (10/7/10):

For further comparison, two different methods were used for solvent removal at the end of Protocol 1. The subsample from sample SL10-2K2 was submerged in hexamethyldisilazane (HMDS) and set out to dry for several days. The two subsamples from sample SL10-1S2AB2 underwent critical point drying for approximately three hours.

Protocol 2A: Two Subsamples

For a comparison of two different aldehydes and ethanol series, Protocol 2 was used. In order to obtain a direct comparison, one subsample each was taken from the same two unfixed samples used in Protocol 1 (SL10-1SAB2 and SL10-2K2). This protocol is outlined as follows:

Day 1 (10/4/10): No sample preparation

Day 2 (10/5/10): Submerge samples in 3% Formalin (made with 60 PSU salinity water). Leave over night.

Day 3 (10/6/10):

(1) Pour off formalin solution and immediately replace with room temperature 60 g/L salt water (to match the salinity of Storrs Lake at the time of sampling to prevent shocking of the samples). Let stand for 10 minutes at room temperature. Do not return samples to refrigerator at any time past this point.

(2) Refresh room temperature 60 g/L salt water. Let stand for 10 minutes at room temperature.
(3) Repeat step 2.
(4) After samples have been submerged in room temperature 60 g/L salt water three times (10 minutes each), pour off the salt water and immediately replace with room temperature 5% ethanol (made with 60 PSU salinity water) solution. Let stand for 15 minutes at room temperature.
(5) Refresh 5% ethanol (made with 60 PSU salinity water) solution. Let stand for another 15 minutes.
(6) After 15 minutes, pour off 5% ethanol solution and immediately replace with room temperature 10% ethanol (made with 60 PSU salinity water) solution. Let stand at room temperature for 15 minutes.
(7) Refresh 10% ethanol (made with 60 PSU salinity water) solution. Let stand for another 15 minutes.
(8) After 15 minutes, pour off 10% ethanol solution and immediately replace with room temperature 25% ethanol (made with 60 PSU salinity water) solution. Let stand at room temperature for 15 minutes.
(9) Refresh 25% ethanol (made with 60 PSU salinity water) solution. Let stand for another 15 minutes.
(10) After 15 minutes, pour off 25% ethanol solution and immediately replace with room temperature 40% ethanol (made with 60 PSU salinity water) solution. Let stand at room temperature for 15 minutes.
(11) Refresh 40% ethanol (made with 60 PSU salinity water) solution. Let stand for another 15 minutes.
(12) After 15 minutes, pour off 40% ethanol solution and immediately replace with room temperature 50% ethanol (made with 60 PSU salinity water) solution. Let stand at room temperature for 15 minutes.
(13) Refresh 50% ethanol (made with 60 PSU salinity water) solution. Let stand for another 15 minutes.
(14) After 15 minutes, pour off 50% ethanol solution and immediately replace with room temperature 75% ethanol (made with 60 PSU salinity water) solution. Let stand at room temperature for 15 minutes.
(15) Refresh 75% ethanol (made with 60 PSU salinity water) solution. Let stand for another 15 minutes.
(16) After 15 minutes, pour off 75% ethanol solution and immediately replace with room temperature 100% ethanol. Let stand at room temperature over night.

Day 4 (10/7/10): Submerge in HMDS and let dry for several days (until completely dry).

Protocol 2B: One subsample

For a comparison between samples that had been recently fixed versus samples that had been sitting in fixative for several months, Protocol 2B was used. This protocol is the

same as Protocol 1B beginning with day 3, but the sample had been fixed for several months, rather than fixing on day 2 overnight. This protocol was tested on a subsample taken from sample SL10-2K3, which had been sitting in 3% formalin (made with 60 PSU salinity water) from the day of sampling in June, 2010 until day 3 of sample preparation (10/6/10).

Mounting and Sputter-coating

After preparation, all samples were mounted on SEM stubs using silver paint. The consistency of these samples did not allow them to stick to carbon tape. The samples were then sputter-coated for 1.5 minutes. The samples were kept in a vacuum-sealed desiccator when not in use.

Results of SEM Protocol Comparisons

It was originally predicted that the different protocols may yield the same basic results and that the fastest protocol would prove to be the best. However, after SEM analysis of each sample, this did not turn out to be the case. Critical point drying appeared to cause the filamentous cyanobacteria, along with other structures, to collapse. HMDS yielded better results, and is easier to employ, than critical point drying (see appendix). In regards to maintaining the structural integrity of the samples, adding salt to the ethanol series (Protocol 2) appeared to work equally as well as using osmium followed by a regular ethanol series (Protocol 1). However, as the salted ethanol (Protocol 2) dried, significant amounts of salt precipitated onto the samples, covering the samples with cubic salt crystals (see appendix). Except for some slight degradation of some crystals, which

may or may not be associated with long-term fixation, there did not appear to be a significant difference in the quality of samples that were fixed during SEM preparation and the sample that had been submerged in formalin for several months. However, it would be beneficial to prepare more samples for use in this comparison. Overall, it appears that Protocol 1, using osmium, a series of unsalted ethanol, and HMDS is the most effective method for preparing these samples for SEM analysis (see appendix).

ESEM and Cryofixation (performed by Christophe Dupraz)

Additional SEM analysis was used on samples taken from Storrs Lake's southern sector previous to this field study by Christophe Dupraz. Dupraz's hydrated samples were observed via the environmental control mode of the ESEM (wet mode). This ESEM is also equipped with Oxford high-resolution cryo transfer system, where samples were frozen (cryofixation) by immersion in nitrogen slush at –210°C. The samples were freeze-fractured, 'etched' (sublimation of excess water by rising temperature up to –95° C for 1 minute) and coated with palladium-gold under vacuum within the microscope preparation chamber. The cryofixation transforms the water to ice having crystalline domain size between 10-100 nm, and thus, are not supposed to modify the three-dimensional organization of even highly hydrated samples.

Petrographic Thin Section Preparation

Stromatolite samples were prepared for petrographic thin sections using a similar chemical drying process to SEM sample preparation. Sample size was reduced using a razor blade to section off portions that demonstrated strong lamination, which were then

broken off from the larger samples. Ethanol solutions were made using 60 PSU salinity water to match the salinity of Storrs Lake at the time of sampling to prevent shocking of the samples. Subsamples were submerged in a 5% ethanol solution for 15 minutes, then the 5% ethanol solution was refreshed, and the subsamples were submerged for an additional 15 minutes. This process was repeated sequentially with 10, 25, 40, 50, and 75% ethanol solutions. The subsamples were then submerged in 100% ethanol three times for 15 minutes each. After the three 15-minute submersions in 100% ethanol, subsamples were submerged in tetramethylsilane (TMS) and left until completely dry.

After drying, subsamples were embedded with epoxy (Struers Epofix or Logitech Epoxypack 301) using a Struers Citovac vacuum system and left to cure for several days prior to petrographic thin section preparation.

Thin sections were studied under normal light microscopy, and additional examination was done with fluorescence by Christophe Dupraz (Transmitted light 12V100W halogen Koehler illumination) using an Olympus petrographic BH-2 and BX60 equipped with fluorescence using a mercury arc lamp (excitation wave length of 395-440 nm, emission > 470 nm). Color contrast of fluorescence pictures were later enhanced with color management software (Adobe Photoshop).

RESULTS

FIELD OBSERVATIONS

Observations were made along two transects in the southern sector of Storrs Lake, between June 18 and June 20, 2010. Sampling and environmental data collection also took place along, and in the vicinity of, these transects. The salinity of the lake during this field study was ~60 PSU, with a water temperature of ~40° C. The pH of water samples from these two transects ranged from ~8.1 to ~8.6. The lake water was red-brown in color and very turbid, with visibility only one or two centimeters below the water surface. The lake water had a distinct smell of sulfide and organic acids (resulting from fermentation), and had a thick, slimy feel, due to extracellular polymeric substances (EPS) suspended in the water column. The red-brown color of the water observed in the southern sector during this study was also observed in the northern sector of Storrs Lake by Mann and Nelson (1989), and was explained by organic matter suspended in the water column, along with pink pigmentation of halophilic bacteria.

Figures #11 & #12: Photographs of core samples from Transect 1 showing the stratification of water, ooze, and sediment

The southern sector of Storrs Lake can be divided into zones based on the sedimentary and microbial features observed along the transects.

Zone I: Pleistocene Rock

The lake area is divided from the road by a narrow border of mangroves and other flora, which then gives way to an exposed area of grey, Pleistocene-age limestone. Some small brush and mangroves are also found in this zone, but it is mainly barren. The rock is cracked and uneven throughout this zone. This area of exposed Pleistocene limestone bedrock is consistent in both transects.

Figure #13: Photograph of Pleistocene limestone from Transect 1

Figure #14: Photograph of Pleistocene limestone from Transect 2

Zone II: Stabilized Sediment and *Dichothrix* Knobs

Continuing towards the water, the Pleistocene bedrock was covered by a region of stabilized sediment. Numerous small, laminated *Dichothrix* knobs were found in the stabilized sediment zone, and samples were taken of these for further analysis. It was apparent from the presence of these *Dichothrix* knobs, as well as from significant salt deposits surrounding them, that this stabilized sediment zone is submerged during certain

periods of the year, although it was exposed during the time of this field study. The sediment was dry and covered with salt in Transect 1, but wet and muddy in Transect 2, located slightly to the south. Calcium carbonate crust was also observed in this zone in Transect 1, but not in Transect 2.

Figure #15: Photograph of dry stabilized sediment from Transect 1

Figure #16: Photograph of muddy stabilized sediment from Transect 2

Figure #17: Photograph of *Dichothrix* knobs from Transect 1

Figure #18: Photograph of *Dichothrix* knobs from Transect 2

Zone III (A): EPS and 'Jelly Bombs'

At the entrance to the water, in both transects, there was a zone of thick extracellular polymeric substances (EPS) with ropy to foamy consistencies. Lenses of greenish to reddish 'slime' can also be found floating amongst the EPS zone. This translucent substance was referred to as 'thrombolitic pie mounds' by Mann and Nelson (1989), 'ectoplasm' by McNeese (1988), or 'jelly bombs' (Paerl, pers. comm.). The latter name

will be used in this paper. 'Jelly bombs' consist of green cyanobacteria covered with thick, cohesive EPS and salt crust. The jelly bombs begin as coin-sized, flat discs within the anoxic zone of the microbial mat at the bottom of the lake, and then grow into larger 'balloon' morphologies that can float to the surface. The jelly bombs (or 'thrombolitic pie mounds') were described by Mann and Nelson (1989) as being primarily composed of the filamentous cyanobacterium *Phormidium henersonii* and associated with different coccoid bacteria and large amounts of EPS.

This zone is created when EPS throughout the lake is pushed toward the shoreline by the wind. Strong wind was observed churning up the EPS, creating foam, similar in consistency to foamy dish soap. When the wind pushed the EPS together more slowly, it created a ropy texture. Salt precipitant from evaporating hypersaline water can create a crust on top of this ropy EPS, resulting in a cohesive, leather-like texture. At the time of this field study, this EPS zone was confined to a narrow (~5 m wide) band along the shoreline at Transect 1. However, this zone was wider (~8 m) and more broken up at Transect 2. This type of ropy EPS was also observed wrapped around mangroves in deeper parts of the lake.

Figure #19: Photograph of EPS zone from Transect 1

Figure #20: Photograph of ‘Jelly Bomb’

Figure #21: Photograph of EPS zone from Transect 2

Zone III (B): Microbial Mat

Beginning at the shoreline (below the EPS zone), and continuing outwards, the lake bottom is covered with a thick (~4-10 cm), laminated soft microbial mat above the Pleistocene limestone bedrock. This soft mat is particularly thick along Transect 2. The soft mat displays typical microbial mat development (e.g. DesMarais, 1995; Garcia-Pichel et al., 1994; Konhauser, 2007), with a brown, muddy layer on the mat surface, overlying a green layer of cyanobacteria, overlying a pinkish purple layer (likely comprised of purple-sulfur bacteria), with a layer of dark brown/black organic matter on the bottom of the mat. Along Transect 2, the mat is so thick that a very distinct black trail was left behind by stirring up the organic matter after walking through the soft mat.

Light microscopy reveals the brown layer on the top 3 to 4 mm of the mat to be composed of empty bacterial sheaths, extracellular polymeric substance (EPS) and pigments (gloeocapsin, scytonemin).

Figure #22: Photograph of Zone III (B) from Transect 1 (soft microbial mat is not visible through the water)

Figure #23: Photograph of undisturbed soft microbial mat from Transect 2

Figure #24: Photograph after walking through soft microbial mat from Transect 2

Zone IV: *Scytonema* Knobs

About 40 meters from the start of both transects, at a depth of approximately 20 centimeters, begins a zone of stromatolitic knobs. These knobs range in height from a few centimeters to about 20 centimeters, and they are much harder and more cohesive than the *Dichothrix* knobs. These laminated structures are growing through, and are surrounded by the thick, soft microbial mat. Some of the shorter knobs, particularly at the beginning of this zone, have not yet breeched the surface of the soft microbial mat, while others are tall enough to be visible through the surface of the turbid lake water, though still fully submerged. The substrate of these knobs varies from the Pleistocene bedrock, to mangrove roots, to the mat itself.

Just below the surface of the stromatolitic knobs is a green layer of cyanobacteria. Later analysis revealed a mix of filamentous and coccoid cyanobacteria, with the dominant species identified as *Scytonema* sp.

The green cyanobacterial layer in the stromatolitic knobs overlies a pinkish purple layer, most likely composed of purple sulfur bacteria. The bottom of the knobs below these layers is comprised of dark-brown to black organic matter.

Figure #25: Photograph of submerged *Scytonema* knobs from Transect 1

Figure #26: Photograph of submerged *Scytonema* knobs from Transect 2

Figure #27: Photograph of irregular *Scytonema* knob from Transect 1

Figure #28: Photograph of columnar *Scytonema* knob from Transect 2

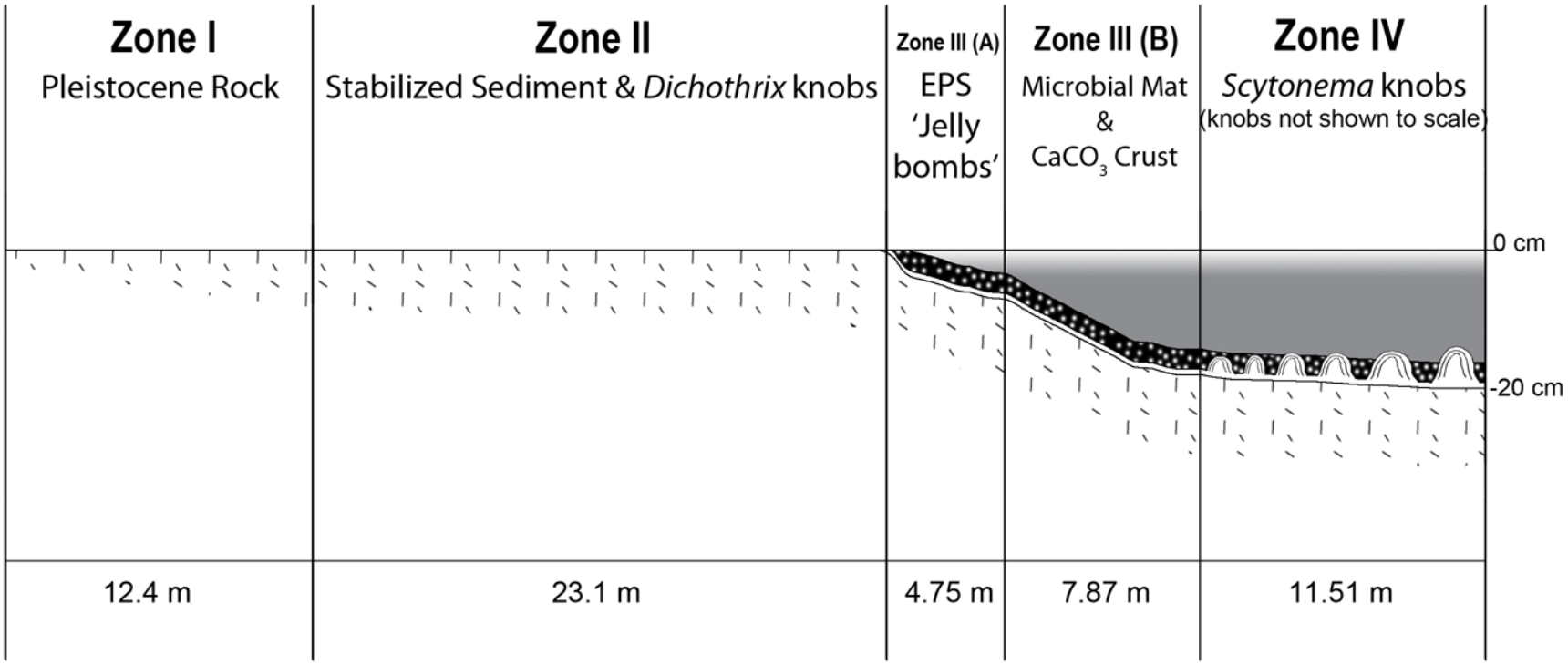

Figure #29: Zones of microbial and sedimentary features along Transect 1.
Distances of zones are shown to scale (1 cm = 2.5 m).
Depth is vertically exaggerated ~27.6 times (1 mm = 1 cm depth)

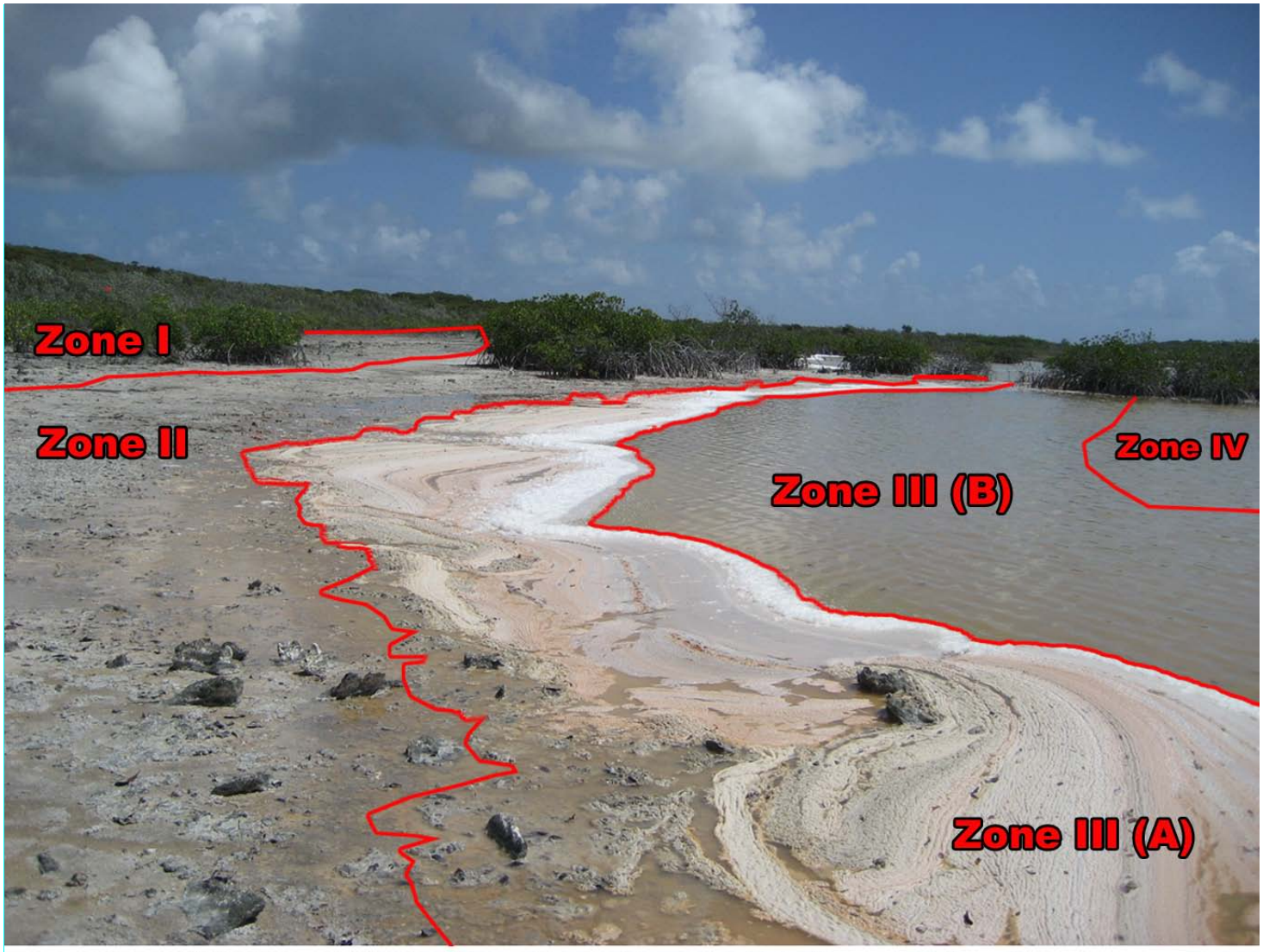

Figure #30: Storrs Lake Southern Sector Transect 1 Photograph with outlined zones

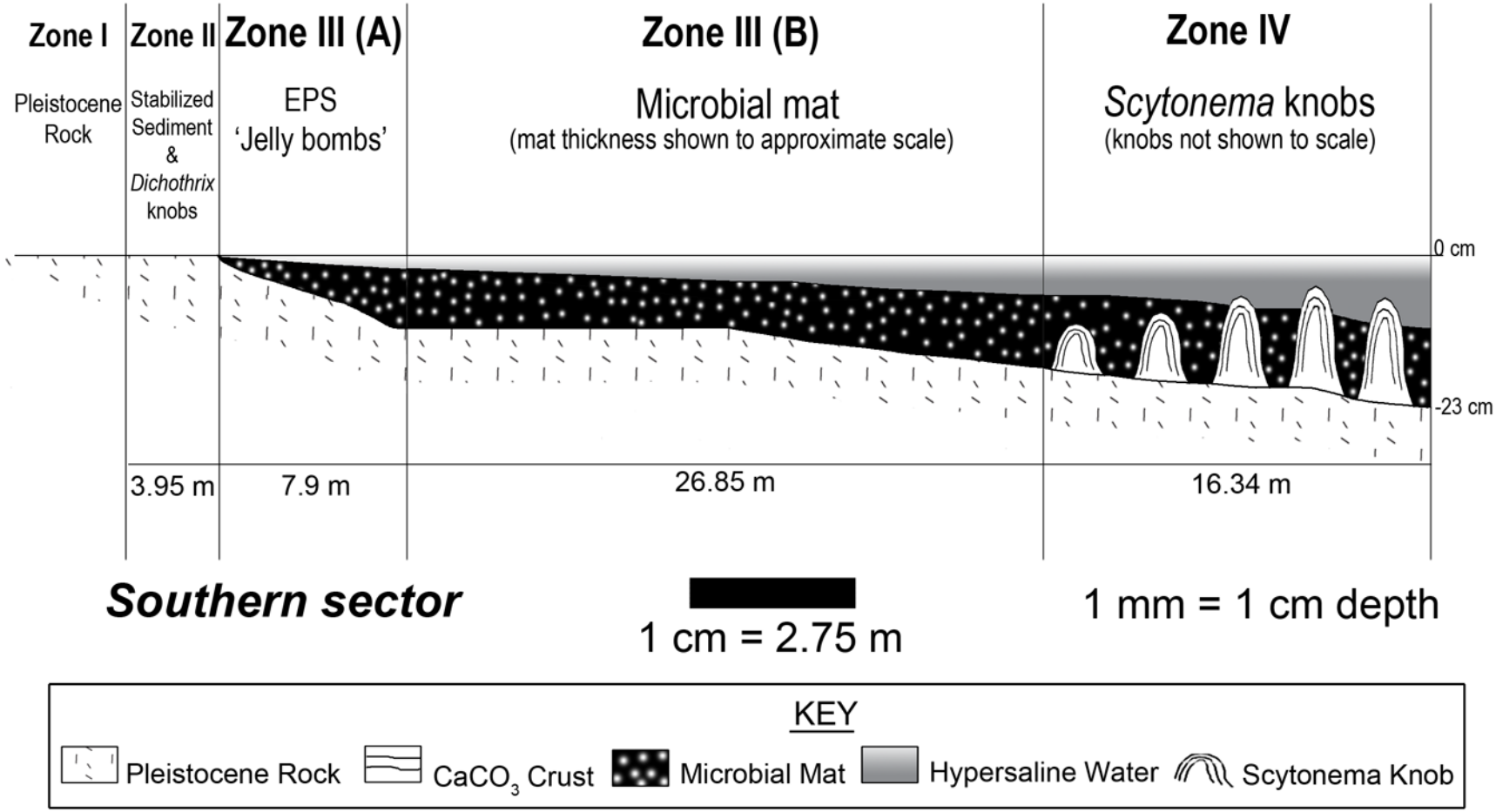

Figure #31: Zones of microbial and sedimentary features along Transect 2.
Distances of zones are shown to scale (1 cm = 2.5 m).
Depth is vertically exaggerated ~27.6 times (1 mm = 1 cm depth).
Thicknesses of microbial mats are shown to approximate scale (measured at intervals and extrapolated out).

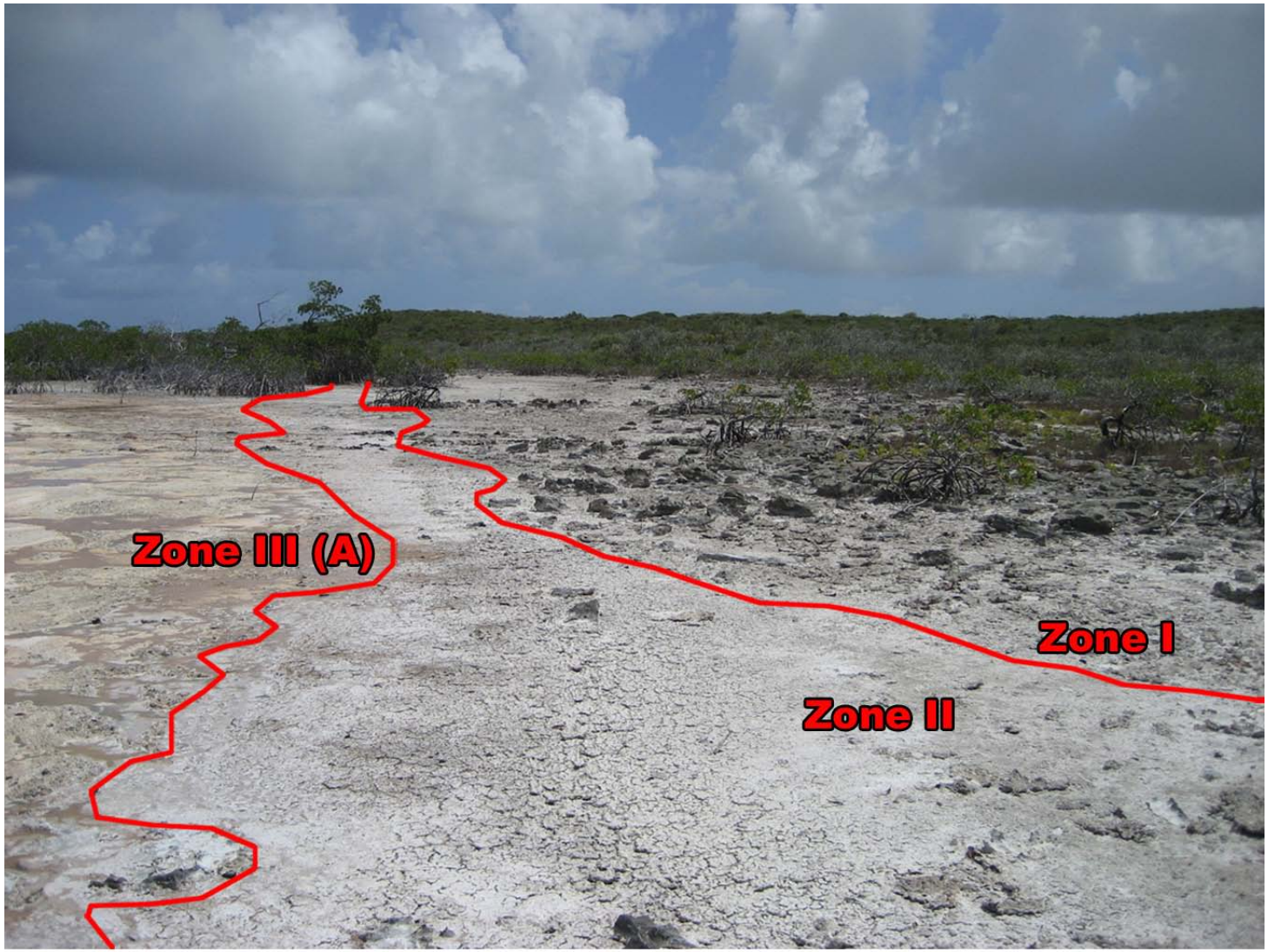

Figure #32: Storrs Lake Southern Sector Transect 2 Photograph with outlined zones

Table #1: Environmental Data from Transect 1

Transect 1	**6/20/10 AM**			
Location	**Zone**	**Zone Description**	**Zone Width**	**Depth**
N 24° 2.381' W 74° 27.063'	--	Mangroves adjacent to road	--	--
N 24° 2.378' W 74° 27.055'	I	Pleistocene rock	12.4 m	Dry, Exposed
N 24° 2.369' W 74° 27.047'	II	Stabilized sediment & *Dichothrix* knobs	23.1 m	Dry, Exposed
N 24° 2.368' W 74° 27.044'	III (A)	EPS and 'Jelly bombs'	4.75 m	7 cm
N 24° 2.365' W 74° 27.038'	III (B)	Soft microbial mat & $CaCO_3$ crust	7.87 m	17 cm
N 24° 2.361' W 74° 27.034'	IV	*Scytonema* knobs	11.51 m*	20 cm

*End of mapped transect, but *Scytonema* knobs continue further

Table #2: Environmental Data from Transect 2

Transect 2	**6/20/10 PM**				
Location	**Zone**	**Zone Description**	**Zone Width**	**Mat Thickness**	**Depth to bedrock**
N 24° 2.264' W 74° 26.972'	I	Pleistocene rock	Road-End of Zone II	---	Dry, exposed
N 24° 2.261' W 74° 26.971'	II	Stabilized sediment & Dichothrix knobs	3.95 m	---	Muddy, Exposed
N 24° 2.260' W 74° 26.965'	III (A)	EPS & 'Jelly bombs'	7.9 m	0-9 cm	0-11 cm
N 24° 2.249' W 74° 26.956'	III (B)	Soft microbial mat	26.85 m	11 cm	17 cm
N 24° 2.244' W 74° 26.948'	IV	*Scytonema* knobs	16.34 m*	~7 cm	23 cm

*End of mapped transect, but *Scytonema* knobs continue further

Table #3a: Sampling Data from Transect 1

Transect 1	**6/19/10 AM-PM**			
Location	**Samples**	**H_2O Temp.**	**Depth**	**Salinity**
N 24° 2.378' W 74° 27.045'	EPS, H_2O, $CaCO_3$ crust	43.2° C	4-6 cm	63.3 PSU
N 24° 2.380' W 74° 27.055'	*Dichothrix* knobs	---	Dry, Exposed	---

N 24° 2.380' W 74° 27.047'	$CaCO_3$ crust	---	Dry, Exposed	---
N 24° 2.378' W 74° 27.047'	'Jelly bomb,' Soft microbial mat, $CaCO_3$ crust	---	Water's Edge	---
N 24° 2.380' W 74° 27.038'	H_2O, *Scytonema* knobs, $CaCO_3$ ooze	40.9° C	18 cm	59.4 PSU

Table #3b: Sampling Data from Transect 1

Transect 1	**6/20/10 AM**			
Location	**Samples**	**H_2O Temp.**	**Depth**	**Salinity**
N 24° 2.382' W 74° 27.038'	H_2O, $CaCO_3$ ooze	30.5° C	17 cm	59.6 PSU

Table #4: Sampling Data from Transect 2

Transect 2	**6/20/10 AM-PM**			
Location	**Samples**	**H_2O Temp.**	**Depth**	**Salinity**
N 24° 2.270' W 74° 26.984'	*Dichothrix* knobs	---	Dry, Exposed	---
N 24° 2.240' W 74° 26.950'	H_2O, *Scytonema* knobs, $CaCO_3$ ooze	36.0° C	20 cm	58.1 PSU
N 24° 2.249' W 74° 26.964'	H_2O, Soft microbial mat	41.2° C	4 cm	65.1 PSU

MORPHOLOGY OF MICROBIALITES IN SOUTHERN STORRS LAKE

The morphology of microbialites can be described in detail by their macrostructure, mesostructure, and microstructures (Figure #3). Two main types of microbialites occurred along the two transects in the southern sector of Storrs Lake. These are the small *Dichothrix* knobs found in the exposed portion along the shoreline of both transects at the time of sampling, and the *Scytonema* knobs found fully submerged further lakeward along both transects.

***Dichothrix* Knobs**

***Dichothrix* Knobs – Macrostructure**

The *Dichothrix* knobs were found only in the exposed portion of the lake during the time of sampling. It is clear that this region is submerged at certain times of the year, but is exposed during the dry season. The *Dichothrix* knobs are small (~5-10 cm long X ~1-4 cm tall), oblong, rounded "blisters" that are stuck to the surface of the stabilized sediment (Figure #33). They are brown-blackish on the outside surface, and many were covered with white salt crust due to evaporation of the hypersaline water which submerges them during the wet season. Once removed from the sediment, their undersides are a red-brown color, and there is void space in the internal center of the knobs (Figure #34).

Figure #33: Photograph of *Dichothrix* knob sample from Transect 1

Figure #34: Photograph of void space inside *Dichothrix* knob

The *Dichothrix* knobs in Transect 1 were slightly taller and more bulbous (Figure #17) than those of Transect 2, which were flatter and closer to the sediment (Figure #18). The stabilized sediment surrounding the *Dichothrix* knobs in Transect 1 was completely dry (Figure #15), but the knobs themselves, and the sediment immediately beneath the knobs were still wet (Figure #35). The sediment surrounding the flatter *Dichothrix* knobs in Transect 2 was wetter and muddy, and the knobs themselves were wet as well. The

difference in the height of the knobs is likely due to the moisture content of the sediment around them. In dry conditions, shrinking into a tighter knob to have less surface area in contact with the dry sediment could be a survival strategy for the *Dichothrix* community. Shrinking of the sediment around the knobs during desiccation could also potentially cause the knobs to bubble up.

Figure #35: Photograph of damp sediment beneath sampled *Dichothrix* knobs

Dichothrix Knobs – Mesostructure

The *Dichothrix* knobs vary in their mesostructure. Many are clotted and thrombolitic, and some of the clots are organized into layers, creating laminated thrombolites (Figure #36). Some of the knobs, particularly the flatter knobs from Transect 2, display very little organized mesostructure, and could qualify as leiolites. The majority of *Dichothrix* knobs observed in this study, however, are thrombolites or laminated thrombolites.

Figure #36: Photograph of *Dichothrix* knob showing laminated clotted mesostructure

Dichothrix Knobs – Microstructure

Thin section analysis reveals the microstructure of the *Dichothrix* knobs to be a combination of agglutinated trapping and binding, which makes up the majority of the microstructure, and some organomineralization. The areas of trapping and binding within the *Dichothrix* knobs are mostly clotted, with some crude lamination (Figure #37). The trapped sediment grains are composed of ostracode and gastropod shells, foraminifera, micritized ooids and other, unidentified grains (Figure #38). Though the knobs are dominated by trapping and binding, some areas of organomineralization exist within the *Dichothrix* knobs. The precipitation is comprised mostly of micrite (<5 μm), and small holes can be seen in the micrite where filaments were cut perpendicularly (Figure #39). Some areas of sparite/microsparite (5-20 μm) are also present around these micritic grains, possibly due to recrystallization. Many of the clotted structures and clotted laminae are separated by significant pore space (~0.5-1 millimeter), and the remains of filaments can be seen in some of this pore space.

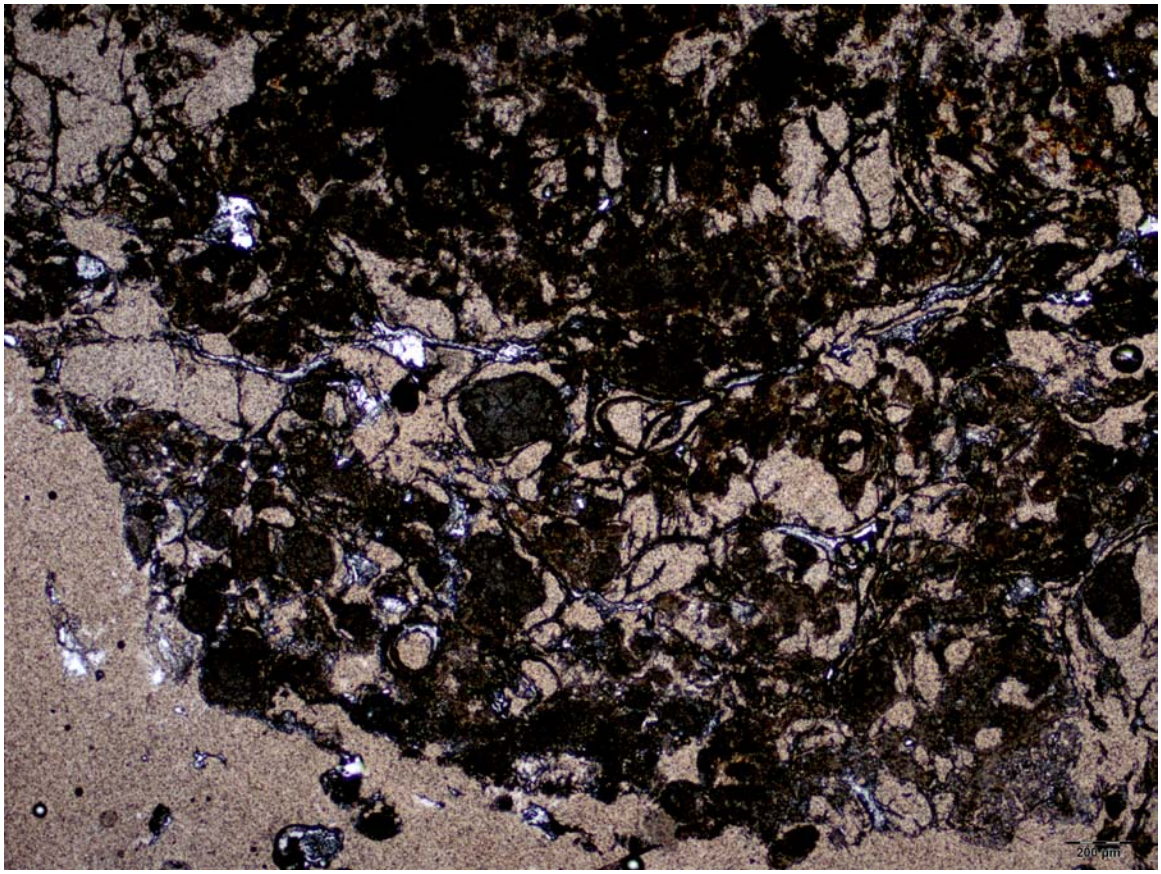

Figure #37: Thin section micrograph of *Dichothrix* knob showing crudely laminated clots

Figure #38: Thin section micrograph of *Dichothrix* knob showing trapped grains

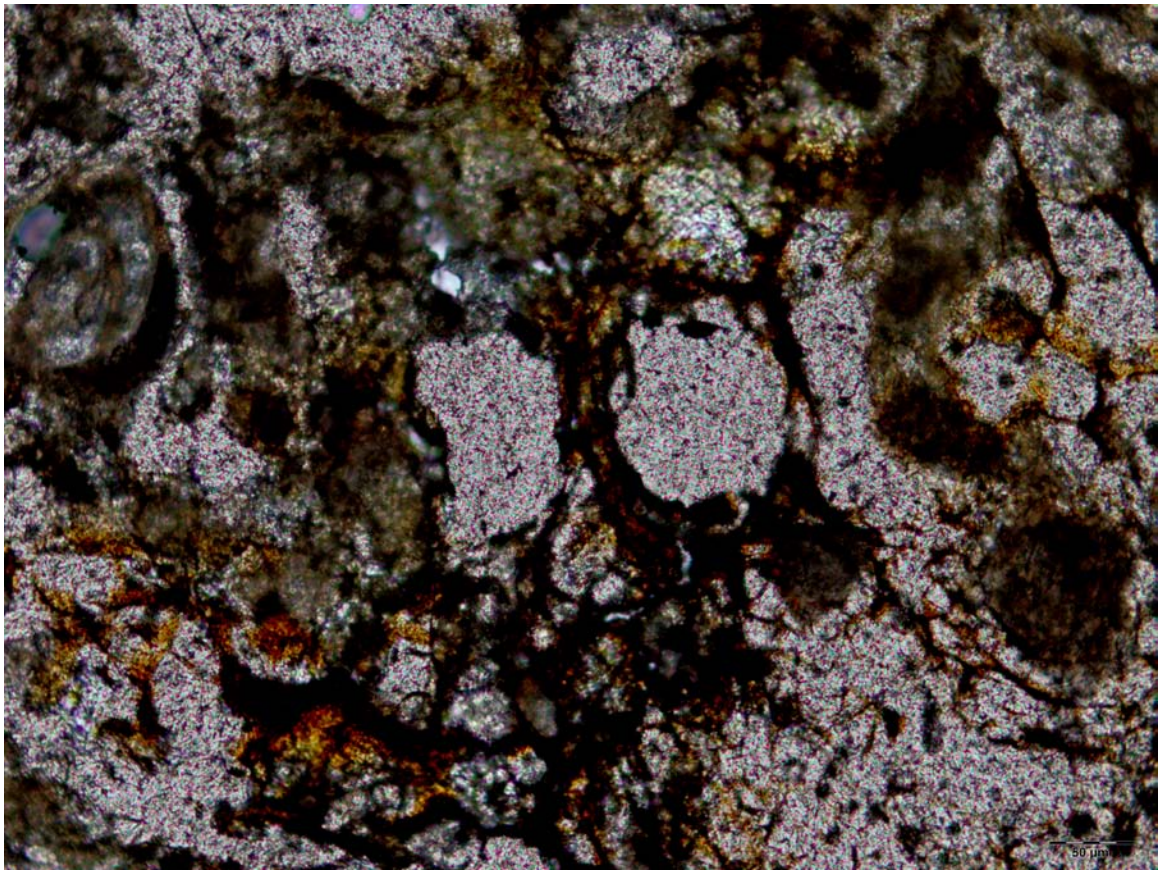

Figure #39: Thin section micrograph of *Dichothrix* knob showing precipitation around cyanobacterial 'ghosts'

Dichothrix Knobs – Bacterial Identification

Planavsky and colleagues (2009) identified *Dichothrix* as being one of the main cyanobacteria involved in the formation of thrombolitic structures in Highborne Cay, Bahamas. The filamentous cyanobacteria was identified by Planavsky and colleagues "based on the presence of common lateral false branching, with the branch first running parallel to the original trichome, as well as the presence of basal heterocysts, obligatory sheaths, narrowing apical ends, and a lack of akinetes" (Planavsky et al., 2009). Further study by Myshrall et al. (2010) on the same structures, confirmed the identification of *Dichothrix* in small, thrombolitic "button microbialites" in Highborne Cay using 16S rRNA gene sequencing. The internal meso- and microstructures of the "button"

thrombolites described by Myshrall et al. (2010) appear consistent with the small thrombolitic knobs found along the edge's of Storrs Lake in this study.

In their chapter on limestones in The Ecology of Cyanobacteria, Pentecost and Whitton (2000) described *Dichothrix* as one of the common types of cyanobacteria that form carbonate structures around the edges of lakes that are dry and exposed periodically.

Because *Dichothrix* has been identified as the major filamentous cyanobacterium responsible for thrombolitic microbialites elsewhere in the Bahamas, it is probable that *Dichothrix* could be responsible for the thrombolitic structures found in Storrs Lake, which are similar in their microstructure, but of vastly different salinity, temperature, and water composition. The location of these knobs in the exposed region along the lake edge further implies that *Dichothrix* could be the primary cyanobacterium creating these small microbialites. Thus, for the purposes of this study, *Dichothrix* has been named as the dominant filamentous cyanobacterium responsible for the creation of the small knobs around the shoreline of Storrs Lake. However, microbial and genetic analysis is needed to confirm the identification of the cyanobacteria in Storrs Lake. It is also possible that the same species of cyanobacteria is primarily responsible for all of the microbialites in Storrs Lake.

***Scytonema* Knobs**

***Scytonema* Knobs – Macrostructure**

The *Scytonema* knobs found submerged further lakeward at ~20 cm depth are larger and more cohesive than the *Dichothrix* knobs. The macrostructures of these *Scytonema* knobs range from irregular (Figures #27) to columnar knobs (Figure #28). These knobs range in height from a few centimeters, to about 20 centimeters, and they range in diameter from ~6-12 cm. Some of the taller columnar knobs, whose tops are several centimeters above the soft microbial mat that surrounds them, are topped with a thick carbonate cap, which are a light tan color (Figure #28). Many of the shorter knobs, where the tops are closer to-or have not yet broken through-the soft microbial mat, are comprised of carbonate that is darker in color (Figure #40 a & b). This darker color is likely the result of more organics on the knobs closer to and within the mat, as well as reduced iron and manganese resulting from lower oxygen content within the deeper part of the mat.

Figures #40 a & b: Photographs of irregular *Scytonema* knobs with dark carbonate

Scytonema Knobs – Mesostructure

The *Scytonema* knobs are stromatolitic in mesostructure; in cross section, they show well-developed millimeter-scale concentric laminations (Figures #41 a & b). These fine laminations occur throughout the *Scytonema* knobs, and different colored layers can be seen where different types of bacteria are the most dense: a green cyanobacterial layer near the top of the knobs (or immediately below the carbonate cap on the taller columnar knobs), a pink/purple layer underneath (possibly purple sulfur bacteria), with dark organic matter under that.

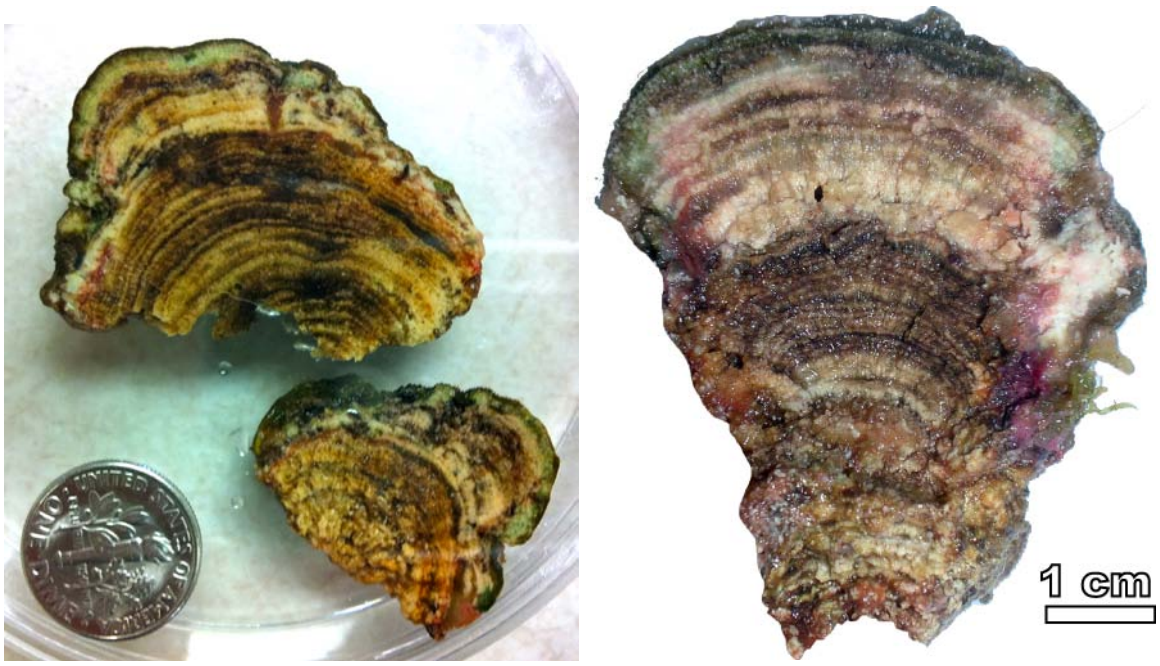

Figures #41 a & b: *Scytonema* knobs in cross section showing concentric lamination and bacterial layers

Scytonema Knobs – Microstructure

The laminated mesostructure of the *Scytonema* stromatolite knobs results from the organomineralization of dense micritic layers separated by millimeter-sized porous

intervals (Figure #42). Small holes in the micrite represent ‘ghosts’ of the *Scytonema* filaments that are responsible for the organomineralization (Figure #43), and some organics are preserved in some thin sections (Figure #44). Much of the micrite is surrounded by sparite/microsparite (5-20 µm) (Figure #45).

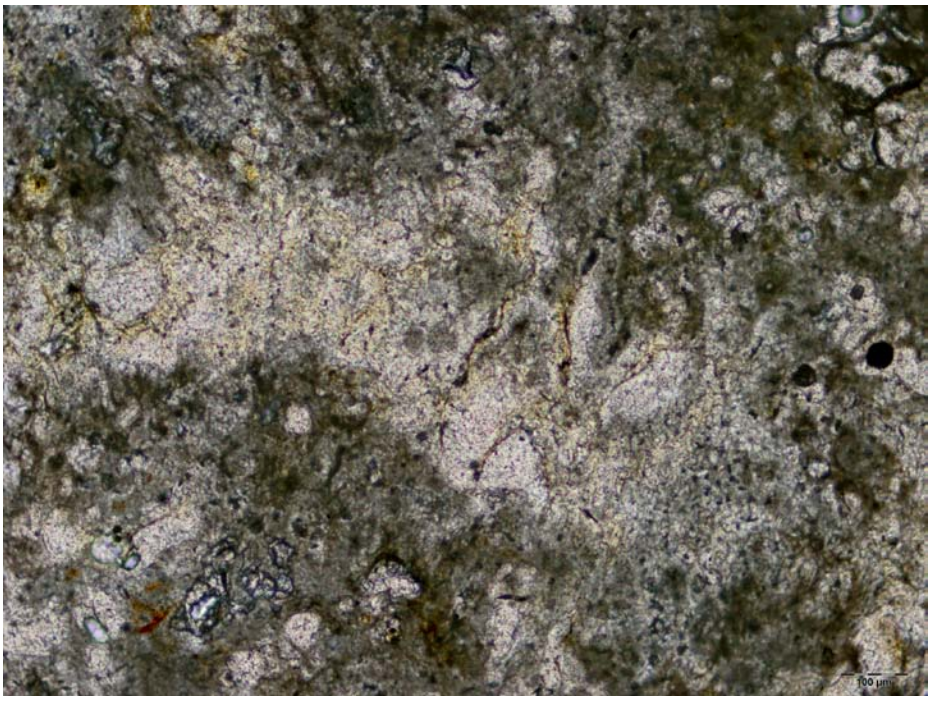

Figure #42: Thin section micrograph of *Scytonema* knob showing laminations

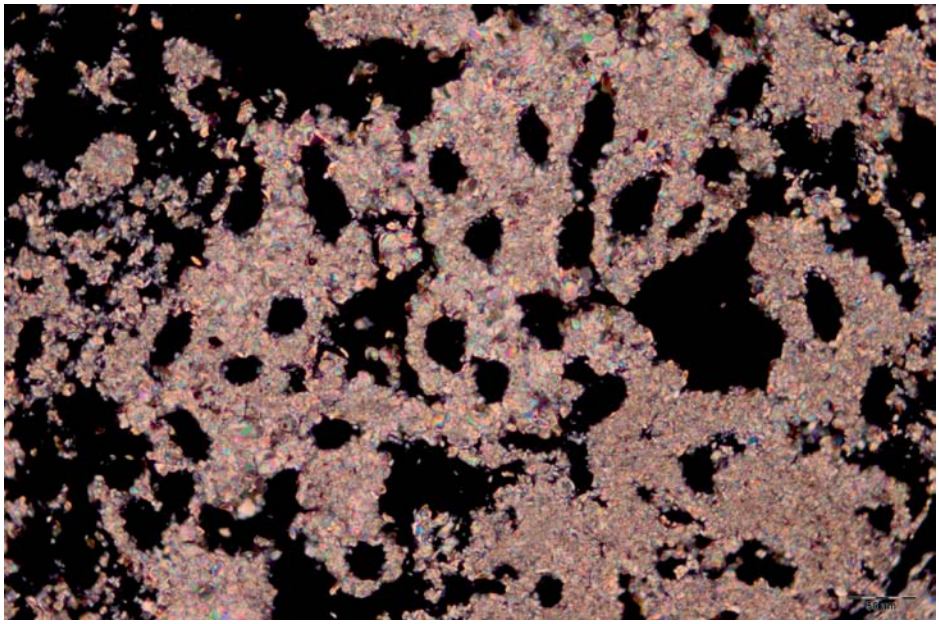

Figure #43: Thin section micrograph of *Scytonema* knob showing ‘ghosts’ of *Scytonema* filaments

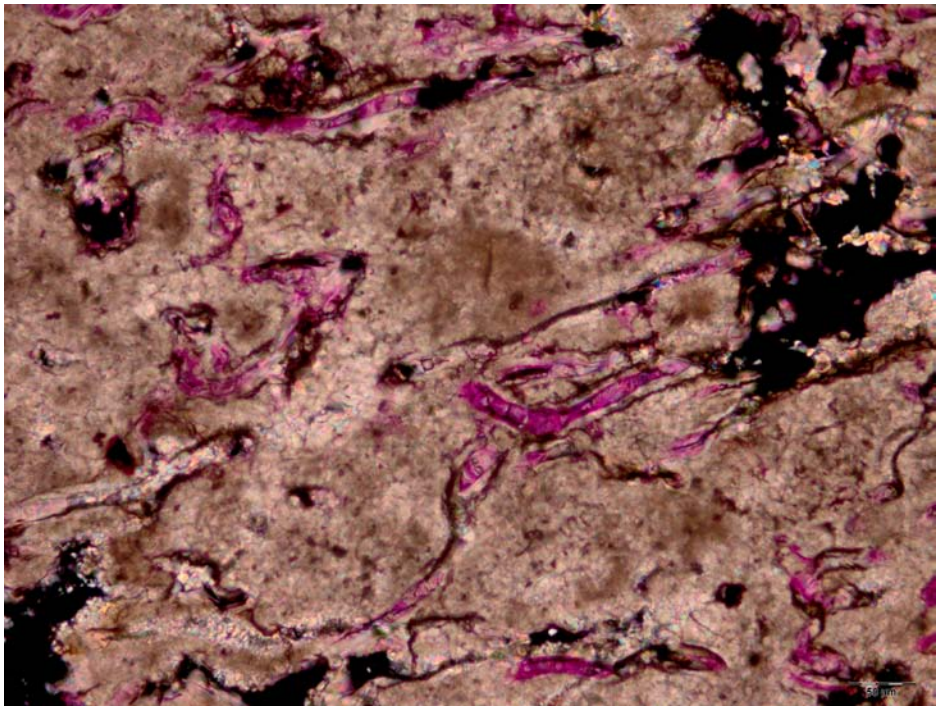

Figure #44: Thin section micrograph of *Scytonema* knob showing preservation of organics

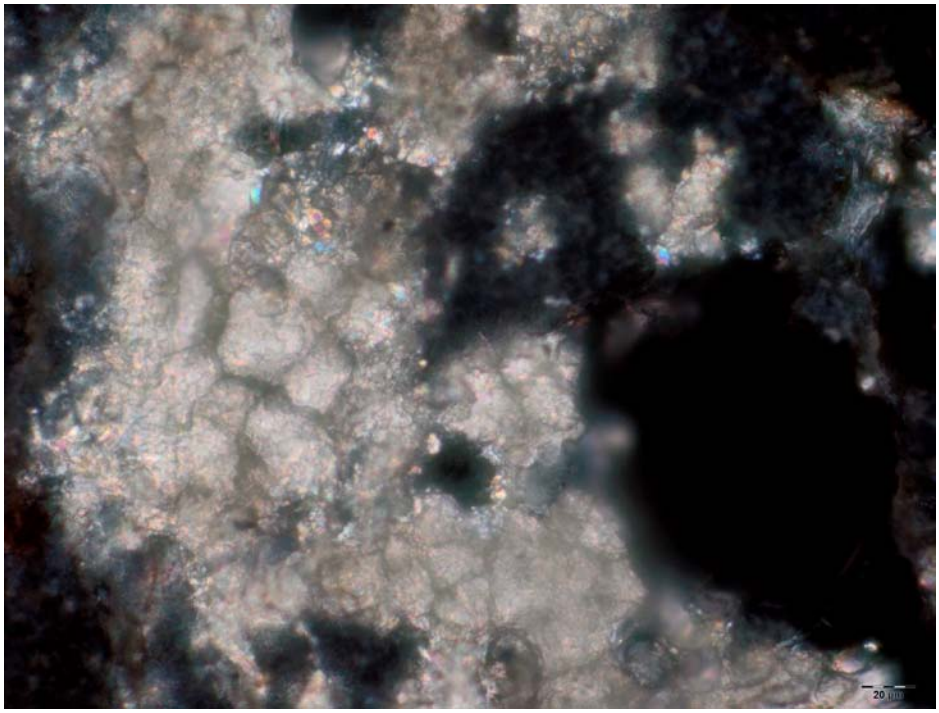

Figure #45: Thin section micrograph of *Scytonema* knob showing micrite surrounded by sparite/microsparite (5-20 µm)

Although precipitation of micrite is highly dominant, some trapping and binding of sediment, such as ostracode and gastropod shells, foraminifera, diatoms, and ooid grains, can be found within the stromatolitic knobs (Figure #46), as well as scattered patches of micropeloidal micrite (~40 µm in diameter) (Figure #47). These trapped grains and micropeloids are primarily found within the more porous layers, in between the dense micrite laminae.

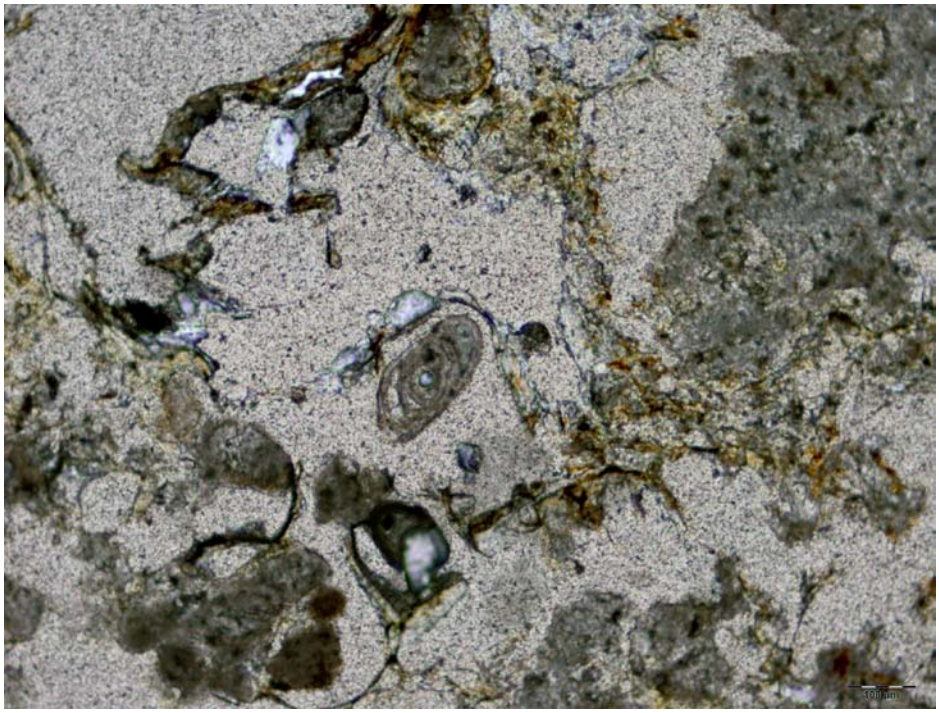

Figure #46: Thin section micrograph of *Scytonema* knob showing trapping and binding

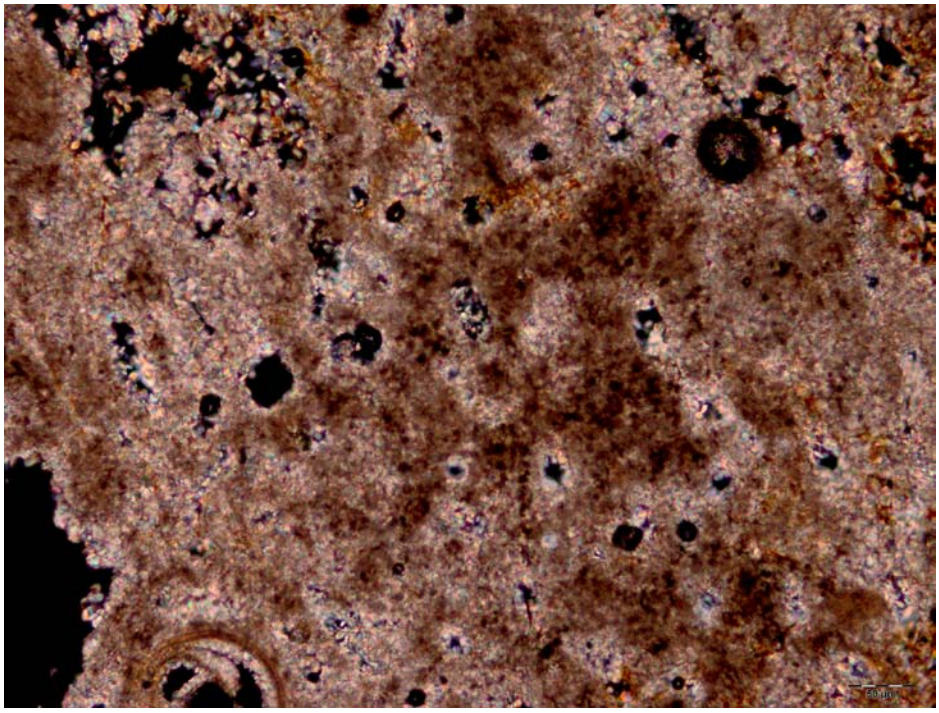

Figure #47: Thin section micrograph of *Scytonema* knob showing micropeloidal structures

SEM imaging reveals abundant cyanobacterial filaments of varying sizes (Figure #48 a & b), as well as coccoidal bacteria (FIgure #49), both in close association with mineral precipitation. Cryofixation SEM analysis preserves the 3-dimensional structure of the EPS, which displays vacuolar framework or 'honeycomb structure' as illustrated by Défarge et al. (1996) and Trichet et al. (2001) (Figure #50 a & b). Empty spaces inside these vacuoles were filled by water that was 'etched' during sample sublimation (see methods). Filamentous and coccoidal cyanobacteria are embedded in this 3-dimensional EPS framework (Figure #50 a & b). Micritic precipitation occurs surrounding, but not in, the sheaths of filamentous cyanobacteria, as well as within the EPS matrix. Precipitation within the EPS matrix cannot be observed with dried SEM samples, as the EPS collapses during the drying process. SEM analysis reveals that the micritic precipitation within the EPS matrix begins as nanospherolites (200-500 nanometers in diameter), which nucleate on the walls of the vacuolar framework of the EPS and can be observed under cryo SEM (Figure #51). If the precipitation had begun as larger, micritic crystals, it would have destroyed the framework of the EPS matrix. Larger micropeloidal structures can also be observed replacing some areas of the EPS framework under cryo SEM (Figure #52).

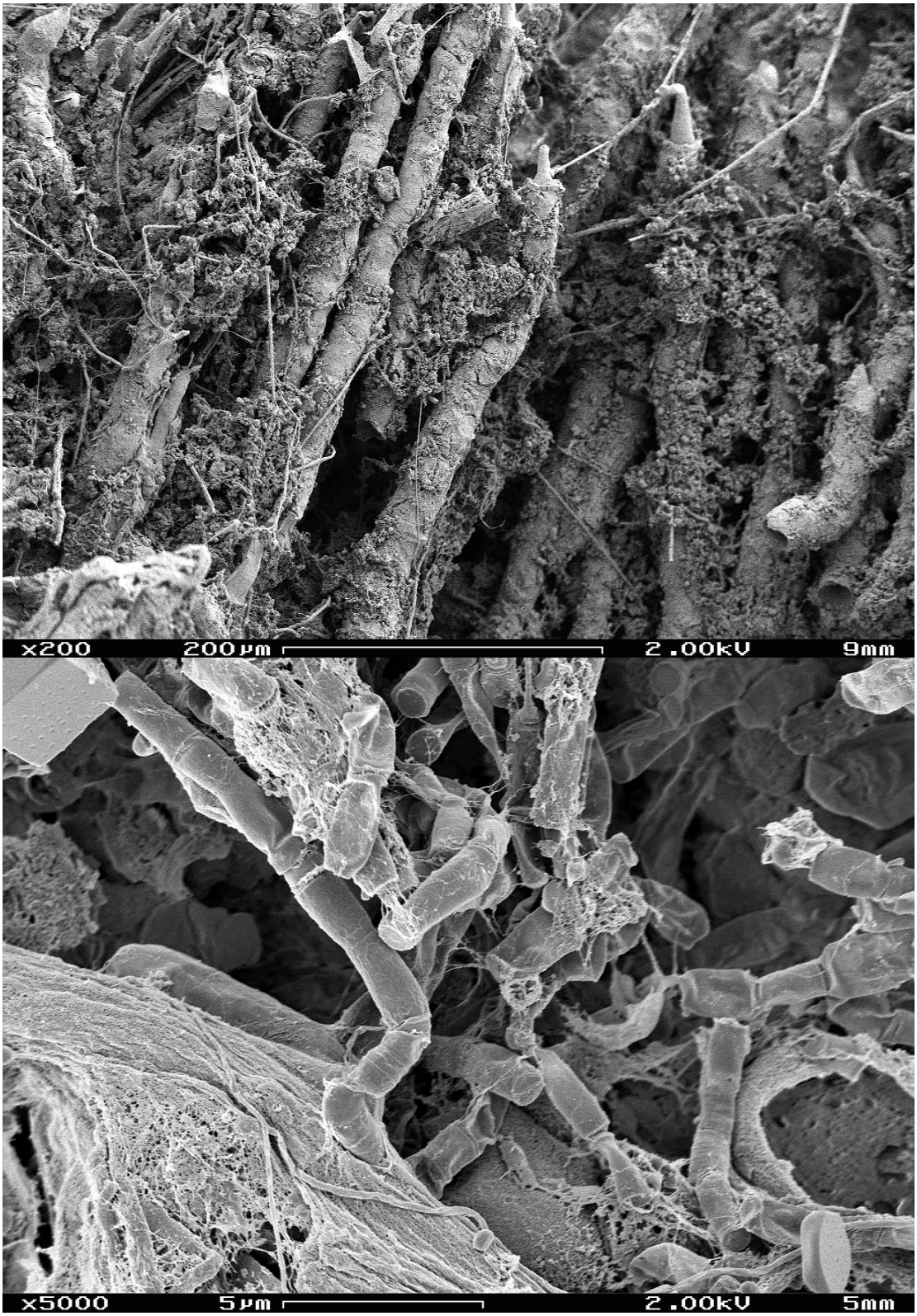

Figures #48 a & b: SEM micrographs of *Scytonema* knob showing cyanobacterial filaments

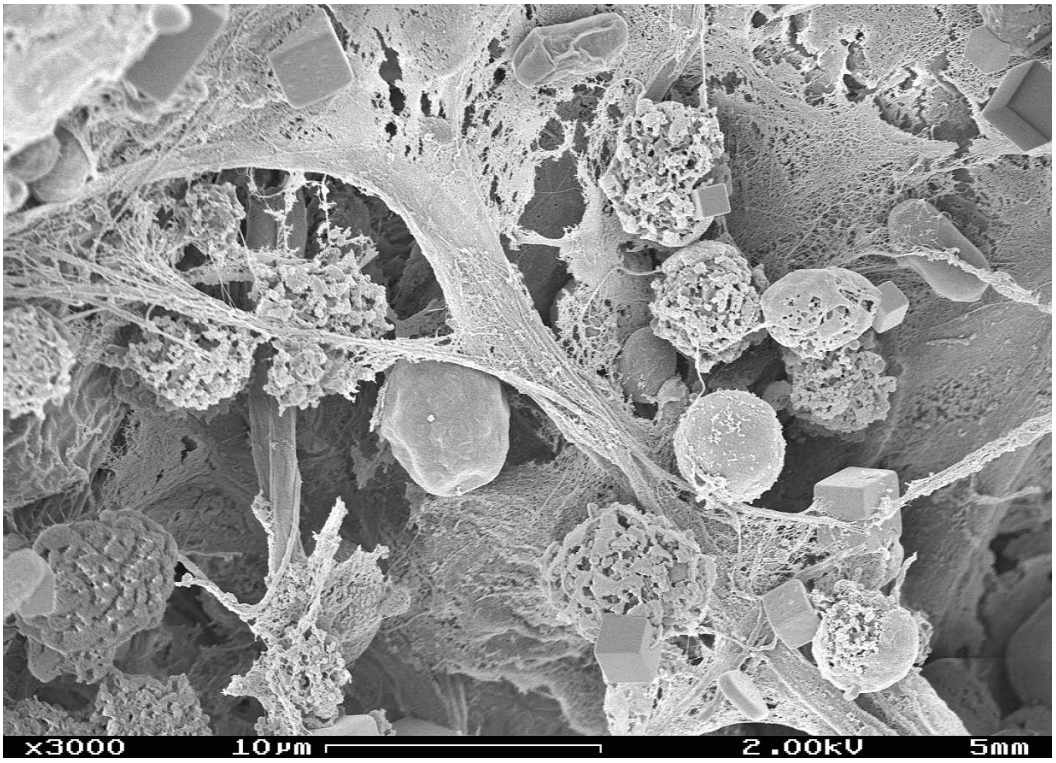

Figure #49: SEM micrograph of *Scytonema* knob showing coccoidal bacteria and micropeloidal structures

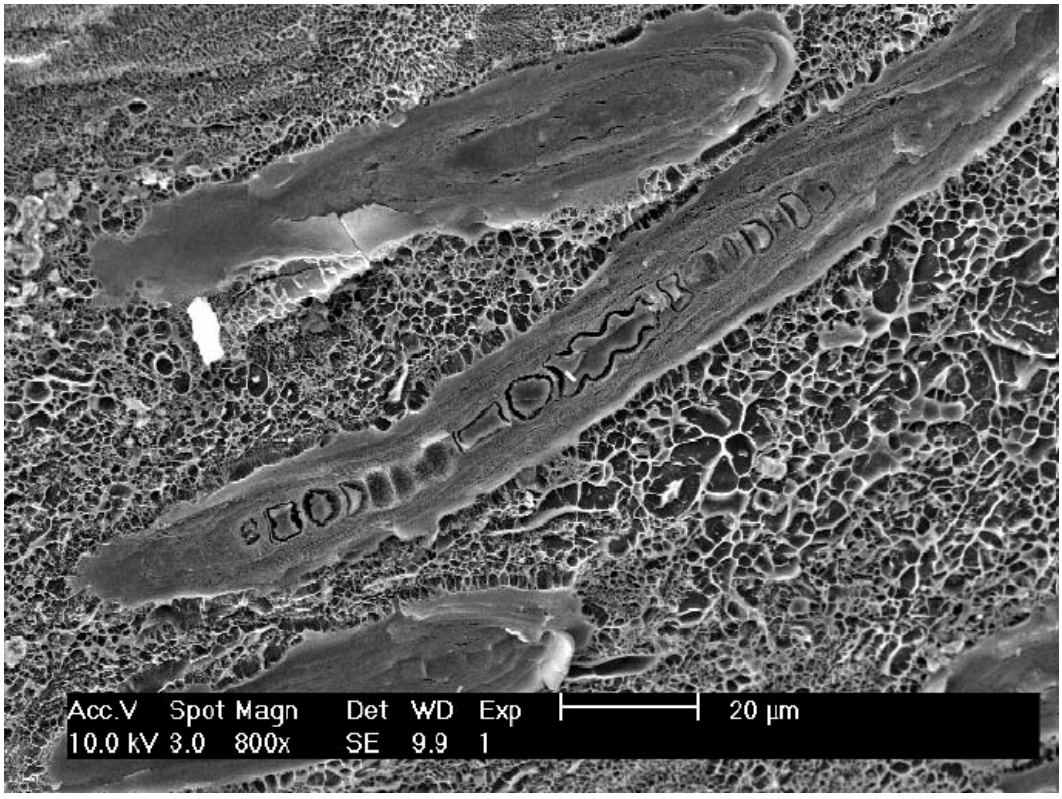

Figure #50 a: Cryo SEM micrograph of *Scytonema* knob showing cyanobacterial filaments embedded in EPS vacuolar framework

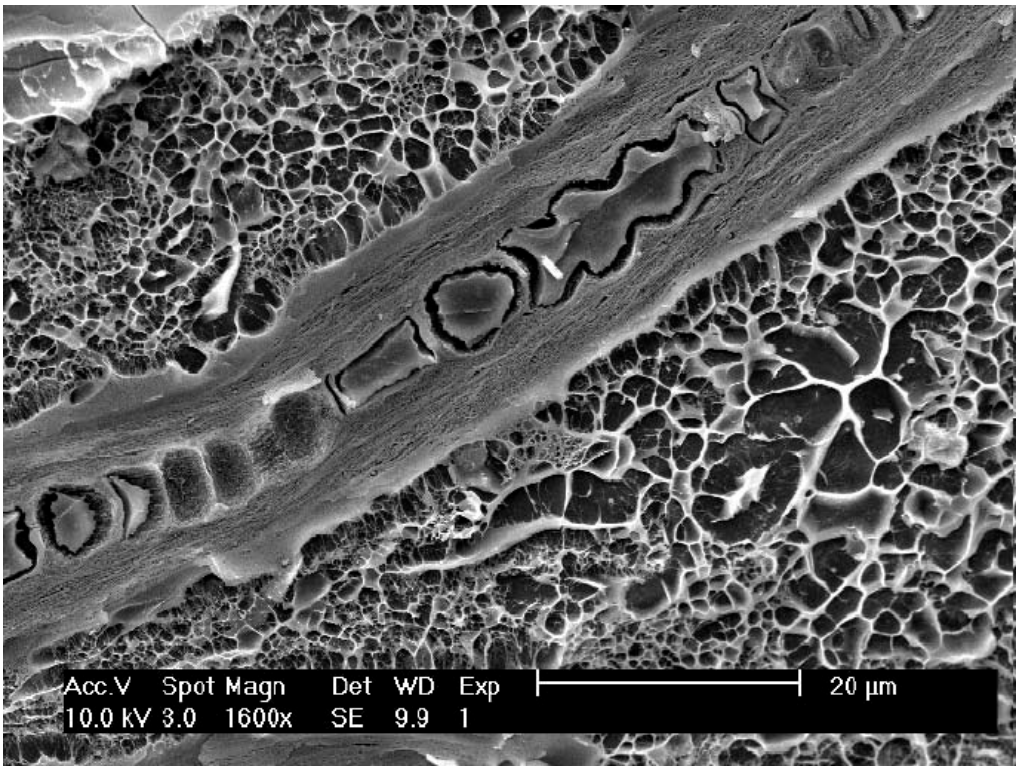

Figure #50 b: Cryo SEM micrograph of *Scytonema* knob showing cyanobacterial filaments embedded in EPS vacuolar framework

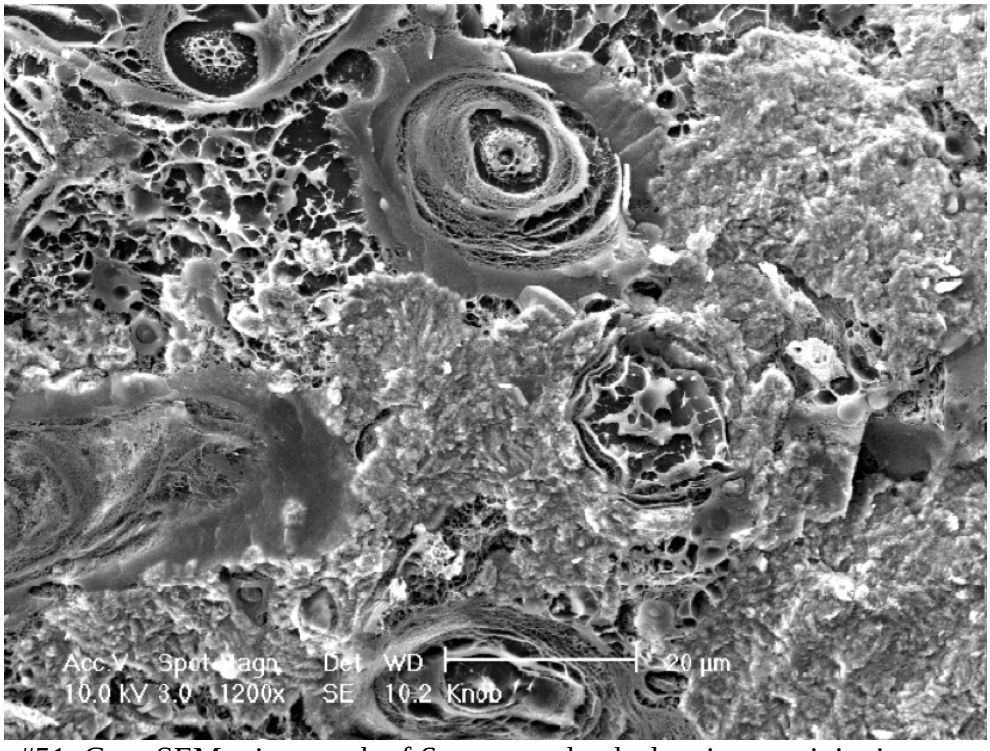

Figure #51: Cryo SEM micrograph of *Scytonema* knob showing precipitation on vacuole walls of EPS

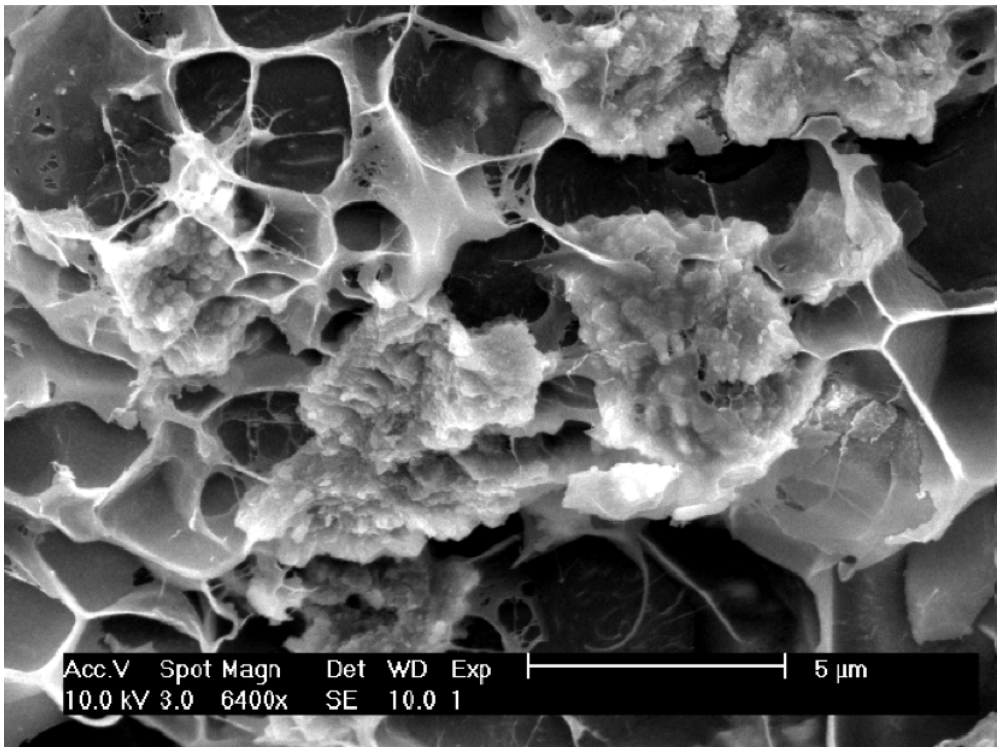

Figure #52: Cryo SEM micrograph of *Scytonema* knob showing micropeloidal structures replacing EPS

***Scytonema* Knobs – Bacterial Identification**

Pentecost (1989) identified *Scytonema* as the dominant cyanobacterium in mat profiles from several locations throughout the Bahamas, including several location in Storrs Lake's northern sector, as well as the narrows separating the northern and southern sectors, stating that the greatest biomass was located in the upper 4 millimeters of the mats. It is likely then, that *Scytonema* is also the dominant cyanobacterium in the soft microbial mats and microbialites found in Storrs Lake's southern sector as well.

Scytonema was also identified as the dominant cyanobacterium in the stromatolitic knobs in Storrs Lake's southern sector by Dupraz et al. (2006).

Scytonema was identified in the stromatolitic knobs from Storrs Lake by Dupraz using light microscopy, as well as by examining SEM images of the filaments, which show size and features consistent with *Scytonema*. Dupraz has identified *Scytonema* as a major cyanobacterium in other stromatolitic structures in Storrs Lake in previous studies as well (e.g. Dupraz et al., 2006). As with the *Dichothrix*, however, microbial and genetic analysis is needed to be certain of the identification.

Macro-, Meso-, Microstructure of Fossil Stromatolites

Fossil stromatolite samples from Mauritania, Africa, belonging to Dupraz, can be compared to the stromatolitic *Scytonema* knobs from Storrs Lake's southern sector. These samples are Late Proterozoic in age, and have similar irregular branching to columnar macrostructures as the modern Storrs Lake knobs (Figure #53). The fossil stromatolites are also consistent with the Storrs Lake knobs in their mesostructure, showing distinct, concentric laminations. Like the Storrs Lake knobs, the fossil stromatolites are micritic in their microstructure. However, the fossil stromatolites have been completely recrystallized/dolomitized, destroying the original microstructure. Organics are not preserved in any of the fossil samples, providing no information about the microbial community that may have formed them. Despite a lack of detailed information about their origin, the fossil stromatolites do bear strong morphological similarities to the Storrs Lake knobs, providing a good basis for comparison.

Figure #53: Late Proterozoic fossil stromatolites from Mauritania, Africa

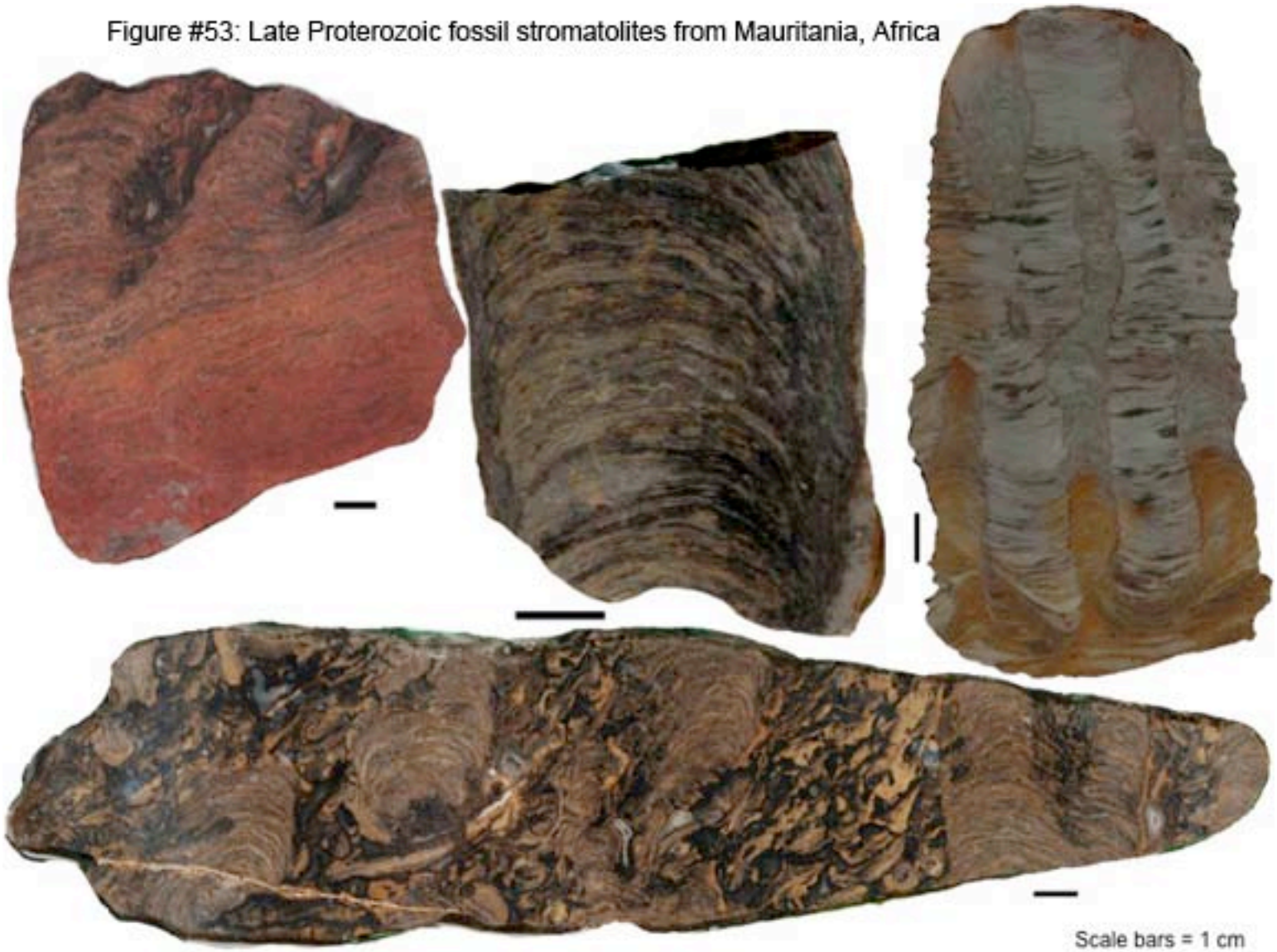

Scale bars = 1 cm

MICROBIAL ACTIVITY PROFILES

Microscopic observations were complemented with *in situ* measurements of microbial activity via microelectrode measurements. Depth profiles of [O_2] revealed distinct differences between the soft laminated microbial mat and the *Scytonema* knobs under similar light conditions.

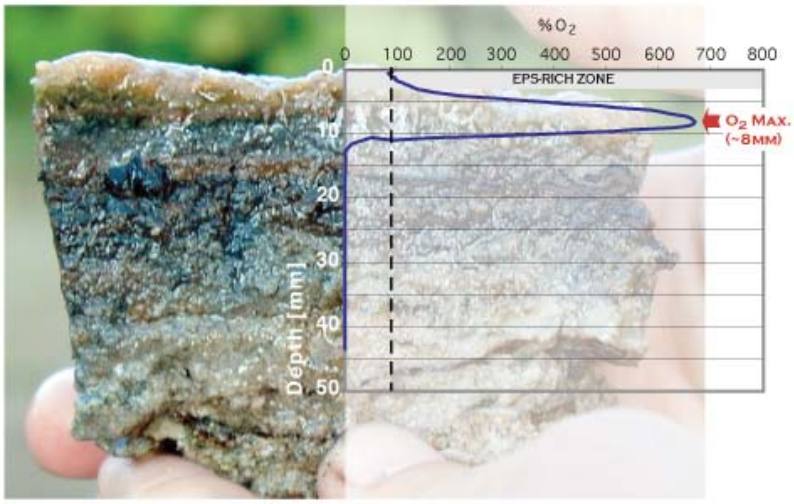

Figure #54a: Microbial Activity Profile of Soft Microbial Mat

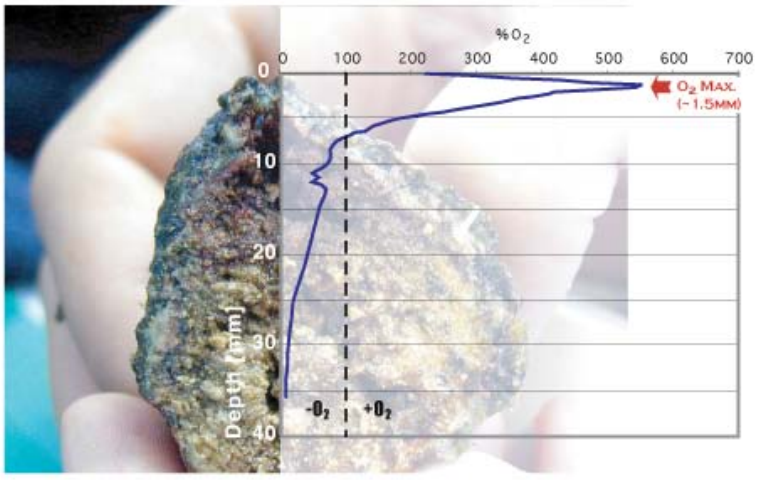

Figure #54b: Microbial Activity Profile of *Scytonema* Knob

Oxygen Profiles in Soft Microbial Mat

Within the first 3 mm of the soft mat, O_2 remains in equilibrium with the level measured in the water column (Figure #54a). This zone corresponds to a light brownish layer of empty sheaths of filamentous cyanobacteria, EPS and pigments. O_2 content rapidly increased around 5 mm depth and reached a maximum of 700% O_2-saturation at 8 mm depth. This peak in O_2 coincides with an intense green layer of cyanobacteria in the mat (Figure #54a) and results from a maximum of oxygenic metabolic activity. The O_2 profile dropped rapidly around 10 mm, and the mat became anoxic at ~12 mm.

Oxygen Profiles in *Scytonema* Knobs

O_2 profiles performed in the *Scytonema* knobs showed a maximum concentration higher in the knobs than in the soft mats (1.5 mm, Figure #54). The [O_2] doubled as the needle touched the surface of the knobs (Figure #54b), which indicates oxygenic photosynthetic activity within the green layer of *Scytonema* directly coating the surface of the knobs, with an oxygen concentration increasing to a depth of 1.5 mm. This first layer did not show signs of calcium carbonate precipitation and was not covered by a layer of empty filaments and EPS as observed in the soft mat. Below 1.5 mm into the knob surface, oxygen level rapidly decreased, and the deeper part of the knobs (at ~7 mm) start to became anoxic.

Comparison of Oxygen Profiles

In both cases, drastic increases and decreases of oxygen content within a few millimeters of depth indicate rapid O_2 production and consumption. The production is due to

oxygenic photosynthetic activity, and the consumption results from both aerobic respiration and reoxidation of sulfide (produced deeper in the mat by sulfate-reducing bacteria). Occasional interruptions of light input by cloud or artificial screening lead to a rapid-instantaneous collapse of [O_2], which indicates very high rates of O_2 consumption in both the soft mats and knobs. The boundary between oxic and anoxic environments is colonized by anoxygenic phototrophs (purple-sulfur bacteria) attested by red layers (Figure #54). These and also colorless sulfide-oxidizing chemolithotrophic bacteria (SOB) feed on sulfide produced by sulfate-reducing bacteria (SRB) in the lower anoxic environment. Chemolithotrophic bacteria that oxidize sulfide using O_2 are also situated in the oxic/anoxic transition zone and contribute to the rapid consumption of oxygen. The main difference between the soft mat and the stromatolitic knobs is the presence of a 3-4 mm thick brown organic-rich layer at the top of the soft mat, which does not show activity of oxygenic phototrophs.

HYDROCHEMISTRY OF STORRS LAKE'S SOUTHERN SECTOR

The following table (Table #5) shows the measured pH, salinity, and sampling temperature of each water sample, as well as the averaged results of ion chromatography analysis. This table also includes the alkalinity of Storrs Lake in the form of bicarbonate as determined by titration. "Storrs Lake 1" was taken at the shallow end (6 cm deep) of Transect 1 (See Figure #10), "Storrs Lake 2" was taken at the deeper end (18 cm deep) of Transect 1, "Storrs Lake 3" was taken at the deeper end (20 cm deep) of Transect 2, and "Storrs Lake 4" was taken at the shallow end (4 cm deep) of Transect 2.

For comparison, this table (Table #5) also includes the measured pH of sea water adjacent to Storrs Lake on San Salvador island's eastern shore, as well as the alkalinity of this sea water in the form of bicarbonate as determined by titration. The average temperature, salinity, and ion constituents of standard sea water have also been included in this table for comparison.

	Storrs Lake 1	**Storrs Lake 2**	**Storrs Lake 3**	**Storrs Lake 4**	**Sea Water**
pH	8.64	8.15	8.23	8.57	8.26
Sampling Temp. (°C)	43.2	40.9	36.0	41.2	28
Salinity (PSU)	63.3	59.4	58.1	65.1	35
Alkalinity (mg/L HCO_3^-)	803	803	803	803	141
Ca^{2+} (ppm)	528.35	690.03	711.46	716.40	416.00
Mg^{2+} (ppm)	6325.61	6732.84	6643.68	6159.74	1295.00
Na^+ (ppm)	26034.84	27232.98	27089.51	26105.27	10752.00
Cl^- (ppm)	45825.87	44957.43	41265.58	48151.65	19345.00
SO_4^{2-} (ppm)	6419.94	6237.56	5392.92	6763.09	2701.00
Br^- (ppm)	180.89	176.99	98.47	167.35	66.00
PO_4^{3-} (ppm)	331.05	360.60	408.87	386.85	390.00

Table #5: Hydrochemical Data Table

Considering the high salinity of Storrs Lake, the high concentrations of sodium and chloride found in the water samples are expected. Calcium concentrations are slightly lower than expected, especially in relation to the much higher magnesium concentrations found in the Storrs Lake samples. This could be due to the fact that calcium carbonate is being precipitated in the microbialite structures, which would explain the lower-than-expected levels dissolved in the water column. Even the precipitation of high-magnesium calcite would remove much more calcium ions than magnesium ions from the water column.

	Storrs Lake 1	Storrs Lake 2	Storrs Lake 3	Storrs Lake 4	Sea Water
SI Calcite	1.92	1.70	1.73	2.01	0.86
SI Aragonite	1.78	1.57	1.59	1.87	0.72
SI Dolomite	5.49	4.97	4.98	5.53	2.63
SI Gypsum	-0.58	-0.49	-0.51	-0.41	-0.65

Table #6: Saturation Indices

As shown in Table #6, Storrs Lake is supersaturated with respect to calcite, aragonite, and dolomite, and undersaturated with respect to gypsum. Thus, precipitation of calcite and aragonite is geochemically favorable (i.e., possible with or without the involvement of the microbial mats found in the lake). Storrs Lake is undersaturated with respect to gypsum, so dissolution of gypsum would be geochemically favorable.

The Dolomite Problem

While the saturation index is extremely high in Storrs Lake with respect to dolomite, as well as being high in sea water, primary dolomite rarely forms abiotically in nature (and is even nearly impossible to form at room temperature in the laboratory due to kinetic inhibition), but rather forms as a secondary replacement mineral of calcite or aragonite (Land, 1998; van Lith et al., 2003). Sulfate-reducing bacteria, however, can help to precipitate primary dolomite by increasing the pH and carbonate alkalinity, as well as by removing sulfate, which inhibits dolomite formation (van Lith et al., 2003). "Since sulfate occurs in seawater as a Mg^{2+}–SO_4^{2-} ion pair, its removal also increases the availability of "free" Mg^{2+} cations in the microenvironment around the cell for dolomite precipitation" (Konhauser, 2007; also see van Lith et al., 2003). Since sulfate-reducing bacteria are present in the stromatolitic structures of Storrs Lake (Paull et al., 1992), the

likelihood of primary dolomite precipitation is increased. However, the carbonate found in these stromatolites has been identified as high-magnesium calcite (Neumann et al., 1989), and no primary dolomite has been observed.

ORGANOMINERALIZATION PROCESS

Calcium Sequestration within the EPS Matrix

Acidic groups within the EPS matrix created by the microbial community can bind calcium and magnesium as part of biofilm formation, making the EPS stronger by cross-linking the EPS molecules (e.g. Dupraz et al., 2009). For example, carboxyl groups found in the EPS biofilm have a similar shape to a carbonate anion (Figure #55) (e.g. Dupraz et al., 2009). Therefore, the carboxyl groups in the biofilm can trap a large amount of calcium cations the same way that carbonate does (e.g. Dupraz et al., 2009). This initially inhibits the precipitation of calcium carbonate by removing calcium from the system (e.g. Dupraz et al., 2009) (Figure #56). Therefore, in order for calcium carbonate precipitation to occur, either the calcium binding must be stopped, or the bound calcium must be released.

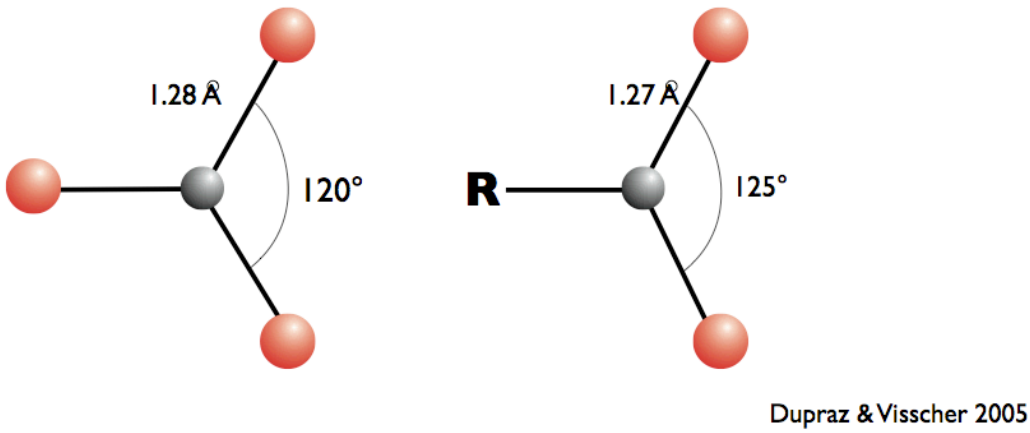

Figure #55: Similarity of CO_3^{2-} (left) to Carboyxl Group (right)

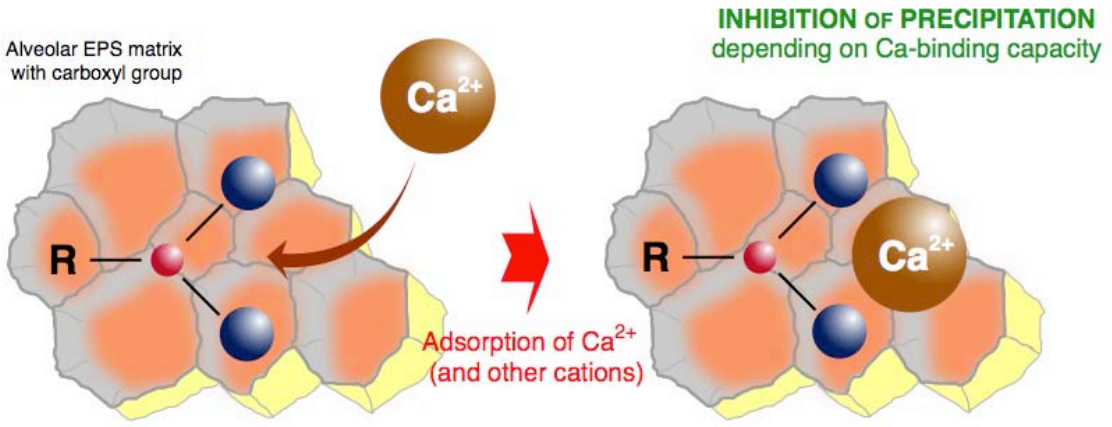

Figure #56: Ca-binding and inhibition of $CaCO_3$ precipitation by carboxyl groups in EPS matrix

Extrinsic Supersaturation of the Binding Capacity

A scenario under which calcium sequestration is stopped is an extrinsic supersaturation of the binding capacity of the EPS. The acidic groups will continue to sequester calcium within the EPS. However, if there is a continuous supply of calcium ions from the surrounding environment, the binding capacity of the acidic groups will eventually be reached, and free calcium ions from the surrounding environment will no longer be able to adsorb to them. The free calcium ions will then be available within the EPS, overcoming the inhibition of calcium carbonate precipitation (e.g. Dupraz et al., 2009) (Figure #57).

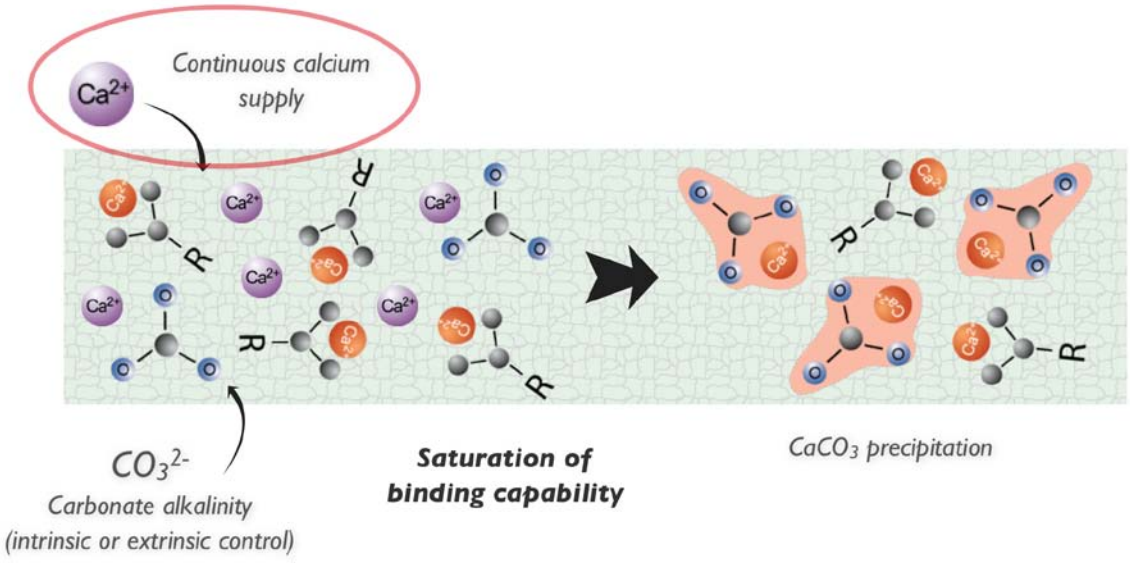

Figure #57: Extrinsic supersaturation of the binding capacity

EPS Degradation by Sulfate-Reducing Bacteria

The sequestered calcium can be released through the degradation of the EPS in which it is trapped. Heterotrophic metabolisms, such as sulfate reduction, can degrade the EPS. Sulfate-reducing bacteria (SRBs) are the terminal degraders of organic matter produced by cyanobacteria and other organisms and increase the carbonate alkalinity by bicarbonate formation leading to the following equation:

$$<2CH_2O> + SO_4^{2-} \rightarrow 2HCO_3^- + 2H_2S \quad (3)$$

(e.g. Patterson & Walter, 1994; Dupraz et al., 2009)

This degradation releases free calcium ions that were previously sequestered by the EPS/organic matter back into the surrounding environment, making them available for calcium carbonate precipitation (e.g. Dupraz et al., 2009). Chemical and physiochemical alternation of EPS (e.g. by oxygen radicals, UV and hydroxides) can lead to the same result of calcium release (Dupraz et al., 2009).

Alkalinity Engine

Once free calcium ions become available, calcium carbonate precipitation is no longer inhibited, and can occur if the carbonate alkalinity is increased, whether geochemically or through a microbially-driven "alkalinity engine" (e.g. Dupraz et al., 2009).

"Alkalinity has historically been defined as the number of equivalents of a strong acid required to neutralize 1 L of water at 20°C. The obtained end-point, corresponding to the second equivalence point of the carbonate system, was operationally defined and results were then commonly given as eq L^{-1}. The recent definition of alkalinity is based on the implementation of the Brønsted–Lowry concept of acids and bases by Rakestrow (1949) who defined alkalinity as the excess of bases (proton acceptors) over acids (proton donors)" (Reimer, 2011). "Total alkalinity is one of the few measurable quantities in natural waters that allows, together with other properties, to calculate concentrations of single species of the carbonate system such as CO_2, HCO_3^-, CO_3^{2-}, H^+, and OH^- (Wolf-Gladrow et al., 2007), and further on, the saturation state of the waters with respect to certain carbonate minerals. Therefore, alkalinity represents a hydrogeochemical key parameter for the understanding of carbonate precipitation, either biologically mediated or not, and its variation through the geological history" (Reimer, 2011). Total alkalinity can be expressed through the following equation:

$$TA \text{ (total alkalinity)} = [HCO_3^-] \text{ (bicarbonate)} + 2[CO_3^{2-}] + [B(OH)_4^-] \text{ (borate)} + [OH^-] - [H^+] \quad (8)$$

"where conceptually the right hand term can be divided up in carbonate alkalinity

(CA = $[HCO_3^-] + 2[CO_3^{2-}]$) as the most dominant contributor, (9)

borate alkalinity, and water alkalinity" (Reimer, 2011).

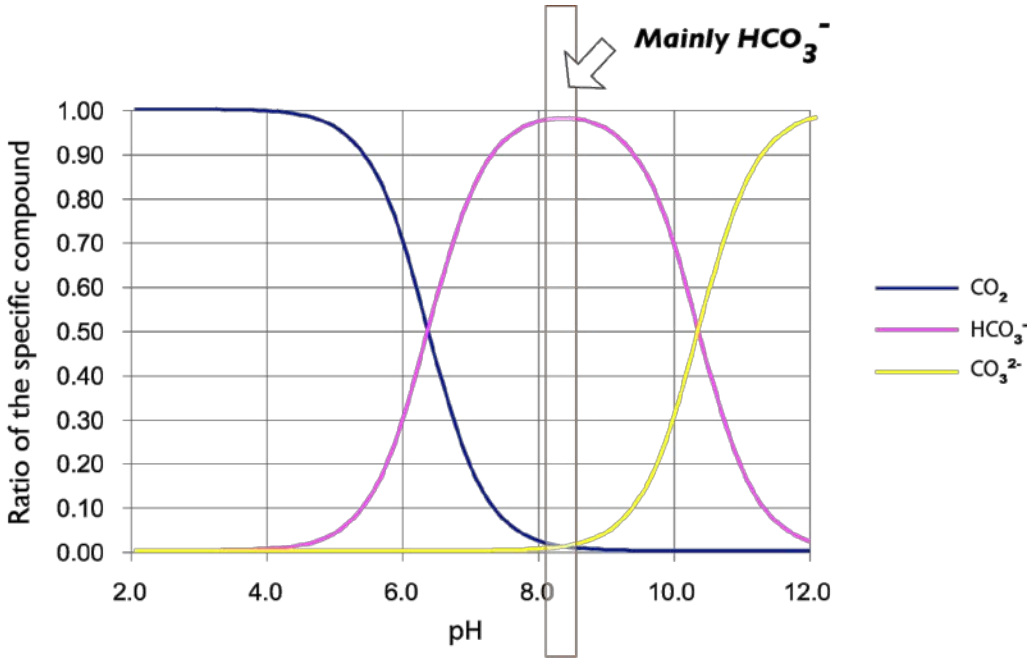

Figure #58: Carbon Speciation

The chemical species that dissolved inorganic carbon (DIC) takes in water is dependent on pH, as illustrated in Figure # 58 (Stumm & Morgan, 1996). Storrs Lake and seawater both have a pH averaging around 8, causing most of the carbonate alkalinity to be in the form of bicarbonate (Figure #58). Therefore, the environment surrounding the bacterial community in the stromatolitic knobs, whether it be water or EPS, will have a carbonate alkalinity that is mostly in the form of bicarbonate. In order for calcium carbonate to precipitate, the carbon species must be pushed from bicarbonate towards carbonate (Stumm & Morgan, 1996). Microbial metabolisms can cause this push.

Alkalinity Engine Driven by Cyanobacteria

The mechanism for organomineralization by cyanobacteria is typically thought to be related to photosynthetic uptake of carbon dioxide (e.g. Thompson et al., 1997; Freytet & Verrecchia, 1998; Merz-Preiß & Riding, 1999), driving an 'alkalinity engine.' The typical equation for photosynthesis is:

$CO_2 + H_2O + light$ ---> $<CH_2O> + O_2$ (Visscher & Stolz, 2005). (10)

However, the carbon species in Storrs Lake's average pH of ~8 is bicarbonate, not carbon dioxide. Since cyanobacteria need carbon dioxide for photosynthesis, but do not have direct access to it, some of these species are able to take in bicarbonate from the surrounding environment and convert it into CO_2 and OH^- ions using an enzyme called carbonic anhydrase (Badger, 2001). The CO_2 can then be used for photosynthesis to create organic matter (Figure #59). The remaining OH^- ions diffuse through the cyanobacterial sheath, locally increasing the carbonate alkalinity within the sheath (Figure #59) (shifting the carbon species toward CO_3^{2-}) (Figure #58) (Dupraz et al., 2011). The OH^- ions react with the bicarbonate in the surrounding environment, creating water and carbonate ions (Dupraz et al., 2011). This should allow carbonate ions to combine with any available free Ca^{2+} and Mg^{2+} ions diffused from the surrounding environment (water or EPS), precipitating high-Mg calcium carbonate, and when the cyanobacteria use CO_2, the bicarbonate is converted to CO_2 and OH^- to reestablish the carbonate equilibrium (Dupraz et al., 2009). Precipitation driven by this mechanism should occur within the cyanobacterial sheaths (Figure #59) (Dupraz et al., 2009).

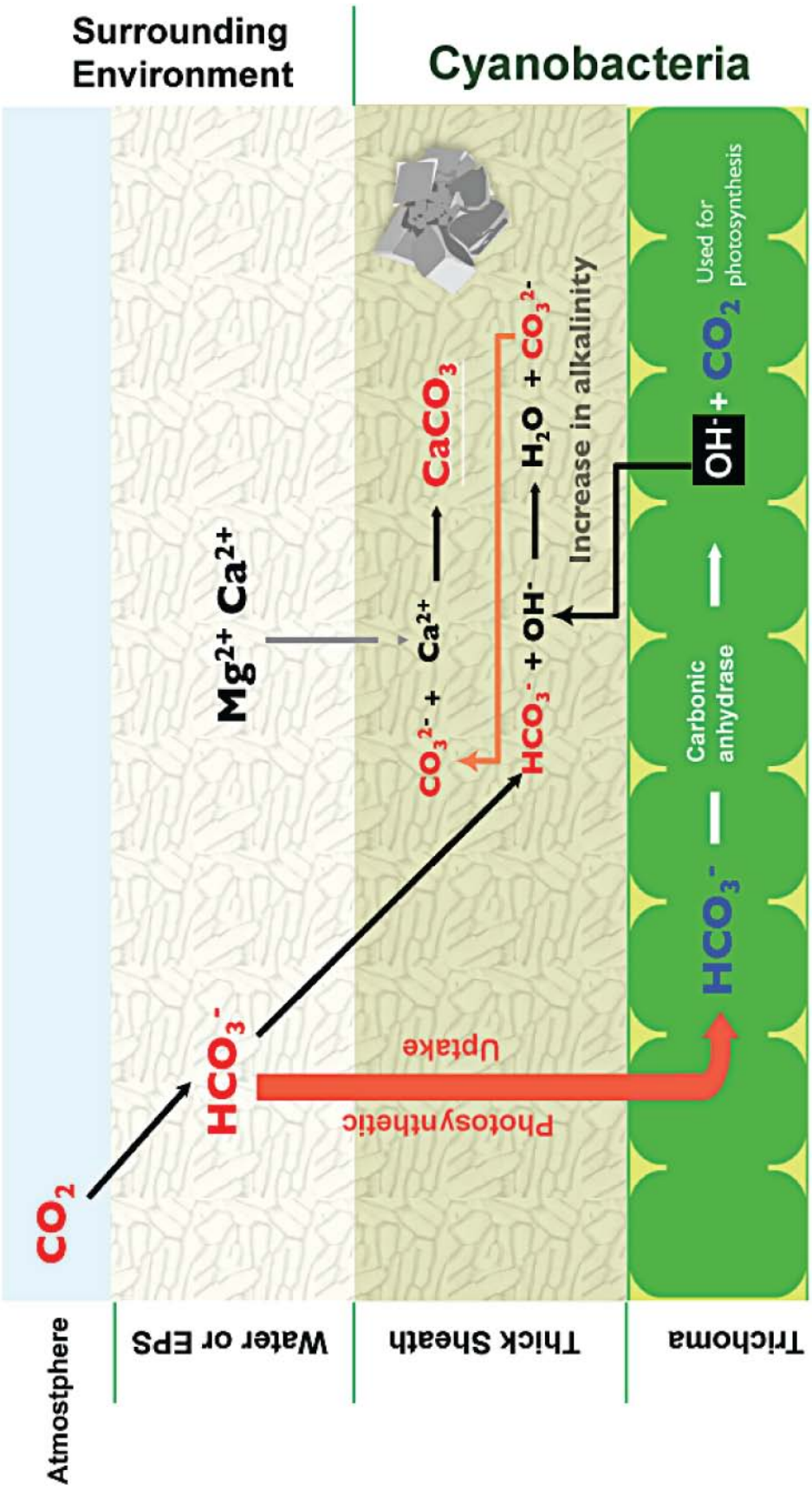

Figure #59: Photosynthetic Alkalinity Engine

Cryofixation SEM analysis, however, shows precipitation *surrounding* the sheaths, with no instances of precipitation *within* the sheaths (Figures #50 a & b). Following this observation, the mode of precipitation by cyanobacteria in Storrs Lake's stromatolitic *Scytonema* knobs is closer to the one described in microbialites in Eleuthera, Bahamas (Dupraz et al., 2004) and to some extent, to the one observed in open marine microbialites in Highborne Cay (e.g., Reid et al., 2000, 2003b). Instead of precipitation occurring within the cyanobacterial sheath, calcium carbonate precipitation progressively replaces the polygonal EPS matrix created by the bacterial community, embedding the filamentous and coccoid bacteria. Within the EPS matrix, precipitation can occur once the Ca-binding capacity is reached and the carbon species is pushed to carbonate (Dupraz et al., 2009). Carbonate anions will bond to free calcium cations in the EPS and/or adsorb to calcium ions that are bound within the acidic groups (Dupraz et al., 2009). This process is controlled extrinsically by the saturation index of carbonate minerals (Table #6), such as calcite and aragonite, which are supersaturated in Storrs Lake (Dupraz et al., 2009).

Alkalinity Engine Driven by Sulfate-Reducing Bacteria (SRB)

Sulfate-reducing bacteria (SRBs) degrade the organic matter created by the cyanobacteria and other organisms and produce bicarbonate through the following equation:

$<2CH_2O> + SO_4^{2-} \rightarrow 2HCO_3^- + 2H_2S$ (Patterson & Walter, 1994) (3)

The organic matter is partially composed of low molecular weight organic acids (LMWOA) (e.g. lactate, acetate), which are strong acids (Dupraz et al., 2009). The

degradation by SRB converts the LMWOA into CO_2, changing the strong acid into a weak acid (Dupraz et al., 2009). This drives the pH of the surrounding environment up, pushing the carbon species (i.e. bicarbonate) toward carbonate (Dupraz et al., 2009). Furthermore, the metabolic reaction for SRB shown above, indicates that per sulfate used, two bicarbonates are produced. As such, SRB increase the carbonate alkalinity of their immediate environment.

The carbonate can bond with free calcium and magnesium ions that are released from the EPS/organic matter during degradation to precipitate high-Mg calcium carbonate (Dupraz et al., 2009). This mechanism of EPS degradation and precipitation could explain the micropeloidal structures found within Storrs Lake's stromatolitic knobs, as the vacuolar framework of the EPS is destroyed through degradation and replaced by calcium carbonate precipitation.

Mineralogy

The mineralogy of the precipitated calcium carbonate in the Storrs Lake stromatolitic knobs, as determined by x-ray diffraction, consists of a solid solution of high-Mg calcite with 12 to 17 mole % Mg^{2+} substituting for Ca^{2+}. Neither low-Mg calcite nor calcite were found. EDS semi-quantitative measurements on micrite and crystals indicate a very small and apparently random variation in the Mg/Ca ratio in the calcite, which indicates a stable mineralogy in the range of high-Mg calcite.

Organomineralization

The micrite that is precipitated around the filamentous cyanobacteria is in turn surrounded by microsparite, then sparite (5-20 μm) in the majority of *Scytonema* stromatolitic knob thin sections, as well as in some *Dichothrix* thrombolitic knob thin sections. Fluorescence microscopy reveals brighter color in the micrite surrounding the *Scytonema* filaments, indicating that this micrite is associated with organic matter and is likely the result of organomineralization by the filamentous cyanobacteria. The surrounding microsparite/sparite is darker, indicating less association with organic matter. The microsparite/sparite may result from recrystallization of the micrite, or simply from the natural progression of precipitation as the organomineralized calcite becomes a nucleus for geochemical precipitation (Figure #60). This pattern of growing precipitation indicates that the cyanobacterial filaments are a nucleus for the precipitation, and that the cyanobacteria may be responsible for the precipitation through photosynthesis and the alkalinity engine. Micropeloidal structures, which are common in the stromatolitic knob thin sections, are likely associated with EPS degradation, and also appear to serve as nuclei for this microsparite/sparite progression of precipitation.

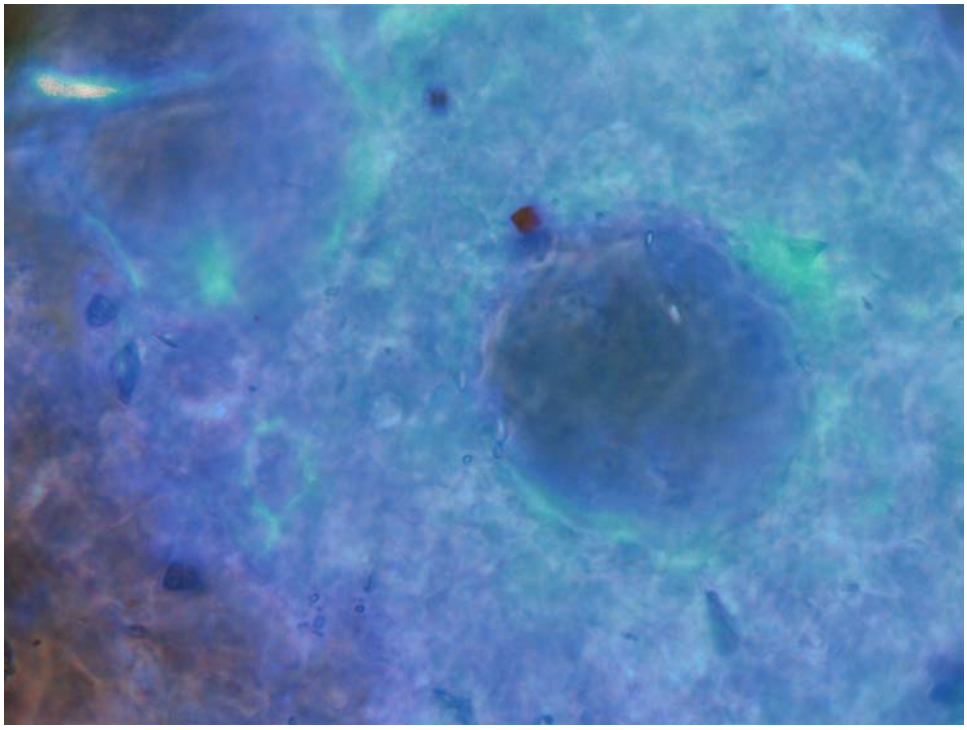

Figure #60: Fluoresent micrograph of *Scytonema* knob showing bright micrite and darker sparite

ISOTOPIC ANALYSES

Isotopic analysis can provide insights into the type of microbial metabolism that is responsible for the organomineralization that forms microbialites.

Stable Carbon Isotopes

For further characterization of calcium carbonate precipitation, the $\delta^{13}C$ ratios of the small stromatolitic knobs and the Pleistocene bedrock were studied (Figure #61). Carbon has two stable isotopes, ^{12}C, which is lighter, and ^{13}C, which is heavier. Biological processes have an affinity for lighter isotopes, so microbial metabolisms tend to take up ^{12}C, leaving the surrounding inorganic carbon reservoir enriched in ^{13}C as the ^{12}C is

depleted by the organisms. The $\delta^{13}C$ ratio will be negative in biomass enriched in ^{12}C, relative to the surrounding environment, which will be depleted in ^{12}C (enriched in ^{13}C).

Isotopic Carbon Signatures of Precipitation through Photosynthesis

Cyanobacteria take up ^{12}C as they create organic matter through photosynthesis, leaving the surrounding environment with a more positive $\delta^{13}C$ ratio. The alkalinity engine results in an increase in the local carbonate alkalinity through OH^- ion diffusion. If free Ca^{2+} ions are available, calcium carbonate will be precipitated in the surrounding, ^{13}C-enriched environment, causing the precipitated calcium carbonate to have a strong positive $\delta^{13}C$ ratio (Merz-Preiß, 1992). However, caution needs to be taken in the interpretation of the carbon isotopic signature: the very high rates of cyanobacterial photosynthesis that is typical for mats rapidly depletes the inorganic carbon pool, particularly the ^{12}C fraction. As such, one may expect a less pronounced effect of the isotope fractionation under these inorganic carbon-limiting conditions.

Isotopic Carbon Signatures of Precipitation through EPS Degradation by Sulfate-Reducing Bacteria

Sulfate-reducing bacteria (SRBs) degrade the organic matter created by the cyanobacteria and other organisms, and produce bicarbonate through the following equation:

$$<2CH_2O> + SO_4^{2-} \dashrightarrow 2HCO_3^- + 2H_2S \quad (3)$$

(Patterson & Walter, 1994)

Because the organic matter has a negative $\delta^{13}C$ ratio, the bicarbonate produced by the SRBs will also have a negative $\delta^{13}C$ ratio. When the pH increases due to the conversion

of LMWOA to CO_2, the negative $\delta^{13}C$ bicarbonate is pushed toward carbonate. Since the original source of the carbonate was the EPS/organic matter, which already had a negative $\delta^{13}C$ ratio, the calcium carbonate will have a strong negative $\delta^{13}C$ ratio (Patterson & Walter, 1994).

Isotopic Carbon Signatures of Stromatolitic Knobs in Storrs Lake

If photosynthesis was solely, or primarily responsible for the calcium carbonate precipitation in the stromatolitic *Scytonema* knobs of Storrs Lake, the calcium carbonate would have a strong positive $\delta^{13}C$ ratio (Merz-Preiß, 1992). If EPS degradation by sulfate-reducing bacteria was solely or primarily responsible for the calcium carbonate precipitation, the calcium carbonate would have a strong negative $\delta^{13}C$ ratio (Patterson & Walter, 1994). It is possible that if both photosynthesis and sulfate-reduction were working in tandem to facilitate calcium carbonate precipitation in the stromatolitic knobs, the calcium carbonate would show a mixed $\delta^{13}C$ signal, neither strongly positive nor strongly negative (Figure #61), but again, the isotopic data must be interpreted cautiously in inorganic carbon-limiting conditions.

Samples taken at the base, middle, and top of the stromatolitic knobs present slightly positive $\delta^{13}C$ ratios, as do the Pleistocene bedrock below the knobs and the larger, subfossil stromatolitic heads in the deeper portion and northern sector of Storrs Lake (Figure #61). The calcium carbonate at the top of the stromatolitic knobs has a $\delta^{13}C$ ratio of approximately +3, with the center of the knobs approaching +2 $\delta^{13}C$, and the base of

the knobs approaching +1.5 $\delta^{13}C$. The Pleistocene bedrock and subfossil stromatolite heads both have a value of +1.5 $\delta^{13}C$.

The slightly positive values of the stromatolitic knobs indicate that the precipitation is microbially mediated, and that the photosynthetically driven alkalinity engine is important for calcium carbonate precipitation. However, if photosynthesis was the sole driver of calcium carbonate precipitation, a stronger positive signal would be expected. It is possible that EPS degradation by SRBs is creating a negative signal that is canceling some of the signal for photosynthesis. This indicates that photosynthesis has a stronger influence on precipitation in the Storrs Lake knobs, but EPS degradation by heterotrophic metabolisms is also an important factor for organomineralization.

Samples from other hypersaline Bahamian field sites, such as Big Pond and Salt Pan on Eleuthera island, all show negative $\delta^{13}C$ ratios (Figure #61), indicating that EPS degradation is the more important factor in calcium carbonate precipitation in these samples (Dupraz et al., 2004; Glunk et al., 2011).

Oxygen Isotope Analysis

$\delta^{18}O$ values were also obtained on the Storrs Lake samples. Both Storrs Lake and other hypersaline Bahamian sites show positive $\delta^{18}O$ values, indicating that these hypersaline environments all have evaporitic conditions, unlike standard sea water, which displays negative $\delta^{18}O$ values (Figure #61).

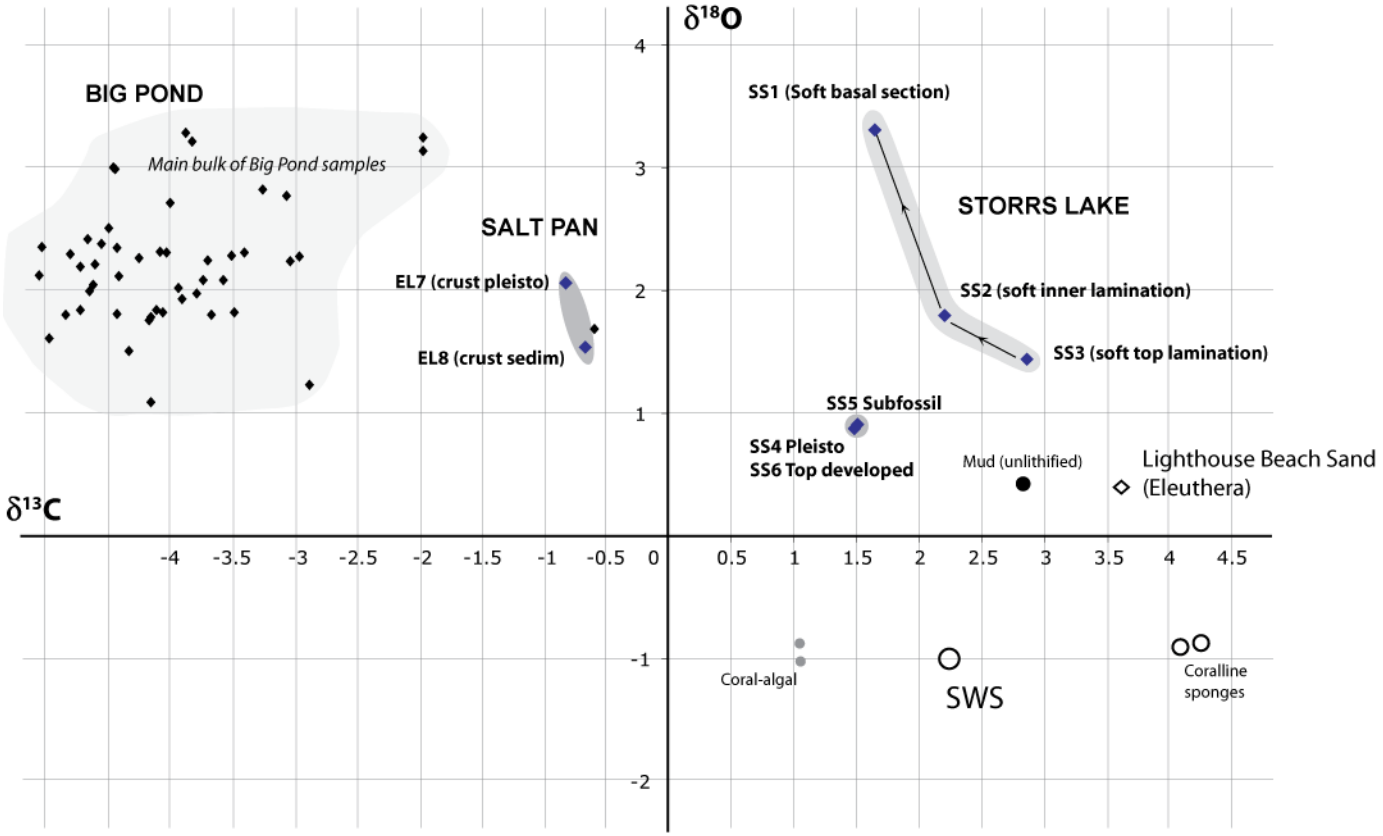

Key:
EL: Eleuthera samples
SS: San Salvador (Storrs Lake samples)
SWS: Sea Water Standard

Figure #61: Isotopic Carbon and Oxygen Data from Storrs Lake, Salt Pan, Big Pond, and Sea Water. Adapted from Dupraz et al., 2004 and Glunk et al., 2011.

LAMINATION

In addition to determining the mechanism for organomineralization in the stromatolitic knobs of Storrs Lake, it is important to determine why the precipitation is organized into layers. The mechanism by which the lamination is formed in the stromatolitic knobs is not fully understood, as there are so many biological and environmental parameters involved.

Alternation of Cyanobacterial Filaments

One of the biological parameters that could provide a possible explanation for the lamination is alternating growth orientations of the *Scytonema* filaments that precipitate the micrite. Filamentous cyanobacteria tend to actively grow their trichomes upwards, with vertical filaments, during warmer temperatures in the spring and summer (Pentecost & Whitton, 2000). In colder winter temperatures, the trichomes grow slower, or not at all, and the filaments lay horizontally (Pentecost & Whitton, 2000). This allows the cyanobacteria to have more surface area to collect sunlight for photosynthesis during the winter when sunlight is less direct and water depth is greater (Pentecost & Whitton, 2000; Monty, 1976). In the summer, when the water is more shallow and the sunlight more direct, a vertical orientation provides sufficient surface area to obtain enough sunlight for photosynthesis without overexposure to the sun (Pentecost & Whitton, 2000, Monty, 1976). These alternating growth orientations within a stromatolite can be described by two main stages (Figure #62): '*Stage 1*' is dominated by a vertical growth orientation of the filaments, high porosity, and little calcium carbonate precipitation, although trapped grains and small patches of micropeloidal micrite (~40 μm in diameter) may be found

along the vertical filaments (Figure #62) (Dupraz et al., 2006). '*Stage 2*' is dominated by horizontally oriented filaments that are associated with a considerable amount of dense micrite (Figure #62) (Dupraz et al., 2006).

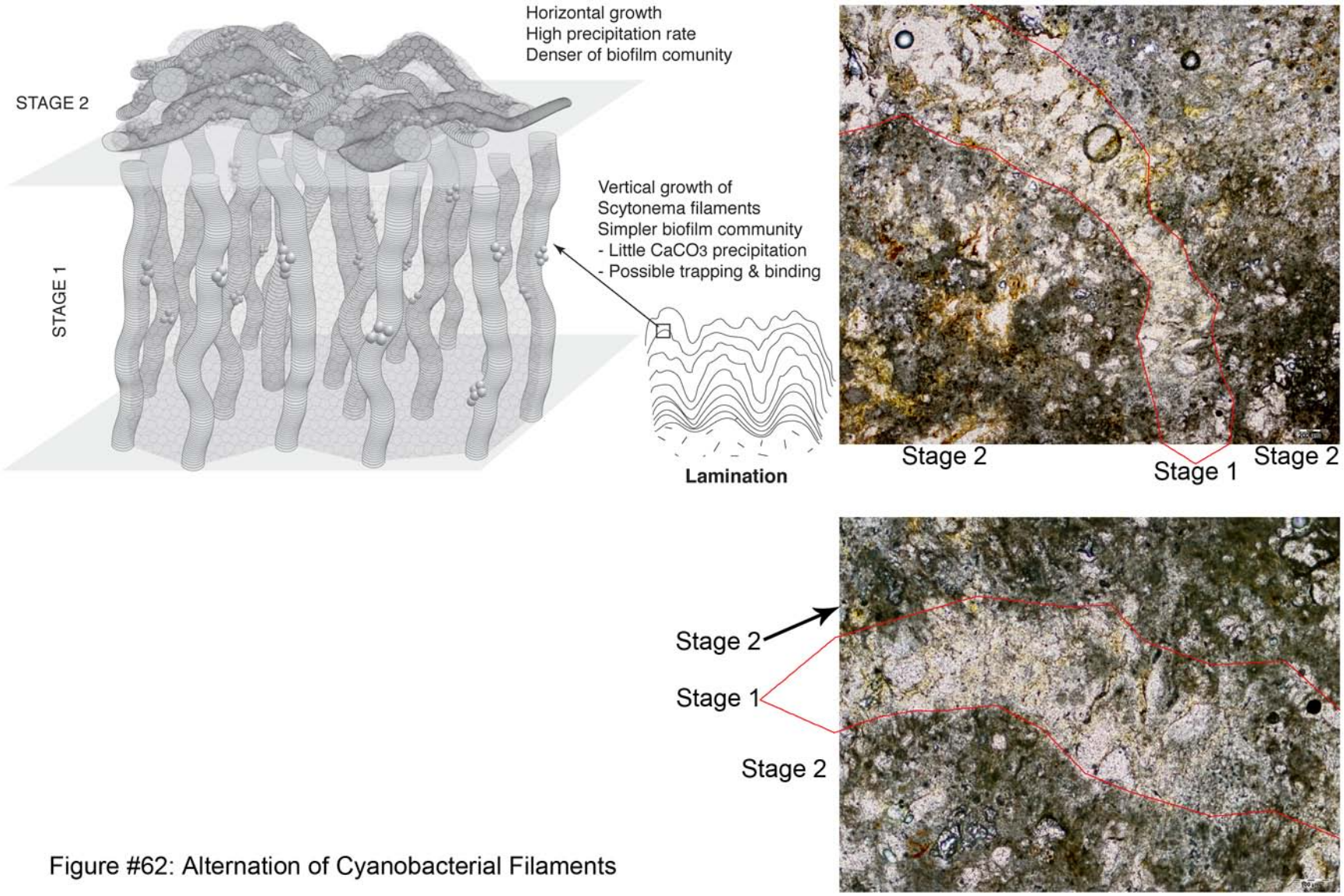

Figure #62: Alternation of Cyanobacterial Filaments

The differences between the two stages are emphasized with fluorescence microscopy, in which organic matter appears bright yellow, calcium carbonate appears green, and areas of porosity (filled with epoxy in thin section) appears red. Patches of yellowish green color are observed in *'Stage 2,'* indicating a close relationship between the organic matter and the calcium carbonate precipitation (Figure #63).

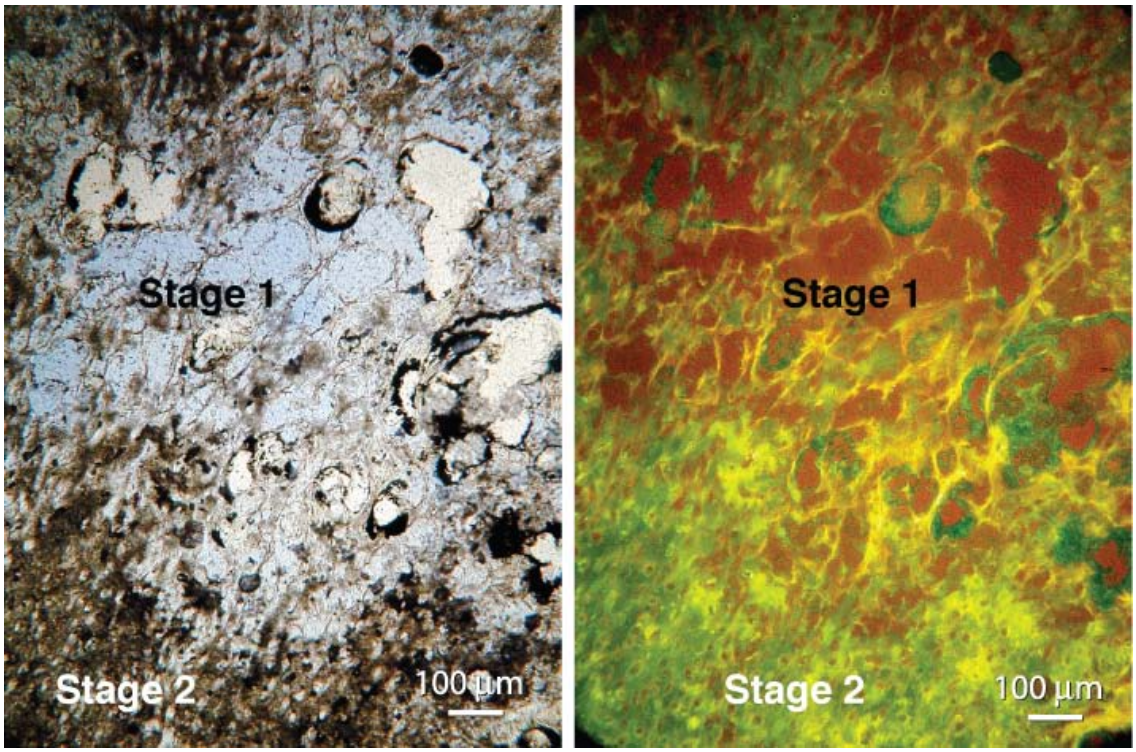

Figure #63: Fluorescence microscopy highlighting filament orientation stages

In some thin sections, this pattern of alternating filament orientation can be observed as small, round holes in the dense micrite where horizontal filaments were cut perpendicularly, and more elongated holes, with little surrounding them, where vertical filaments create porosity between the micritic layers. However, this pattern is only visible when the *Scytonema* knob samples are cut perpendicularly through the middle of

the *Scytonema* knobs. Depending on the orientation of the cuts made during thin section preparation, horizontal filaments may appear elongate and vertical filaments may appear small and round (Figure #64).

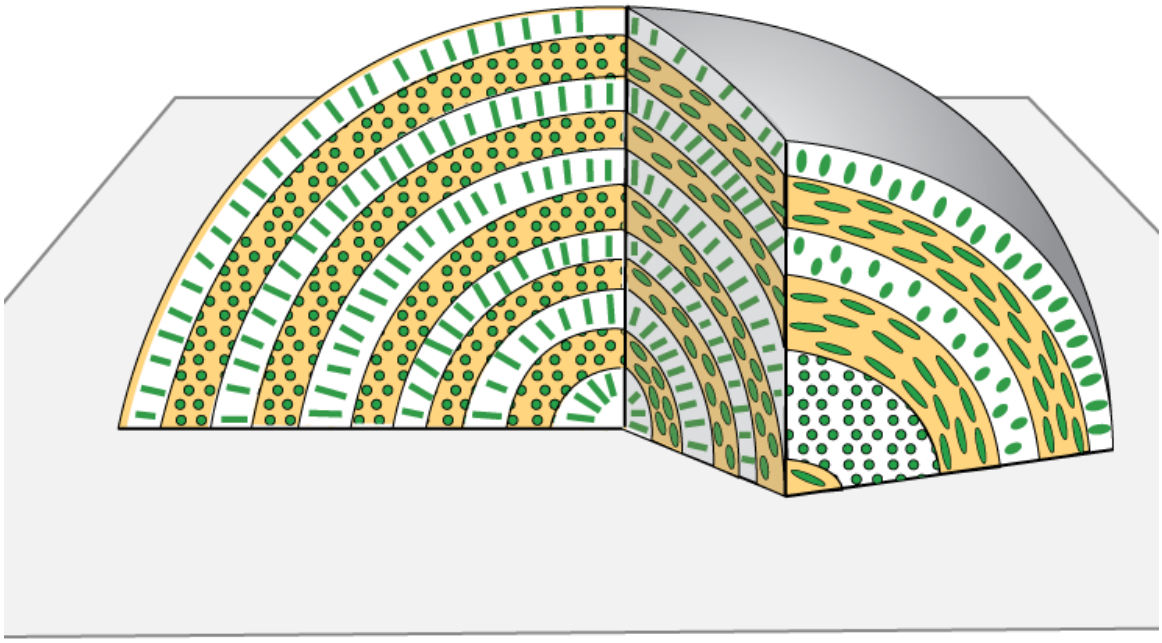

Figure #64: Illustration of filament orientations after sample-cutting

Although it cannot always be observed directly in thin section, the two-stage alternating filament pattern can be demonstrated with computer modeling (Figure #65) (Dupraz et al., 2006). When the orientation of the filaments is the only changing parameter, the modeling is consistent with porosity and little precipitation in association with vertically oriented filaments, and dense precipitation associated with horizontally oriented filaments (Dupraz et al., 2006). In this model, the precipitation rate remains consistent, but the precipitation is compressed into dense layers when filaments are horizontal, and sparse and spread out when filaments are vertical (Dupraz et al., 2006). It is possible that the laminations in the Storrs Lake knob result from a mechanism similar to this simple

model, but the formation of laminae is likely due to a combination of this mechanism and other environmental and microbial parameters.

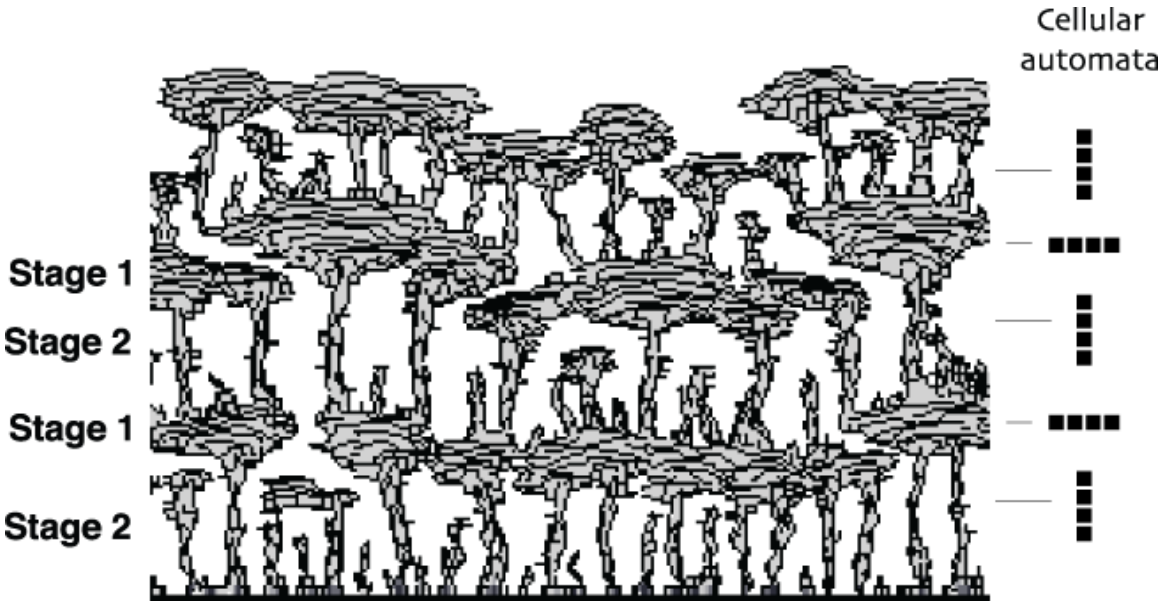

Figure #65: Modeling of laminae formation changing only filament orientations. (Dupraz et al., 2006)

DISCUSSION

Microbialites provide a quintessential example of the link between the geologic and biologic elements of the global carbon cycle, and those of Storrs Lake could provide insights into both modern and fossil microbialites. Storrs Lake is a hypersaline lake that is supersaturated with respect to calcite and aragonite. It should therefore be possible to have carbonate precipitation occur throughout the lake without the influence of microbial metabolism. However, the massive amounts of organic matter created by cyanobacterial photosynthesis in this lake inhibit purely geochemical precipitation by sequestering calcium and magnesium. Carbonate precipitation is instead limited to microbialite structures of differing morphologies in specific zones of the lake: exposed thrombolites

on the shoreline and submerged stromatolites that get progressively larger deeper into the lake.

ZONE FORMATION

Water depth is clearly a key factor in the transition from thrombolitic to distinctly stromatolitic fabrics, as well as in the increasing size of the microbialites along the two Storrs Lake southern sector transects. Depth could play a direct role in this morphological transition, or it could play an indirect role through other environmental factors that change with depth, such as temperature, salinity, and light penetration.

The clotted mesostructure of the thrombolitic *Dichothrix* knobs could be part of the microbial community's strategy for surviving desiccation during the dry season, whereas the stromatolitic *Scytonema* knobs are restricted to a depth where they are submerged year round. As the stromatolitic knobs continue to grow, however, they will eventually become too tall for their own survival, as they will no longer be fully submerged. Once they reach that point, it is likely that the microbial community at the top of the knobs will become inactive, and diagenesis will likely begin to occur. This is supported by the subfossil, inactive status of the larger stromatolitic heads in the deeper and northern portions of Storrs Lake.

HYDROCHEMISTRY

Storrs Lake has a relatively low Ca^{2+} concentration in the water column and a high magnesium to calcium ratio. Both are sequestered by EPS, but more calcium than

magnesium ions are taken up by precipitation, even though the carbonate is in the form of high-Mg calcite.

The lake also has a high concentration of sulfate, allowing sulfate reducers to have highly active metabolisms. This would allow them to actively degrade EPS/organic matter, freeing sequestered calcium and magnesium.

ORGANOMINERALIZATION

Calcium sequestration can be overcome by the extrinsic supersaturation of the binding capacity of acidic groups within the EPS, and then precipitation can occur when the pH increases and drives the carbon species towards carbonate. However, this mechanism is further complicated by the fact that different acidic groups protonate at different pH values, meaning that the binding capacity can also change with pH (Braissant et al., 2007). While an increase in pH will favor precipitation due to the shift in carbon species, it can also cause the acidic groups to deprotonate (release H^+), which would open those sites to bind calcium. If the pH increase is slight, this increase in the binding capacity can counteract the push toward carbonate, and the saturation index will not increase (Dupraz et al., 2009). This effect is especially strong in environments where photosynthesis dominates precipitation through the alkalinity engine. When sulfate-reducing metabolisms work in tandem with photosynthesis, it can help to overcome this problem by degrading the EPS and releasing the calcium.

The carbon species can be driven towards carbonate through the alkalinity engine. However, a purely photosynthetic alkalinity engine should result in carbonate precipitation within the cyanobacterial sheaths, and cryo SEM shows that this is not the case in the Storrs Lake knobs. The cyanobacteria appear to be a nucleation site for precipitation within the EPS matrix, but precipitation is not occurring inside the sheaths. Precipitation through a purely photosynthetic alkalinity engine would also result in calcium carbonate with a strong positive $\delta^{13}C$ ratio. While the calcium carbonate in the stromatolitic knobs does yield a positive $\delta^{13}C$ ratio, the signal is weaker than would be expected for photosynthesis to be the sole factor.

Investigations performed on Bahamian open-marine stromatolites developing in normal salinity (e.g. Reid et al., 1995; Dravis,1983; Dill et al., 1986) have emphasized the central role played by the microbial community succession at the top of the build-ups (Reid et al., 2000). Although cyanobacteria remain the most important organic carbon providers in the microbial mat associated with the Bahamian open-marine stromatolites, uptake of CO_2 linked to cyanobacterial photosynthesis is not the sole mechanism that promotes $CaCO_3$ precipitation. SRB associated with EPS degradation are thought to be co-responsible for aragonite precipitation and laminae formation in Highborne Cay stromatolites (Visscher et al., 2000).

Precipitation outside within the EPS, rather than within the cyanobacterial sheaths, indicates that the EPS matrix plays an important role in the precipitation of calcium carbonate. Precipitation also nucleates on the vacuole walls of the EPS matrix. Given

the weakly positive isotopic signals, it is likely that photosynthesis is a driving force behind calcium carbonate precipitation within the stromatolitic knobs, but is not sufficient to fully explain the precipitation, just as it is insufficient in the open-marine stromatolites. SRB associated with EPS degradation could be working in tandem with photosynthesis by cyanobacteria in driving calcium carbonate precipitation, just as sulfate-reducers are thought to be responsible for precipitation in the Highborne Cay stromatolites. In addition, SRB are not the sole degraders of organic carbon and often rely on partial degradation of complex organic molecules by aerobic heterotrophs. This may influence the carbon isotope signature as well.

If EPS degradation by SRB was solely responsible for calcium carbonate precipitation, the carbonate would have a strong negative $\delta^{13}C$ ratio. Since the carbonate in the Storrs Lake knobs shows a weakly positive $\delta^{13}C$ ratio, EPS degradation cannot be the only driving force for precipitation. However, the weakly positive $\delta^{13}C$ ratio could be the result of a mixed signal, with the strong positive value by photosynthesis being reduced by the strong negative value by EPS degradation. This is further supported by the decreasing positive value further down into the knobs. The $\delta^{13}C$ ratio is slightly higher (~+3 $\delta^{13}C$) towards the top of the knobs, where photosynthesis is the most active, and decreases gradually to +1.5 $\delta^{13}C$ towards the bottom of the knobs where photosynthesis is less active and sulfate-reduction would be more dominant. This would support the idea that the calcium carbonate precipitation is the result of both photosynthesis and EPS degradation working together. Cryo SEM images showing the replacement of the EPS matrix by micropeloidal structures demonstrate that EPS degradation is occurring in the

Storrs Lake knobs. These images also show nanospherolite nucleation within the vacuolar structure of the EPS, providing strong evidence that both types of precipitation are occurring at the same time. It is simply a question of whether both forms are highly significant, if one form is highly dominant over the other, or if even more is involved in driving the precipitation.

In order to make a stronger case for the hypothesis that both photosynthesis and EPS degradation are significant drivers of calcium carbonate precipitation, further isotopic analysis is needed to obtain the $\delta^{13}C$ ratio of the reservoir surrounding the knobs, as well as a strong database for the microenvironments within the knobs. It may be that precipitation is always driven by both cyanobacterial and SRB metabolisms (and, as outlined above, possibly additional heterotrophic metabolisms), or alternative microbial metabolisms could be important for calcium carbonate precipitation at different times of the year, or even diurnally (e.g. methanogenesis; Visscher et al., 2010. For example, the photosynthetically driven alkalinity engine may dominate during the day, and EPS degradation by sulfate-reducers may become the dominant driver of precipitation at night when photosynthesis is not occurring. Photosynthesis may also be less dominant in the winter when sunlight is less direct and light penetration is lower due to an increase in water depth. Geochemical precipitation could also become more dominant in the summer when evaporation increases.

It is clear that microbially-driven calcium carbonate precipitation is a complex process. This process is complicated even further by the fact that Storrs Lake is supersaturated

with respect to calcite and aragonite, and therefore some precipitation may be simply geochemical precipitation, with the knobs acting as a nucleation site. This could be the case with the carbonate caps on the tops of some of the taller stromatolitic knobs that breached the surface of the soft microbial mat by several centimeters. In thin section, these caps had fewer laminations, and were mostly composed of sparite, rather than beginning as micrite and gradually growing to sparite. These caps could represent a particularly dry season when evaporation led to dense geochemical precipitation with the knobs acting as a nucleation site. It is also possible that the microbial community has less of a role in the creation of the knobs once they breach the soft microbial mat surface.

LAMINAE FORMATION

To further understand the organomineralization process, a mechanism for the formation of lamination in the stromatolitic knobs is needed. The seasonal alternation of cyanobacterial filaments between vertical and horizontal orientations seems to be closely associated with the formation of these laminae. It could be that the alternating orientation pattern is directly responsible for creating the lamination. However, it is also possible that seasonal variability results in a number of parameter shifts that lead to the lamination, and the alternating filaments are simply one of several elements involved in laminae formation. For example, in the winter, when filaments are horizontally oriented, the microbial community is more dense, there is less sunlight, and there is more rainfall. The increase in rainfall leads to an increase in water level, and therefore a decrease in light penetration, a decrease in salinity, and a decrease in the concentrations of all other hydrochemical constituents.

It is possible that the microbial community induces/influences the same rate of calcium carbonate precipitation year-round, but the layers become more dense in the winter when the microbial community is more compact. Computer modeling wherein filament orientations are the only changing parameter, and precipitation rates remain consistent, supports this possibility (Dupraz et al., 2006). It is possible, however, that carbonate precipitation rates do vary with season. For example, with lower light levels in the winter, EPS may not be needed for sun protection, and may be less actively produced. This would mean that less calcium and magnesium would be sequestered in the winter, allowing the denser layers of precipitation. In addition, if EPS is less actively produced in the winter, the rate of degradation by SRB may outweigh EPS production. In a more compressed microbial community, element cycling is also condensed, so the recycling capability is higher, allowing for an increase in EPS turnover. More rapid EPS turnover in the winter would free even more calcium and magnesium for carbonate precipitation.

Given that $\delta^{13}C$ ratios show photosynthesis to be the more dominant metabolism for controlling precipitation in Storrs Lake, it is likely that purely environmental seasonal changes are not in control of the formation of laminae. If this were the case, it would be expected that denser precipitation would occur in the summer when the cyanobacteria would have more access to sunlight. Since the opposite effect is observed in the stromatolitic knobs, it is likely that the filament orientations do have a strong control over lamination, and computer modeling strongly supports this hypothesis (Dupraz et al., 2006).

Other Effects on Lamination

Even though it is likely that laminae formation is related to seasonality, the laminations cannot be used for age-dating in a manner similar to dendrochronology. Although general seasonal conditions are predictable, the environmental and microbial conditions will not be exactly the same each season, and thus their effects on precipitation will vary, if only slightly. If there is a particularly dry summer, for example, there may be more geochemical precipitation using the stromatolitic knobs as a nucleation site due to increased evaporation. An anomalously dry summer could also potentially expose some of the taller stromatolitic knobs, inhibiting precipitation, and potentially damaging the microbial community which may take some time to recover.

Storm events can increase wave energy, potentially causing breakage to some weaker portions of the knobs. Severe storm events, such as hurricanes, can result in drastic changes to the lake, potentially burying some of the stromatolitic knobs completely in sediment, leaving the knobs to either start over, be taken over by a different microbial community, or cease microbialite formation all together. If enough sedimentation occurs in an extremely severe storm event, the lake could even be temporarily drained. Storm events can affect different portions of the lake more strongly than others, having an uneven effect on the knobs throughout the lake.

Stromatolitic knobs that have breached the top of the soft mat are vulnerable to the formation of algal build-ups on top of the knobs. This can cause damage to the top of the

knobs as some eukaryotes can bore into the carbonate layers or locally induce dissolution (Dupraz et al., 2009).

While calcium carbonate precipitation is highly geochemically favored in Storrs Lake, it is possible that some dissolution occurs at various times, particularly at night, within the microenvironments at the top of the stromatolitic knobs. Metabolisms such as fermentation $H_2O + <3CH_2O> + CaCO_3 ---> 2HCO_3^- + <C_2H_6O> + Ca^{2+}$ (11) may induce some calcium carbonate dissolution at the top of the knobs (Dupraz et al., 2009). These metabolisms thrive at night when photosynthesis and other oxygenic metabolisms become inactive (Dupraz et al., 2009).

These variations make it impossible to date the knobs based on the growth of laminations. Carbon-dating, using the unstable (radioactive) isotope of carbon, ^{14}C, would provide a much better mechanism for determining the age of individual knobs. Because of parameters that have uneven effects on the stromatolitic knobs throughout the lake, such as isolated storm events, algal coatings, breakage, dissolution, varying growth rates, etc., it is not possible to use the knobs for stratigraphic correlation either (Paull et al., 1992).

COMPARISON OF MICROBIALITES IN DIFFERENT ENVIRONMENTS

Although many questions remain, this study can provide a strong basis for comparison among the Storrs Lake microbialites, as well as microbialites from other field sites. This diagram displays the basic characteristics of Bahamian microbialites in Storrs Lake, Highborne Cay, Eleuthera, as well as the Sarine River in Switzerland. By comparing these different microbialites, insights can be gained into the ways in which environmental factors can effect the morphologies and organomineralization processes in these microbialites.

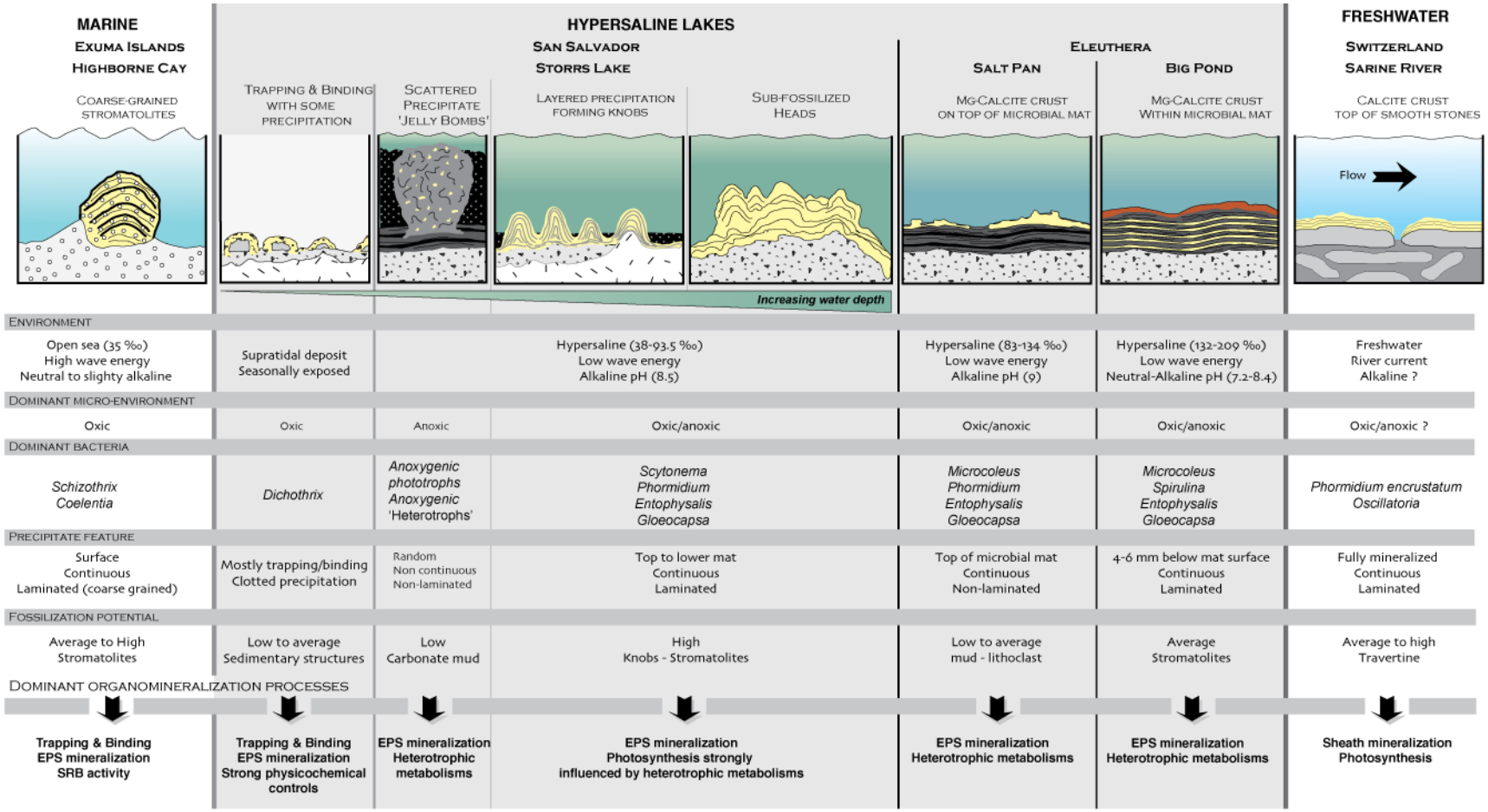

Figure #66: Comparison of Microbialites. Adapted from Reid et al., 2000; Dupraz et al., 2004; Glunk et al., 2011; and Dupraz et al., 2009.

Comparison of Storrs Lake Microbialites

Water depth has already been shown to be an important factor in controlling the morphology of the Storrs Lake microbialites. Small thrombolitic knobs are exposed on the shoreline, formed primarily through trapping and binding with some precipitation. The morphology of these thrombolitic structures is likely the result of a survival mechanism by the microbial community in order to withstand exposure in the supratidal environment. Some small, random precipitation does occur in the anoxic zone of the microbial mat upon entering the water, which then floats to the surface in the form of 'jelly bombs,' made of EPS.

Stromatolitic knobs begin forming at a depth where they will be submerged year-round. The small stromatolitic knobs, and larger, sub-fossil stromatolitic heads within the deeper portions of the lake, share many of the same characteristics. The only major differences between the two are their size, and the fact that the microbial communities are still active in the smaller knobs, while the larger heads no longer seem to be actively forming and some may have begun diagenesis. Computer modeling shows that the small stromatolitic knobs may eventually coalesce to from the larger stromatolitic heads in deeper portions of the lake (Figure #66) (Dupraz et al., 2006). If this modeling is accurate, understanding the formation of the small knobs essentially reveals the mechanism by which the larger heads are formed. The larger heads could become inactive when they reach a height at which they are no longer submerged year-round.

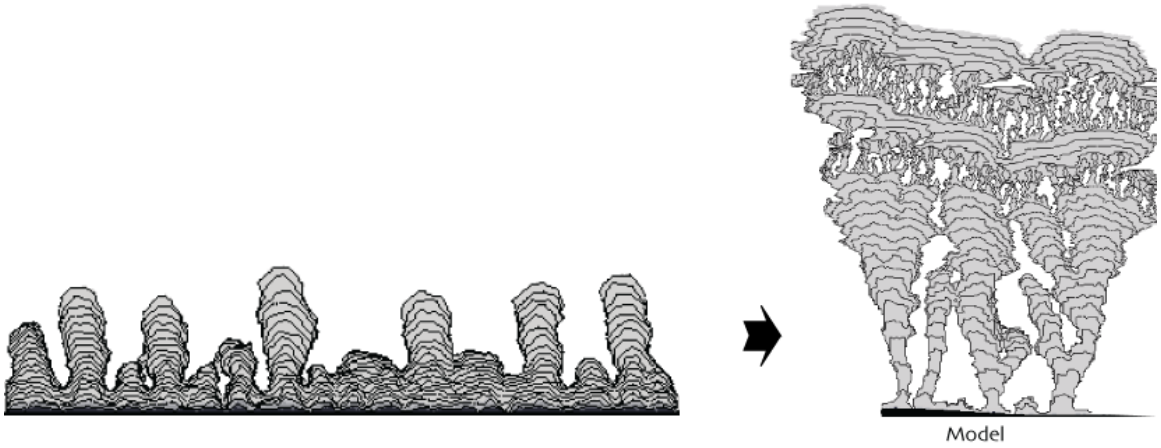

Figure #67: Modeling of small stromatolitic knobs coalescing to form larger stromatolitic heads (Dupraz et al., 2006)

Comparison of Storrs Lake and Other Hypersaline Environments

While Storrs Lake is a hypersaline lake, its salinity (~60 PSU at the time of this field study) is lower than that of other lakes/ponds throughout the Bahamas, including Salt Pan (83-134 PSU) and Big Pond (132-209 PSU) on Eleuthera island, Bahamas (Dupraz et al., 2004; Glunk et al., 2011). Despite some differences, these three examples of hypersaline lakes/ponds are highly comparable environments. $\delta^{18}O$ ratios show that all of these lakes are evaporative environments, all of which are supersaturated with respect to carbonate minerals, with precipitation of high-Mg calcite occurring within well-developed microbial mats comprised of relatively equivalent functional groups (cyanobacteria, sulfate-reducers) of bacteria (Dupraz et al., 2004, Glunk et al., 2011). The pattern of this precipitation is also consistent in all three hypersaline lakes/ponds. Salt Pan and Big Pond both show a microstructure of micritic micropeloidal structures surrounded by microsparite, then sparite, as seen in the Storrs Lake microbialites in areas where EPS is being degraded and replaced by high-Mg calcite (Dupraz et al., 2004, Glunk et al., 2011). Precipitation does not occur within cyanobacterial sheaths in any of these environments

$\delta^{13}C$ ratios show that while the carbonate precipitation in each of these hypersaline environments is microbially mediated, the metabolism responsible for precipitation differs slightly between the lakes/ponds (Dupraz et al., 2004; Glunk et al., 2011). EPS degradation by sulfate-reducing bacteria seems to be important for calcium carbonate precipitation in all three environments, but is most dominant in Big Pond, with the most negative $\delta^{13}C$ ratios (-2 and -5 $\delta^{13}C$), and slightly dominant in Salt Pan, with slightly negative $\delta^{13}C$ ratios (between -0.5 and -1 $\delta^{13}C$) (Dupraz et al., 2004; Glunk et al., 2011). Photosynthesis seems to be dominant over EPS degradation in Storrs Lake, with slightly positive $\delta^{13}C$ ratios (+1.5 to +3 $\delta^{13}C$). While the driving metabolism varies, it is likely that both photosynthesis and sulfate-reducing bacteria are involved in carbonate precipitation, as both metabolisms are active in each of these environments. It is interesting to note that $\delta^{13}C$ ratios become increasingly more negative with increasing salinity in these three hypersaline environments, which may be related to effects of salinity on the microbial community.

While the mechanism for organomineralization is comparable in each of these hypersaline environments, precipitation is organized differently in each. The precipitation in Salt Pan is non-laminated, leiolitic carbonate crust (Dupraz et al., 2004), unlike the laminated mesostructure seen in Storrs Lake and Big Pond (Glunk et al., 2011). Laminae formation associated with the alternation of cyanobacterial filament orientations is found in Storrs Lake's stromatolitic knobs, where photosynthesis appears to be the dominant metabolism for organomineralization, while lamination in Big Pond,

where EPS degradation appears to be the dominant control over organomineralization, is related to periodic episodes of precipitation and non-precipitation (Glunk et al., 2011).

Comparison of Storrs Lake and Highborne Cay, Exuma Islands, Bahamas

Although specific species vary, Highborne Cay, Storrs Lake, Salt Pan, and Big Pond all share the same basic functional groups of bacteria (cyanobacteria, SRBs, etc.) (Dupraz et al., 2004; Glunk et al., 2011; Reid et al., 2000). While trapping and binding of coarse-grained sediments by filamentous cyanobacteria is the primary mechanism for forming the Highborne Cay open-marine stromatolites, *in situ* precipitation of micrite does occur during periods of low wave-energy, due to a combination of photosynthesis and, more dominantly, heterotrophic metabolisms (Reid et al., 2000). This is similar to the mechanism of precipitation observed in hypersaline lakes. EPS degradation by sulfate-reducing bacteria also leads to the precipitation of calcium carbonate within bored grains in the Highborne Cay stromatolites as well (Reid et al., 2000), a smaller-scale version of the same precipitation mechanism that is dominant in Salt Pan and Big Pond, and important in Storrs Lake. Although the mechanisms for organomineralization share similarities between Highborne Cay and Storrs Lake, the mechanisms for lamination are different. The laminations in the Storrs Lake stromatolites are associated with cyanobacterial filament orientations, while the laminations in the Highborne Cay stromatolites are dependent on changing sedimentation rates (Reid et al., 2000).

Thrombolitic structures found at Highborne Cay are frequently exposed along the shoreline (Myshrall et al., 2010), similar to the exposed thrombolites of Storrs Lake.

However, thrombolites at Highborne Cay are frequently buried by sediment due to high-wave energy, and exposed/submerged tidally (Myshrall et al., 2010), while the Storrs Lake thrombolites are exposed nearly year-round without burial. The thrombolites of both Highborne Cay and Storrs Lake show clotted mesostructure created through a combination of micritic precipitation and trapped grains (Myshrall et al., 2010).

Comparison of Storrs Lake and Freshwater Microbialites

Although the microbial community functional groups are relatively equivalent in hypersaline lakes and open marine environments, in freshwater, the sulfur cycle is less important, and cyanobacteria may completely dominate the microbial community, such as in the Sarine River in Fribourg, Switzerland (Dupraz et al., 2009). This could be due to the much lower amounts of organic matter in freshwater ecosystems to feed heterotrophic metabolisms (Dupraz et al., 2009). Without massive amounts of organic matter, calcium sequestration is much less of an issue in freshwater ecosystems than in the hypersaline lakes. Therefore, photosynthetic increases in carbonate alkalinity can drive carbonate precipitation without having to overcome the binding capacity, and without the help of heterotrophs to free calcium through EPS degradation.

Without the calcium sequestration problem, and without the involvement of heterotrophic metabolisms, the mechanism for organomineralization is largely different than in hypersaline lakes and open marine environments. This mechanism results in precipitation within the cyanobacterial sheaths (Dupraz et al., 2009), rather than in the EPS matrix as seen in hypersaline lakes and open marine environments. The formation

of laminae in this photosynthetically dominated system is associated with alternating cyanobacterial filament orientations (Dupraz et al., 2009; Geurts, 1976; Monty, 1976; Freytet & Plet, 1996; Freytet & Verrecchia, 1998), just as it is in Storrs Lake, where photosynthesis is also slightly dominant, despite heavy involvement of heterotrophic metabolisms.

Conclusions from Comparisons

- Stable carbon isotopes indicate that carbonate precipitation is microbially mediated in hypersaline lakes. This is further supported by the corresponding location of precipitation with the most metabolically active portions of microbial mats (Dupraz et al., 2004; Glunk et al., 2011; Reid et al., 2000.; Dupraz et al., 2009).
- Functional groups within microbial communities (cyanobacteria, sulfate-reducing bacteria, etc.) are relatively equivalent amongst hypersaline lakes and in open-marine settings, but heterotrophic bacteria are insignificant or absent in freshwater settings.
- Carbonate precipitation as a function of EPS degradation by heterotrophs is important or dominant in hypersaline lakes and open-marine settings, despite the fact that photosynthesis is still highly active in these environments (Dupraz et al., 2004; Glunk et al., 2011; Reid et al., 2000; Dupraz et al., 2009). However, photosynthesis is the only metabolism driving precipitation in slow-flowing or still freshwater.

- Alternating cyanobacterial filaments control the formation of laminae in Storrs Lake and fresh water travertine where photosynthesis has more control over precipitation, while lamination is a function of periodic shifts in organomineralization in Big Pond and Highborne Cay, where EPS degradation by sulfate-reducing bacteria is the dominant metabolism for controlling precipitation (Dupraz et al., 2004; Reid et al., 2000).
- During quiet periods, in open-marine settings, micritic precipitation forms in a similar mechanism to precipitation in the Storrs Lake knobs (Reid et al., 2000). Similar heterotrophically-driven precipitation occurs in the Storrs Lake EPS matrix, as well as within bored grains in Highborne Cay stromatolites (Reid et al., 2000). It is possible that if, hypothetically, sedimentation rates could increase in Storrs Lake for an extended period of time, trapping and binding of coarse grains could become more important, and the stromatolitic knobs may begin to form morphologies similar to those of Highborne Cay stromatolites. Vice versa, if the ocean could, hypothetically, be quieted for an extended period of time, micritic precipitation could become more dominant, and the Highborne Cay stromatolites may take on a more micritic microstructure. Despite differing morphologies, Highborne Cay and Storrs Lake stromatolites could both be used as a potential analog for the organomineralization process that could have formed ancient stromatolites.

The differences and similarities of all of these microbialites are a testament to the profound impact that environmental conditions can have on the organomineralization

process. Depth has a strong influence on the macro- and mesostructure of microbialites across Storrs Lake. Environmental changes can impact the dominant metabolism that controls precipitation, which can in turn control the micro- and mesostructure of the microbialites. Sedimentation rates can also have a profound impact on the morphology of the microbialites. These many ties between the microbial community and environmental conditions in creating carbonate rock is why microbialites make a perfect example of the link between the biologic and geologic carbon cycle.

THE FUTURE FOR THESE MICROBIALITES

The future of each of these microbialites will depend largely on changes in environmental conditions. A rise in global temperature, for example, could increase evaporation in the hypersaline lakes. Increases in evaporation could cause geochemical precipitation to become more dominant, which could also change the morphology of the microbialites. Major increases in evaporation would eventually expose the microbialites, likely causing the microbial community to become inactive, and diagenesis may begin to occur.

Even without these changes, the stromatolitic knobs in Storrs Lake will eventually be exposed if they continue to grow and coalesce into even larger stromatolitic heads. Once the stromatolites reach a height at which they will no longer be submerged year-round, the microbial community will likely become inactive, as it has in the larger stromatolitic heads. Diagenesis could then start to occur, potentially destroying the original precipitated microstructure over time. However, the laminated mesostructure would remain intact, as would the overall morphology of the knobs and larger heads.

Storrs Lake stromatolitic knobs are strongly lithified, making them cohesive enough to give them a high fossilization potential. The quiet lake setting also gives strong potential for gentle burial, increasing the fossilization potential even more. The larger stromatolitic heads can already be classified as subfossilized.

The Highborne Cay stromatolites, being 70% comprised of trapped coarse grains (Reid et al., 2000), are significantly less cohesive than the Storrs Lake stromatolites, with the exception of the thin micritic layers and fused grains. In the event of sea level regression, long-term exposure would allow the biofilm to dry out, and the sediment grains that hold most of the stromatolites structures together would crumble apart. Layers of precipitated micrite and fused grains could remain intact, but would break off as the bulk of the overall structure crumbled. A sea level regression could potentially make the Highborne Cay stromatolites have a lower fossilization potential than the Storrs Lake stromatolites. However, in the event of a sea level *transgression*, the high chances of burial for the open-marine microbialites due to high-wave energy would increase their fossilization potential. The potentially lower fossilization potential of the coarse-grained, open-marine stromatolites could provide a simple possible explanation for why the fossil stromatolites are mostly micritic. It could be that coarse-grained stromatolites were just as common as micritic stromatolites on the early earth, but simply were not preserved as often.

The carbonate crust of Salt Pan would likely have a low fossilization potential, being preserved only as mud-sized carbonate grains. Some crust could be preserved as larger

lithoclasts, but the crust is too brittle to stay together as a whole. The precipitated stromatolitic layers of Big Pond would have an average fossilization potential, likely similar to the Storrs Lake stromatolites. Freshwater travertine generally has a high fossilization potential (Dupraz et al., 2009). The travertine is fully mineralized, making it cohesive, and forms in slow-moving currents or still water, making gentle burial likely (Dupraz et al., 2009).

The thrombolitic knobs of Storrs Lake have a low preservation potential as whole structures, which crumble easily under little pressure, and are not likely to be buried on the exposed shoreline. However, the individual clotted structures that make up the mesostructure of the thrombolites could be preserved, and could potentially become grainstone. The thrombolites of Highborne Cay may have a higher fossilization potentially due to their frequent burial, but would most likely be preserved as grainstone rather than macroscopic structures, similar to the Storrs Lake thrombolites.

PROPOSAL OF FUTURE RESEARCH ON STORRS LAKE MICROBIALITES

To understand the seasonal changes that effect the Storrs Lake microbialites, long-term study is critical. A comprehensive database of depth, salinity, light penetration, ion concentrations, and saturation indices over several years would provide insights into environmental changes that occur in this lake. This could then be paired with study of seasonal variations in filament orientations, microbial activity, EPS production, and isotopic signatures, to determine the effects of environmental changes on the microbial

community and organomineralization/geochemical precipitation. These long-term observations could explain whether the dominant metabolism controlling precipitation shifts seasonally, or whether geochemical precipitation becomes more important during the dry season when evaporation rates increase. Information on precipitation rates could also provide evidence for the effects of alternating filament orientations on creating lamination, determining if the same amount of precipitation is simply condensed during the winter when filaments are horizontal, or if precipitation increases during this time.

While precipitation has been the strong focus of studies on microbialites in Storrs Lake, more work is needed to determine the effects, or lack thereof, of dissolution in these structures, both diurnally and seasonally. Study of the impacts of storms could be used as a test of the stromatolitic knobs' resilience and fossilization potential.

This study is primarily from the geological perspective on microbialites, but a clear understanding of the microbial community and its metabolisms is essential for a comprehensive view of the organomineralization processes occurring in any of these environments. More isotopic analysis is needed on the stromatolitic knobs and surrounding reservoir to further determine the origin of the mixed signals and metabolic effects on precipitation. Cryo SEM is essential for examining precipitation within the EPS matrix, so this is a critical part of any future work done on these microbialites.

LONG-TERM RESEARCH GOALS

This study contributes insights into the organomineralization process and laminae formation in modern micritic stromatolites. The next big step is to apply these insights to the fossil record.

Storrs Lake stromatolitic knobs are dominated by micritic calcium carbonate precipitation, and appear to have similar macro- and mesostructures to late Proterozoic fossil stromatolites from Mauritania, Africa (Figure #53). This makes the Storrs Lake stromatolitic knobs a good potential modern analog for micritic stromatolites in the fossil record. However, many of the techniques used in this study cannot be applied to fossil stromatolites. For example, the fossil stromatolites are completely recrystallized/dolomitized, and stable carbon isotopes give strong signals for diagenesis. This means that the original microstructure and isotopic signatures are destroyed, so thin section and isotope analysis does not provide information about the original mechanism for precipitation. Organics are not preserved in the fossil stromatolites, giving little information about the microbial community that may have formed them, or their potential effects on laminae formation. More sophisticated techniques are needed to obtain this information, such as microprobes or nanosims.

If more information can be gained in the future about the fossil stromatolites, the insights gained in this study could be used to determine the environment in which they formed, or the microbial community that formed them. For example, if the fossil stromatolites were formed by *in situ* precipitation, cyanobacteria and heterotrophic bacteria may have been

involved in organomineralization, and cyanobacteria could have been involved in laminae formation. If instead, the fossil stromatolites were formed primarily by the trapping and binding of mud-sized grains, a steady supply of sediment would be required, and bacterial biofilms may have been responsible for stabilizing the sediment. Laminae formation in that case could result from a changing environment in which higher-energy trapping and binding alternated with quieter periods of precipitation, similar to Highborne Cay.

A lot more work needs to be done, but this study could provide a small step closer to a better understanding of organomineralization and laminae formation in modern stromatolites, paving the way for gaining insights into the history of Earth's carbon cycle.

REFERENCES

Aitken, J. D., (1967): Classification and environmental significance of cryptalgal limestones and dolomites, with illustrations from the Cambrian and Ordovician of southwestern Alberta. J. – *Sed. Petrol*, 37, 1163-1178.

Allwood, A.C., Walter, M.R., Burch, I.W., Kamber, B.S., (2007): 3.43 billion-year-old stromatolite reef from the Pilbara Craton of Western Australia: Ecosystem-scale insights to early life on Earth. – *Precambrian Research*, 158, 198–227.

Allwood, A.C., Walter, M.R., Kamber, B.S., Marshall, C.P., Burch, I.W., (2006): Stromatolite reef from the Early Archaean era of Australia. – *Nature,* 441, 714-718.

Arp, G., Reimer, A., Reitner, J., (1999): Calcification in cyanobacterial biofilms of alkaline salt lakes. – *Eur. J. Phycol*., 34, 393-403.

Adams, Robert W. (1983): General Guide to the Geological Features of San Salvador. *In* Gerace, D.T. (ed), Field Guide to the Geology of San Salvador. 3rd ed. pp 1-66. CCFL Bahamian Field Station, San Salvador, Bahamas.

Bathurst, Robin G.C., (1975): Carbonate Sediments and their Diagenesis. 2nd ed. Elsevier. Netherlands.

Badger, M., (2001): The roles of carbonic anhydrases in photosynthetic CO_2 concentrating mechanisms. – *Photosynthesis Research,* 77, 83-94.

Bebout, B.M., (1992): Interactions of nitrogen and carbon cycling in microbial mats and stromatolites [PhD thesis]: University of North Carolina at Chapel Hill.

Braga, J. C., Martin, J. M., Riding, R., (1995): Controls on Microbial Dome Fabric Development along a Carbonate-Siliciclastic Shelf-Basin Transect, Miocene, SE Spain. – *Palaios,*10, 347-361.

Braissant, O., Decho, A.W., Dupraz, C., Glunk, C., Przekop, K.M., and Visscher, P.T., (2007): Exopolymeric substances of sulfate-reducing bacteria: Interactions with calcium at alkaline pH and implication for formation of carbonate minerals. – *Geobiology*, 5, 401-411.

Burne, Robert V., and Moore, Linda S., (1987): Microbialites; organosedimentary deposits of benthic microbial communities. – *Palaios,* 2, 241-254.

Carew, James L., and J. E. Mylroie., (1995): Deposition Model and Stratigraphy for the Quaternary Geology of the Bahama Islands. *In* Curran, H.A., and White, B., (eds), Terrestrial and Shallow Marine Geology of the Bahamas and Bermuda. pp 5-32. Geological Society of America Special Paper 300. Boulder, Colorado.

Curran, H. Allen., (1997): Introduction to the Geology of the Bahamas and San Salvador Island, With an Overflight Guide. *In* Curran, H.A., (ed), Guide to Bahamian Ichnology: Pleistocene, Holocene, and Modern Environments. pp 1-10. Bahamian Field Station, San Salvador, Bahamas.

Curran, H. Allen, and White, Brian., (1995): Introduction: Bahamas Geology. *In* Curran, H.A., and White, B. (eds), Terrestrial and Shallow Marine Geology of the Bahamas and Bermuda. pp 1- 3. Geological Society of America Special Paper 300. Boulder, Colorado.

Decho, Alan W., Norman, R. Sean, Visscher, Pieter T., (2010): Quorum Sensing in Natural Environments: Emerging Views from Microbial Mats. – *Trends in Microbiology*, 18, 2, 73-80.

Défarge, C., Trichet, J., Jaunet, A.M., Robert, M., Tribble, J., Sansone, F.J., (1996): Texture of microbial sediments revealed by cryo-scanning electron microscopy. – *Journal of Sedimentary Research*, 66, 935-947.

DesMarais, D.J., (1995). The biogeochemistry of hypersaline microbial mats. *In* Jones, J.G. (ed), Advances in Microbial Ecology. pp. 251-274. Plenum, New York.

Dill, R.F., Shinn, E.A., Jones, A.T., Kelly, K., Steinen, R.P., (1986): Giant subtidal stromatolites forming in normal salinity waters. – *Nature*, 324, 55-58.

Dravis, J.J., (1983): Hardened subtidal stromatolites, Bahamas. – *Science*, 219, 385-386.

Dupraz, C., Visscher, P.T., Reid, P., (2011): Microbialite, Modern. *In* Reitner, Joachim, and Thiel, Volker (eds), Encyclopedia of Geobiology. pp. 617-635. Springer, University of Göttingen, Germany.

Dupraz, C., Reid, R.P., Braissant. O., Decho, A.W., Norman, R.S., Visscher, P.T., (2009): Processes of carbonate precipitation in modern microbial mats. – *Earth Science Review*, 96, 141–162.

Dupraz, C., Patissina, R., Verrecchia, E.P., (2006): Simulation of stromatolite morphospace using 'DLA-CA' growth model': translation of energy in morphology. – *Sedimentary Geology*, 185, 185-203.

Dupraz, C., and Visscher, P.T., (2005): Microbial lithification in marine stromatolites and hypersaline mats. – *Trends in Microbiology*, 13, 9, 429-438.

Dupraz C., Visscher P.T., Baumgartner L.K. Reid R.P., (2004): Microbe-mineral interactions: early carbonate precipitation in a hypersaline lake (Eleuthera Island, Bahamas). – *Sedimentology*, 51, 745-765.

Dupraz, C., and Strasser, A., (2002): Nutritional modes in coral-microbialite reefs (Jurassic, Oxfordian, Switzerland): Evolution of trophic structure as a response to environmental change. – *Palaios*, 17, 449-471.

Dupraz, C., and Strasser, A., (1999): Microbialites and micro-encrusters in shallow coral bioherms (Middle-Late Oxfordian, Swiss Jura Mountains). – *Facies*, 40, 101-130.

Feldmann, M., and McKenzie, J., (1998): Stromatolite-thrombolite association in a modern environment, Lee Stocking Island, Bahamas. – *Palaios*, 13, 201-212.

Fowler, Alexandré., (2009): Taphonomy of a Modern Coral Reef in the Bahamas as a Tool for Modeling Patch Reef Ecosystem Transitions and Depositional Environments in the Fossil Record [Undergraduate Thesis]: Hartwick College Department of Geological and Environmental Sciences Senior Thesis. Faculty Advisor: Dr. David Griffing.

Freytet, P., Verrecchia, E.P., (1999): Calcitic radial palisadic fabric in freshwater stromatolites: diagenetic and recrystallized feature or physicochemical sinter crust. – *Sedimentary Geology*, 126, 97-102.

Freytet, P., and Verrecchia, E.P., (1998): Freshwater Organisms that Build Stromatolites: a Synopsis of Biocrystallization by Prokaryotic and Eukaryotic Algae. – *Sedimentology*, 45, 535-563.

Freytet, P., and Plet, A., (1996): Modern freshwater microbial carbonates: the *Phormidium* stromatolites (Tufa-travertine) of southeastern Burgundy (Paris Basin, France). – *Facies*, 34, 219–238.

Garcia-Pichel, F., (1994): A Model for Internal Self-Shading in Planktonic Organisms and its Implications for the Usefulness of Ultraviolet Sunscreens. – *Limnology and Oceanography*, 39, 1704-1717.

Geurts, M.A., (1976): Genèse et stratigraphie des travertins de fond de vallée en Belgique. – *Acta Geographica Lovaniensia*, 16, 1–66.

Ginsburg, R.N., (1991): Controversies about stromatolites: vices and virtues. *In* Müller, D.W., McKenzie, J.A., and Weissert, H., (eds), Controversies in Modern Geology. pp. 25-36. Academic press Limited, London.

Glunk, C., Dupraz, C., Braissant, O., Gallagher, K.L., Verrecchia, E.P., Visscher, P.T., (2011): Microbially Mediated Carbonate Precipitation in a Hypersaline Lake, Big Pond (Eleuthera, Bahamas). – *Sedimentology*, 58, 720-738.

Golubic, S., and Hofmann, H. J., (1976): Comparison of Holocene and Mid-Precambrian Entophysalidaceae (Cyanophyta) in Stromatolitic Algal Mats: Cell Division and Degradation. – *Journal of Paleontology*, 50, 1074-1082.

Grotzinger, J.P., and Knoll, A.H., (1999): Stromatolites in Precambrian carbonates: evolutionary mileposts or environmental dipsticks?. – *Annu. Rev. Earth Planet. Sci.*, 27, 313-358.

Hattin, Donald T., (1982): Holocene Lithification of Carbonate Sediments, San Salvador Island, Bahamas. *In* Gerace, D.T. (ed.) Proceedings of the First Symposium on the Geology of the Bahamas. pp. 45-62. CCFL Field Station, San Salvador, Bahamas.

Hofmann, H.J., Grey, A.H., Hickman, A.H., Thorpe, R.I., (1999): Origin of 3.45 Ga coniform stromatolites in Warrawoona Group, Western Australia. – *Geological Society of America Bulletin*, 111, 1256-1262.

Kah, L.C., and Grotzinger, J.P., (1992): Early Proterozoic (1.9 Ga) thrombolites of the Rocknest Formation, Northwest Territories. – *Palaios*, 7, 305–315.

Kalkowsky, E., (1908): O€olith und Stromatolith im norddeutschen Buntsandstein. – *Zeitschrift der Deutschen geologischen Gesellschaft*, 60, 68–125, pls 4–11.

Kennard, J.M., and James, N.P., (1986): Thrombolites and stromatolites : Two distinct types of microbial structures. – *Palaios*, 1, 492-503.

Konhauser, K., (2007). Introduction to Geomicrobiology. Blackwell Science. UK.

Land, L.S., (1998): Failure to precipitate dolomite at 25°C from dilute solution despite 1000-fold oversaturation after 32 years. – *Aquatic Geochemistry*, 4, 361-368.

Mann, C. John., and Hoffman, Larry R., (1984): Algal mounds in Storr's Lake, San Salvador, Bahamas. *In* Gerace, D.T. (ed), Proceedings of the Second Symposium on the Geology of the Bahamas. pp. 41-51. CCFL Bahamian Field Station, San Salvador, Bahamas.

Mann, C.J., and Nelson, W.M., (1989): Microbialitic structures in Storr's Lake, San Salvador Island, Bahamas Islands. – *Palaios*, 4, 287-293.

McNeese, L.R., (1988): Modern Stromatolites in hypersaline Storr's Lake, San Salvador, Bahamas [Masters Thesis]: University of North Carolina Chapel Hill.

Merz-Preiß, M., (1992): The biology of carbonate precipitation by cyanobacteria. – *Facies* 26, 81-102.

Merz-Preiß, M., and Riding, R., (1999): Cyanobacterial Tufa Calcification in Two Freshwater Streams: Ambient Environment, Chemical Thresholds and Biological Processes. – *Sed. Geol.*, 126, 103–124.

Monty, C.L.V., (1977): Evolving concepts on the nature and the ecological significance of stromatolites. *In* Flügel, E. (Ed.), Fossil algae. pp. 15-35. Springer-Verlag, Berlin, Heidelberg, New York.

Monty, C.L.V., (1976): The origin and development of crypalgal fabric. *In*: Walter, M.R. (Ed.), Stromatolites. Developments in Sedimentology, 20, 193–249.

Moore, L.S., and Burne, R.V., (1994): The modern thrombolites of Lake Clifton, Western Australia. *In* J. Bertrand-Sarfati and C. Monty (eds.), Phanerozoic Stromatolites II. pp. 3–19. Kluwer Academic Publishers, Dor-drecht.

Mullins, H.T., and Lynts, G.W., (1977): Origin of the Northwestern Bahama Platform: Review and Reinterpretation. – *Geological Society of America Bulletin*, 88, 1147-1161.

Myshrall, K.L., Mobberley, J.M., Green, S.J., Visscher, P.T., Havemann, S.A., Reid, R.P., Foster, J.S., (2010): Biogeochemical Cycling and Microbial Diversity in the Thrombolitic Microbialites of Highborne Cay, Bahamas. – *Geobiology*, 8, 337-354.

Neumann, C.A., Bebout, B.M., McNeese, L.R., Paul, C.K., Paerl, H.W., (1989): Modern stromatolites and associated mats: San Salvador, Bahamas. *In*: Mylroie, J. (ed), Proceedings of the 4th Symposium on the Geology of the Bahamas. pp. 235-251. Bahamas Field Station, San Salvador, Bahamas.

Paerl, H.W. personal communication with Dupraz, C., 2007.

Patterson, William P., and Walter, Lynn M., (1994): Depletion of ^{13}C in seawater $\sum CO_2$ on modern carbonate platforms: Significance for the carbon isotopic record of carbonates. – *Geology*, 22, 10, 885-888.

Paull, C.K., Neumann, A.C., Bebout, B., Zabielski, V., Showers, W., (1992): Growth rate and stable isotopic character of modern stromatolites from San Salvador, Bahamas. – *Palaeogeography Palaeoclimatology, Palaeoecology*, 95, 335-344.

Pentecost, A., (1989): Observations on the *Scytonema* Mats of San Salvador, Bahamas. *In* Mylroie, John E. (ed), Proceedings of the Fourth Symposium on the Geology of the Bahamas. pp. 295-302. CCFL Bahamian Field Station, San Salvador, Bahamas.

Pentecost, A., and Riding, R., (1986): Calcification in cyanobacteria. Leadbeater, B.S.C., Riding, R. (Eds.), Biomineralization in lower plants and animals. – *Clarendon press, Oxford*, 73-90.

Pentecost, A., and Whitton, B.A., (2000): Limestones. *In* Whitton, B.A. and Potts, M. (eds), The Ecology of Cyanobacteria. pp. 257-279. Kluwer, Amsterdam.

Planavsky, N., Reid, R.P., Lyons, T.W., Myshrall, K.L., Visscher, P.T., (2009): Formation and Diagenesis of Modern Marine Calcified Cyanobacteria. – *Geobiology*, 7, 566-576.

Rakestrow, N.W., (1949): The conception of alkalinity or excess base of seawater. – *Journal of Marine Research*, 8, 14-20.

a) Reid, R.P, James, N.P., Macintyre, I.G., Dupraz, C., Burne, R.V., (2003): Shark Bay Stromatolites: Microfabrics and reinterpretation of origins. – *Facies*, 49, 45-53.

b) Reid, R.P., Dupraz, C., Visscher, P.T., Decho, A.W., Sumner, D.Y., (2003): Microbial processes forming modern marine stromatolites: microbe-mineral interactions with a three-billion-year rock record. *In* Krumbein, W.E., Paterson, D.M., Zavarzin, G.A. (eds.), Fossil and Recent Biofilms - a natural history of life on Earth. pp. 103-118. Kluwer Academic Publishers.

Reid, R.P., Visscher, P.T., Decho, A.W., Stolz, J.F., Bebout, B.M., Dupraz, C., Macintyre, I.G., Paerl, H.W., Pinckney, J.L., Prufert-Bebout, L., Steppe, T.F., DesMarais, D.J., (2000): The Role of Microbes in Accretion, Lamination and Early Lithification of Modern Marine Stromatolites. – *Nature*, 406, 989-992.

Reid, R.P., MacIntyre, I.G., Browne, K.M., Steneck, and R.S., Miller, T., (1995): Modern marine stromatolites in the Exuma Cays, Bahamas: Uncommonly Common. – *Facies*, 33, 1-18.

Reimer, Adreas., (2011): Alkalinity. *In* Reitner, Joachim, and Thiel, Volker (eds), Encyclopedia of Geobiology. pp. 20-24. Springer, University of Göttingen, Germany.

Riding, R., (2011): Microbialites, stromatolites, and thrombolites. In J. Reitner and V. Thiel (eds), Encyclopedia of Geobiology. – *Encyclopedia of Earth Science Series, Springer, Heidelberg*, 635-654.

Riding, R., (2000): Microbial carbonates: the geological record of calcified bacterial-algal mats and biofilms. – *Sedimentology*, 47, 179-214.

Riding, R., (1991): Classification of microbial carbonates. *In* Riding, R. (ed.), Calcareous Algae and Stromatolites. pp. 21-51. Springer-Verlag, New York.

Riding, R., Awramika, S.M., Winsborougha, B.M., Griffina, K.M., Dill, R.F., (1991): Bahamian giant stromatolites: microbial composition of surface mats. – *Geological Magazine*, 128, 227-234

Semikhatov, M.A., Gebelein, C.D., Cloud, P., Awramik, S.M., Benmore, W.C., (1979): Stromatolite morphogenesis - progress and problems. – *Can. J. Earth Sci.*, 16, 992-1015.

Seong-Joo, L., Browne, K.M., Golubic, S., (2000): On stromatolites lamination. *In* Riding, R.E., Awramik, S.M. (eds.), Microbial Sediments. pp. 16-24. Springer-Verlag, Berlin, Heidelberg, New-York.

Shapiro, R.S., (2000): A comment on the systematic confusion of thrombolites. – *Palaios*, 15, 166-169.

Stumm, W., and Morgan, J.J., (1996): Aquatic Chemistry. John Wiley & Sons, New York.

Thompson, J.B., Schultze-Lam, S., Beveridge, J., Des Marais, D.J., (1997): Whiting Events: Biogenic Origin Due to the Photosynthetic Activity of Cyanobacterial Picoplankton. – *Limnol. Oceanogr.*, 42, 133-141.

Thompson, J.B., and Ferris, F.G., (1990): Cyanobacterial precipitation of gypsum, calcite, and magnesite from natural alkaline lake water. – *Geology*, 18, 995-998.

Trichet, J., Défarge, C., Tribble, J., Tribble, G., Sansone, F., (2001): Christmas Islands lagoonal lakes, models for the deposition of carbonate-evaporite-organic laminated sediments. – *Sedimentary Geology*, 140, 177-189.

Trichet, J., and Défarge, C., (1995): Non-biologically supported organomineralization. – *Bull. Inst. Océanographique Monaco, no. spec.*, 14, 203-236.

Turner, E.C., James, N.P., Narbonne, G.M., (2000): Taphonomic control on microstructure in Early Neoproterozoic reefal stromatolites and thrombolites. – *Palaios*, 15, 87-111.

van Lith, Y., Warthmann, R., Vasconcelos, C., McKenzie, J.A., (2003): Sulfate-reducing bacteria induce low-temperature Ca-dolomite and high Mg-calcite formation. – *Geobiology*, 1, 71–79.

Verrecchia, E.P., Freytet, P., Verrecchia, K.E., and Dumont, J.L., (1995): Spherulites in calcrete laminar crusts: biogenic $CaCO_3$, precipitation as a major contributor to crust formation. – *J. Sed. Research*, A65, 690-700.

Visscher, P.T., Dupraz, C., Braissant, O., Gallagher, K.L., Glunk, C., Casillas, L., Reed, R.E.S., (2010): Biogeochemistry of carbon cycling in hypersaline mats: Linking the present to the past through biosignatures. *In* Seckbach, J., and Oren, A. (eds) Cellular Origin, Life in Extreme Habitats and Astrobiology, 14: Microbial Mats. pp. 443-468. Springer. Verlag., Berlin.

Visscher, P.T., Reid, R.P., Bebout, B.M., (2000): Microscale observations of sulfate reduction: Correlation of microbial activity with lithified micritic laminae in modern marine stromatolites. – *Geology,* 28, 919-922.

Visscher, P.T., Beukema J., van Gemerden H., (1991): In situ characterization of sediments: measurements of oxygen and sulfide profiles. – *Limnol. Oceanogr*., 36, 1476-1480.

Visscher, P.T., and Stolz, J.F., (2005): Microbial mats as bioreactors: populations, processes and products. – *Paelogeogr. Paleoclimatol. Paleooecol*., 219, 87-100.

Wolf-Gladrow, D.A., Zeebe, R.E., Klaas, C., Körtzinger, A., Dickson, A.G., (2007): Total alkalinity: The explicit conservative expression and its application to biogeochemical processes. – *Marine Chemistry*, 106, 287-300.

Zabielski, V.P., (1991). The depositional history of Storr's Lake San Salvador Island, Bahamas [PhD thesis]: University of North Carolina Chapel Hill.

Zavarzin, G.A., (2002): Microbial geochemical calcium cycle. – *Microbiology,* 71, 1-17.

APPENDIX

COMPARISON OF SEM SAMPLE PREPARATION PROTOCOLS

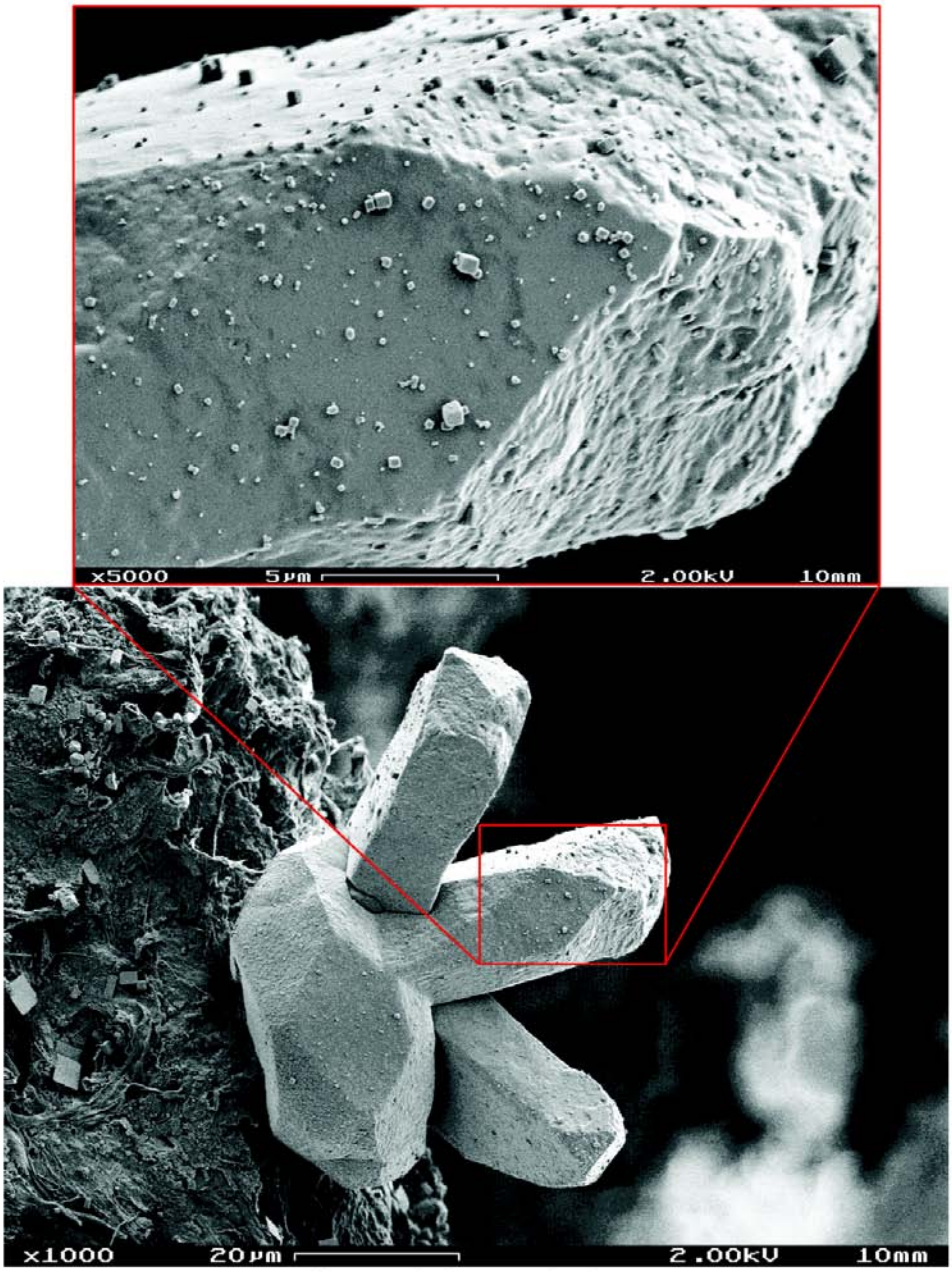

Crystal degradation,
possibly due to long-term Fixation

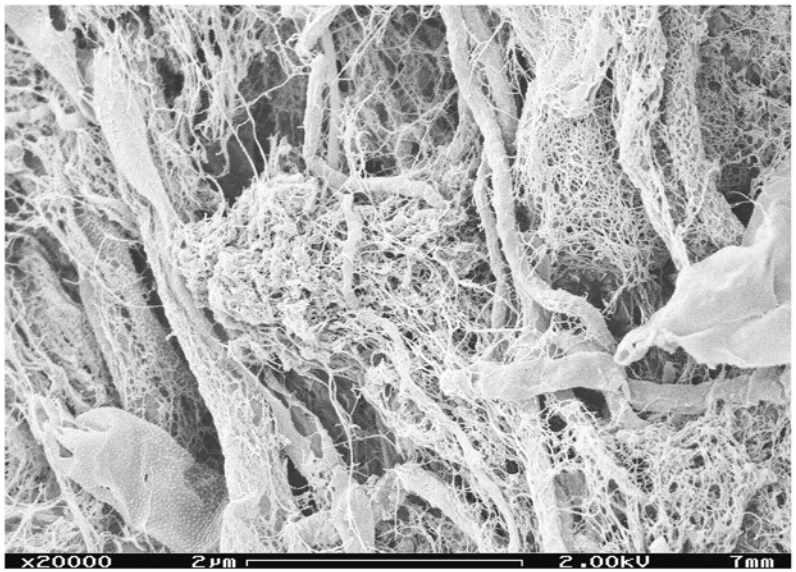

Critical Point Drying

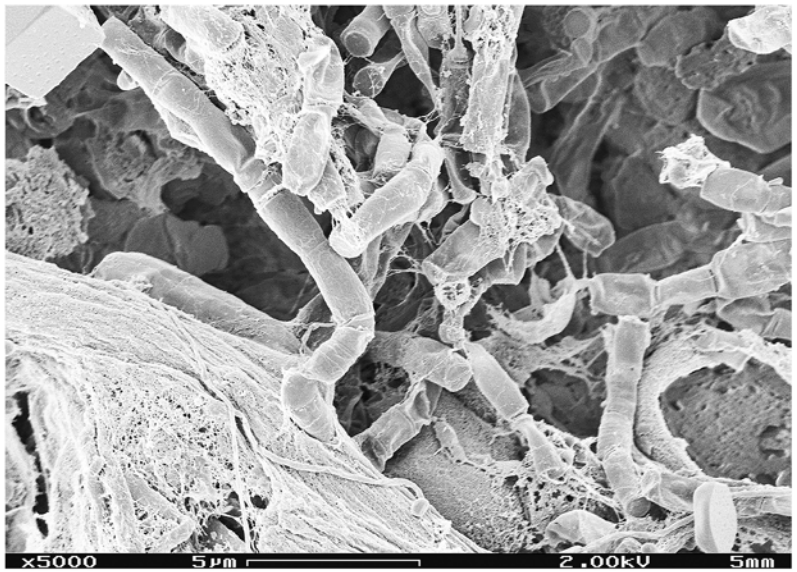

HMDS

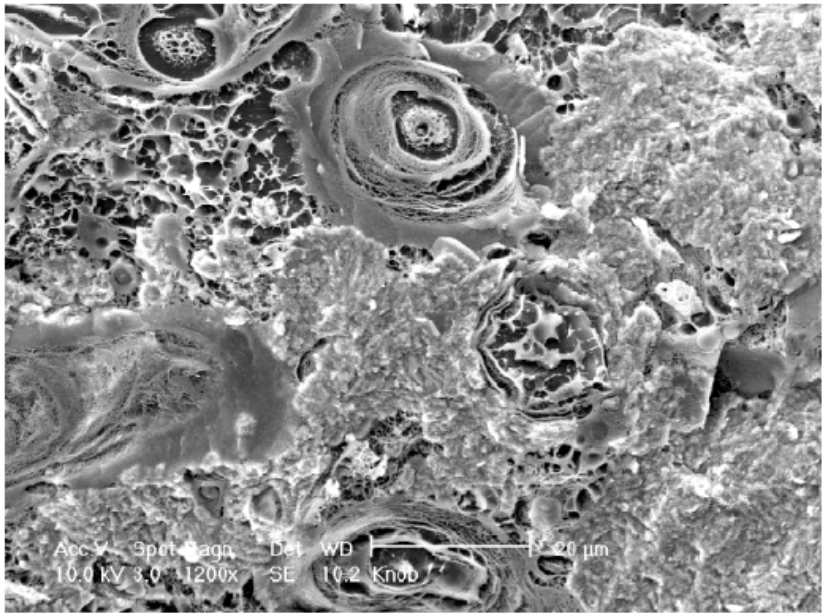
Acc.V Spot Magn Det WD
10.0 kV 3.0 1200x SE 10.2 Knob
20 µm

Cryo

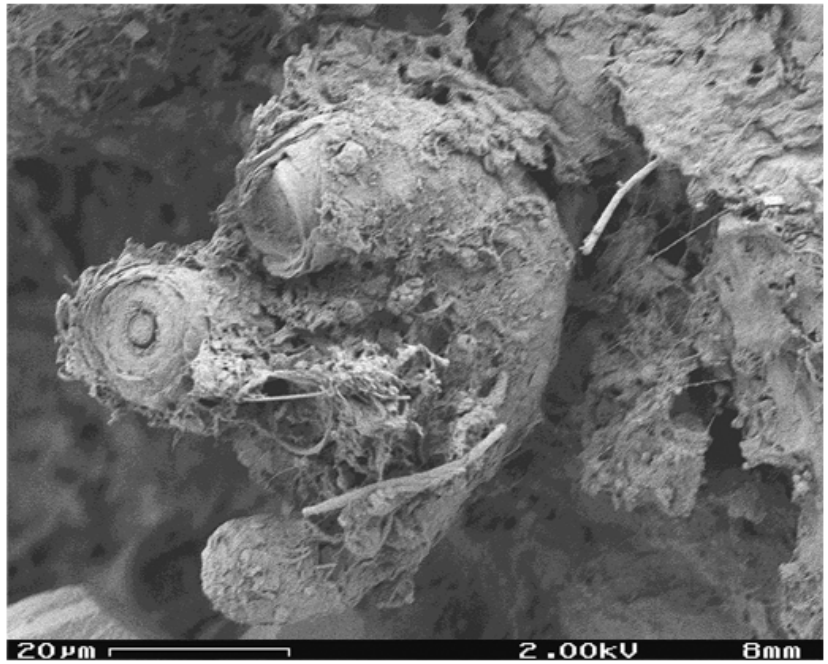
20µm
2.00kV
8mm

HMDS

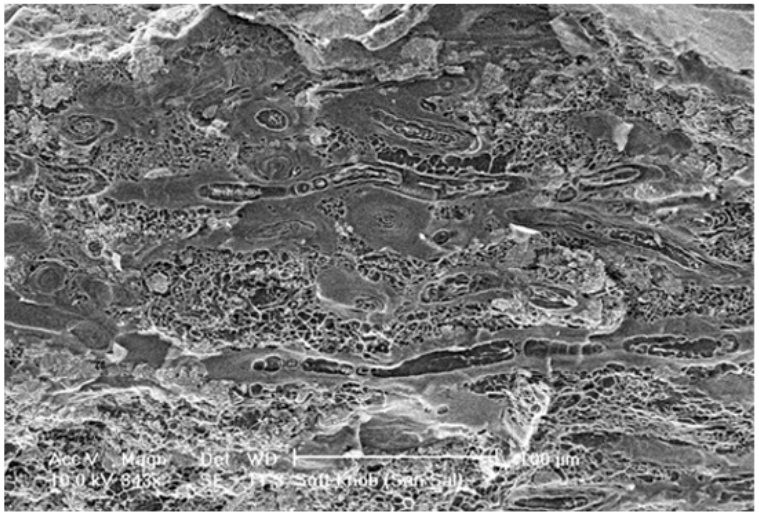

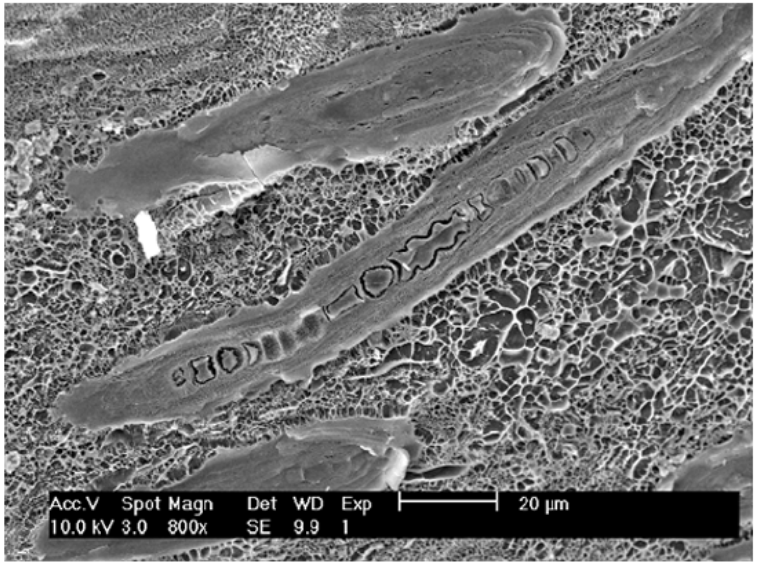

Cryo

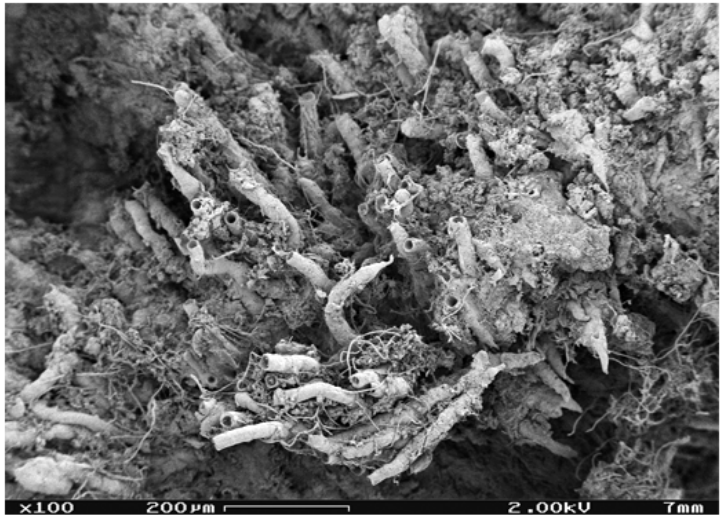

Critical Point Drying

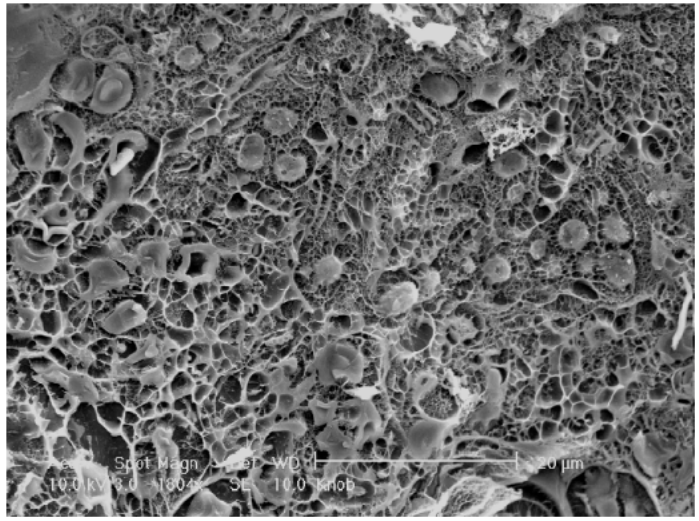

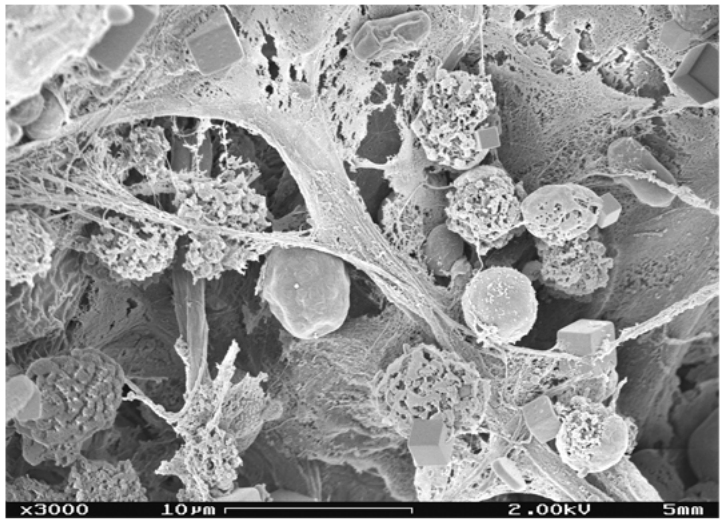
x3000 10µm 2.00kV 5mm

HMDS

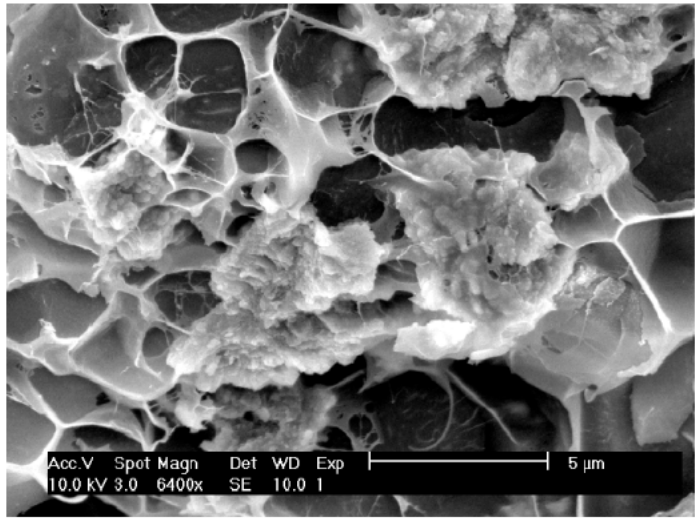
Acc.V Spot Magn Det WD Exp 5 µm
10.0 kV 3.0 6400x SE 10.0 1

Cryo

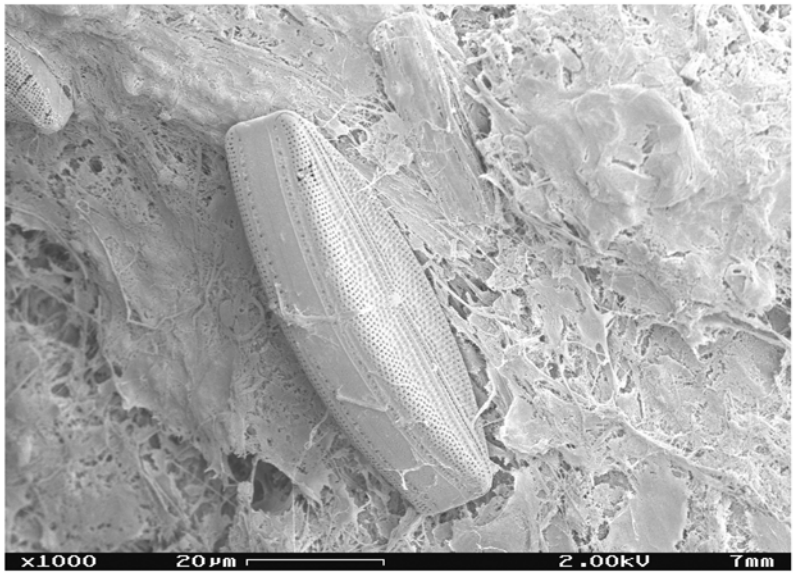

Osmium

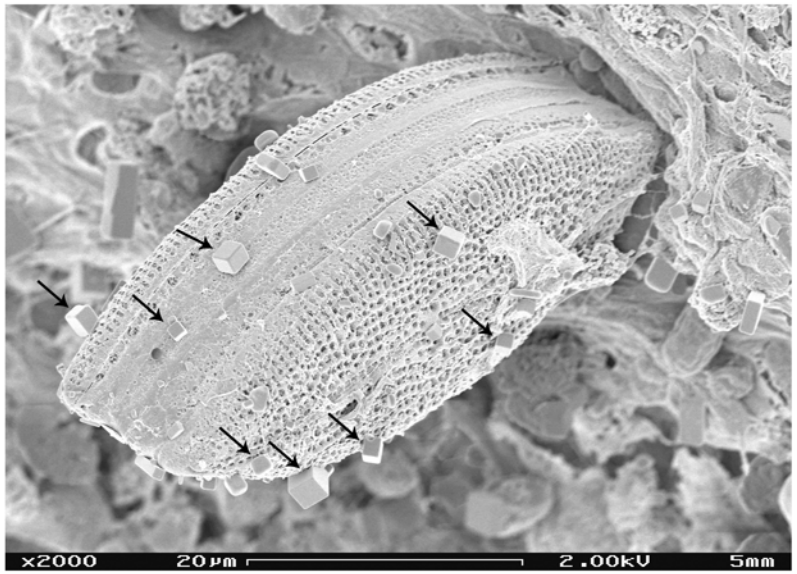

Salted ethanol series

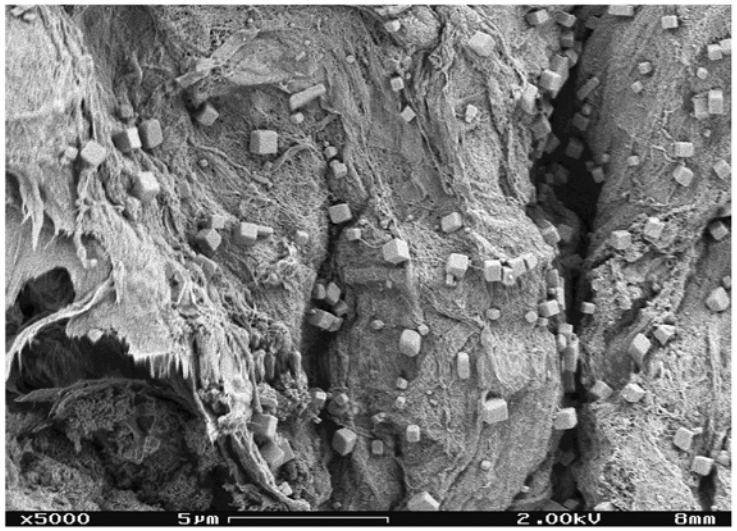

PHREEQ OUTPUTS

STORRS LAKE 1

```
Database file:  phreeqc.dat
------------------
Reading data base.
------------------
SOLUTION_MASTER_SPECIES
SOLUTION_SPECIES
PHASES
EXCHANGE_MASTER_SPECIES
EXCHANGE_SPECIES
SURFACE_MASTER_SPECIES
SURFACE_SPECIES
RATES
END
-----------------------------------
Reading input data for simulation 1.
-----------------------------------
TITLE SL10-1WF
SOLUTION 1
pH 8.64
temp 43.2
pe
density 1.03772
units ppm
Br 180.89
Ca 528.35
C 803 as HCO3
Cl 45825.87
Mg 6325.61
P 105.94
Na 26034.84
S 6419.94 as SO4-2
END
-----
TITLE
-----
 SL10-1WF
-------------------------------------------
Beginning of initial solution calculations.
-------------------------------------------
Initial solution 1.
-----------------------------Solution composition----------------------
Elements           Molality       Moles
Br                 2.477e-03   2.477e-03
C                  1.440e-02   1.440e-02
Ca                 1.443e-02   1.443e-02
Cl                 1.415e+00   1.415e+00
Mg                 2.847e-01   2.847e-01
Na                 1.239e+00   1.239e+00
P                  3.743e-03   3.743e-03
S                  7.314e-02   7.314e-02
```



```
----------------------------Description of solution--------------------
```

```
pH  =   8.640
                                        pe  =   8.640
                          Activity of water  =   0.949
                             Ionic strength  =   1.863e+00
                           Mass of water (kg)  =   1.000e+00
                  Total alkalinity (eq/kg)  =   2.859e-02
                           Total CO2 (mol/kg)  =   1.440e-02
                         Temperature (deg C)  =  43.200
                   Electrical balance (eq)  =   2.420e-01
 Percent error, 100*(Cat-|An|)/(Cat+|An|)  =   7.57
                                  Iterations  =   9
                                     Total H  = 1.110214e+02
                                     Total O  = 5.585756e+01
----------------------------Distribution of species----------------------
Log       Log         Log
Species             Molality    Activity  Molality  Activity     Gamma
OH-                2.763e-05   1.456e-05    -4.559    -4.837    -0.278
H+                 3.175e-09   2.291e-09    -8.498    -8.640    -0.142
H2O                5.551e+01   9.494e-01    -0.023    -0.023     0.000
Br                2.477e-03
Br-                2.477e-03   1.227e-03    -2.606    -2.911    -0.305
C(-4)             0.000e+00
CH4                0.000e+00   0.000e+00  -121.360  -121.174     0.186
C(4)              1.440e-02
MgCO3              4.084e-03   6.272e-03    -2.389    -2.203     0.186
HCO3-              3.590e-03   2.219e-03    -2.445    -2.654    -0.209
NaCO3-             2.562e-03   2.506e-03    -2.591    -2.601    -0.010
MgHCO3+            2.441e-03   2.388e-03    -2.612    -2.622    -0.010
NaHCO3             7.614e-04   1.169e-03    -3.118    -2.932     0.186
CO3-2              4.141e-04   6.047e-05    -3.383    -4.218    -0.836
CaCO3              3.537e-04   5.431e-04    -3.451    -3.265     0.186
CaHCO3+            1.875e-04   1.159e-04    -3.727    -3.936    -0.209
CO2                6.827e-06   1.048e-05    -5.166    -4.979     0.186
Ca                1.443e-02
Ca+2               1.269e-02   3.380e-03    -1.897    -2.471    -0.574
CaSO4              1.095e-03   1.681e-03    -2.961    -2.774     0.186
CaCO3              3.537e-04   5.431e-04    -3.451    -3.265     0.186
CaHCO3+            1.875e-04   1.159e-04    -3.727    -3.936    -0.209
CaPO4-             7.152e-05   6.996e-05    -4.146    -4.155    -0.010
CaHPO4             3.192e-05   4.902e-05    -4.496    -4.310     0.186
CaOH+              2.376e-07   2.324e-07    -6.624    -6.634    -0.010
CaH2PO4+           7.916e-08   7.742e-08    -7.102    -7.111    -0.010
CaHSO4+            3.004e-11   2.938e-11   -10.522   -10.532    -0.010
Cl                1.415e+00
Cl-                1.415e+00   7.947e-01     0.151    -0.100    -0.250
H(0)              2.141e-38
H2                 1.070e-38   1.644e-38   -37.970   -37.784     0.186
Mg                2.847e-01
Mg+2               2.328e-01   8.219e-02    -0.633    -1.085    -0.452
MgSO4              4.146e-02   6.366e-02    -1.382    -1.196     0.186
MgCO3              4.084e-03   6.272e-03    -2.389    -2.203     0.186
MgHCO3+            2.441e-03   2.388e-03    -2.612    -2.622    -0.010
MgPO4-             2.346e-03   2.295e-03    -2.630    -2.639    -0.010
MgHPO4             1.050e-03   1.612e-03    -2.979    -2.793     0.186
```

```
MgOH+              5.950e-04   5.820e-04    -3.225    -3.235    -0.010
MgH2PO4+           2.452e-06   2.398e-06    -5.611    -5.620    -0.010
Na                1.239e+00
Na+                1.225e+00   9.370e-01     0.088    -0.028    -0.116
NaSO4-             1.137e-02   1.112e-02    -1.944    -1.954    -0.010
NaCO3-             2.562e-03   2.506e-03    -2.591    -2.601    -0.010
NaHCO3             7.614e-04   1.169e-03    -3.118    -2.932     0.186
NaHPO4-            3.587e-05   3.509e-05    -4.445    -4.455    -0.010
NaOH               1.671e-06   2.566e-06    -5.777    -5.591     0.186
O(0)              6.217e-12
O2                 3.109e-12   4.774e-12   -11.507   -11.321     0.186
P                 3.743e-03
MgPO4-             2.346e-03   2.295e-03    -2.630    -2.639    -0.010
MgHPO4             1.050e-03   1.612e-03    -2.979    -2.793     0.186
HPO4-2             2.029e-04   1.920e-05    -3.693    -4.717    -1.024
CaPO4-             7.152e-05   6.996e-05    -4.146    -4.155    -0.010
NaHPO4-            3.587e-05   3.509e-05    -4.445    -4.455    -0.010
CaHPO4             3.192e-05   4.902e-05    -4.496    -4.310     0.186
MgH2PO4+           2.452e-06   2.398e-06    -5.611    -5.620    -0.010
H2PO4-             1.111e-06   6.436e-07    -5.954    -6.191    -0.237
PO4-3              1.071e-06   5.324e-09    -5.970    -8.274    -2.304
CaH2PO4+           7.916e-08   7.742e-08    -7.102    -7.111    -0.010
S(-2)             0.000e+00
HS-                0.000e+00   0.000e+00  -118.070  -118.349    -0.278
H2S                0.000e+00   0.000e+00  -120.432  -120.245     0.186
S-2                0.000e+00   0.000e+00  -121.234  -122.116    -0.882
S(6)              7.314e-02
MgSO4              4.146e-02   6.366e-02    -1.382    -1.196     0.186
SO4-2              1.921e-02   2.124e-03    -1.716    -2.673    -0.956
NaSO4-             1.137e-02   1.112e-02    -1.944    -1.954    -0.010
CaSO4              1.095e-03   1.681e-03    -2.961    -2.774     0.186
HSO4-              7.393e-10   7.231e-10    -9.131    -9.141    -0.010
CaHSO4+            3.004e-11   2.938e-11   -10.522   -10.532    -0.010
------------------------------Saturation indices-----------------------
--------
Phase               SI log IAP  log KT
Anhydrite        -0.66   -5.14   -4.48  CaSO4
Aragonite         1.78   -6.69   -8.47  CaCO3
Calcite           1.92   -6.69   -8.60  CaCO3
CH4(g)         -118.17 -159.67  -41.50  CH4
CO2(g)           -3.33  -21.48  -18.15  CO2
Dolomite          5.49  -11.99  -17.49  CaMg(CO3)2
Gypsum           -0.58   -5.19   -4.60  CaSO4:2H2O
H2(g)           -34.56  -34.56   -0.00  H2
H2O(g)           -1.09   -0.02    1.07  H2O
H2S(g)         -119.06 -158.10  -39.05  H2S
Halite           -1.75   -0.13    1.62  NaCl
Hydroxyapatite   12.98  -28.56  -41.54  Ca5(PO4)3OH
O2(g)            -8.28   69.07   77.36  O2
Sulfur          -90.17 -123.54  -33.38  S
------------------
End of simulation.
------------------
------------------------------------
Reading input data for simulation 2.
------------------------------------
```

```
-----------
End of run.
-----------
No memory leaks
```


STORRS LAKE 2

```
Database file:  phreeqc.dat
------------------
Reading data base.
------------------
SOLUTION_MASTER_SPECIES
SOLUTION_SPECIES
PHASES
EXCHANGE_MASTER_SPECIES
EXCHANGE_SPECIES
SURFACE_MASTER_SPECIES
SURFACE_SPECIES
RATES
END
-----------------------------------
Reading input data for simulation 1.
-----------------------------------
TITLE SL10-2WF
SOLUTION 1
pH 8.15
temp 40.9
pe
density 1.035807
units ppm
Br 176.99
Ca 690.03
C 803 as HCO3
Cl 44957.43
Mg 6732.84
P 115.39
Na 27232.98
S 6237.56 as SO4-2
END
-----
TITLE
-----
 SL10-2WF
-------------------------------------------
Beginning of initial solution calculations.
-------------------------------------------
Initial solution 1.
-----------------------------Solution composition----------------------
Elements           Molality       Moles
Br                2.426e-03   2.426e-03
C                 1.441e-02   1.441e-02
Ca                1.886e-02   1.886e-02
```

```
Cl                1.389e+00   1.389e+00
Mg                3.033e-01   3.033e-01
Na                1.297e+00   1.297e+00
P                 4.080e-03   4.080e-03
S                 7.111e-02   7.111e-02
```

```
----------------------------Description of solution----------------------------
                                    pH  =   8.150
                                    pe  =   8.150
                         Activity of water  =   0.948
                            Ionic strength  =   1.927e+00
                        Mass of water (kg)  =   1.000e+00
                  Total alkalinity (eq/kg)  =   2.366e-02
                        Total CO2 (mol/kg)  =   1.441e-02
                       Temperature (deg C)  =  40.900
                    Electrical balance (eq)  =   3.805e-01
 Percent error, 100*(Cat-|An|)/(Cat+|An|)  =  11.61
                                Iterations  =   9
                                   Total H  = 1.110261e+02
                                   Total O  = 5.585039e+01
----------------------------Distribution of species----------------------------
Log       Log         Log
Species             Molality    Activity  Molality  Activity     Gamma
OH-                 7.731e-06   4.066e-06    -5.112    -5.391    -0.279
H+                  9.812e-09   7.079e-09    -8.008    -8.150    -0.142
H2O                 5.551e+01   9.484e-01    -0.023    -0.023     0.000
Br                 2.426e-03
Br-                 2.426e-03   1.199e-03    -2.615    -2.921    -0.306
C(-4)              0.000e+00
CH4                 0.000e+00   0.000e+00  -112.565  -112.373     0.193
C(4)               1.441e-02
HCO3-               5.348e-03   3.304e-03    -2.272    -2.481    -0.209
MgHCO3+             3.919e-03   3.903e-03    -2.407    -2.409    -0.002
MgCO3               2.034e-03   3.170e-03    -2.692    -2.499     0.193
NaHCO3              1.183e-03   1.843e-03    -2.927    -2.734     0.193
NaCO3-              1.125e-03   1.121e-03    -2.949    -2.950    -0.002
CaHCO3+             3.717e-04   2.296e-04    -3.430    -3.639    -0.209
CaCO3               2.068e-04   3.223e-04    -3.684    -3.492     0.193
CO3-2               1.945e-04   2.834e-05    -3.711    -4.548    -0.836
CO2                 3.126e-05   4.872e-05    -4.505    -4.312     0.193
Ca                 1.886e-02
Ca+2                1.680e-02   4.573e-03    -1.775    -2.340    -0.565
CaSO4               1.344e-03   2.095e-03    -2.872    -2.679     0.193
CaHCO3+             3.717e-04   2.296e-04    -3.430    -3.639    -0.209
CaCO3               2.068e-04   3.223e-04    -3.684    -3.492     0.193
CaHPO4              7.576e-05   1.181e-04    -4.121    -3.928     0.193
CaPO4-              5.265e-05   5.244e-05    -4.279    -4.280    -0.002
CaH2PO4+            5.845e-07   5.822e-07    -6.233    -6.235    -0.002
CaOH+               1.021e-07   1.017e-07    -6.991    -6.993    -0.002
CaHSO4+             1.094e-10   1.090e-10    -9.961    -9.963    -0.002
Cl                 1.389e+00
Cl-                 1.389e+00   7.806e-01     0.143    -0.108    -0.250
H(0)               1.964e-36
H2                  9.819e-37   1.530e-36   -36.008   -35.815     0.193
Mg                 3.033e-01
```

```
Mg+2              2.531e-01   9.182e-02    -0.597    -1.037    -0.440
MgSO4             4.063e-02   6.331e-02    -1.391    -1.199     0.193
MgHCO3+           3.919e-03   3.903e-03    -2.407    -2.409    -0.002
MgHPO4            2.057e-03   3.205e-03    -2.687    -2.494     0.193
MgCO3             2.034e-03   3.170e-03    -2.692    -2.499     0.193
MgPO4-            1.426e-03   1.421e-03    -2.846    -2.848    -0.002
```

```
MgOH+             1.752e-04   1.745e-04    -3.756    -3.758    -0.002
MgH2PO4+          1.495e-05   1.489e-05    -4.825    -4.827    -0.002
Na               1.297e+00
Na+               1.284e+00   9.921e-01     0.109    -0.003    -0.112
NaSO4-            1.095e-02   1.091e-02    -1.960    -1.962    -0.002
NaHCO3            1.183e-03   1.843e-03    -2.927    -2.734     0.193
NaCO3-            1.125e-03   1.121e-03    -2.949    -2.950    -0.002
NaHPO4-           6.898e-05   6.871e-05    -4.161    -4.163    -0.002
NaOH              5.635e-07   8.781e-07    -6.249    -6.056     0.193
O(0)             1.529e-16
O2                7.645e-17   1.191e-16   -16.117   -15.924     0.193
P                4.080e-03
MgHPO4            2.057e-03   3.205e-03    -2.687    -2.494     0.193
MgPO4-            1.426e-03   1.421e-03    -2.846    -2.848    -0.002
HPO4-2            3.772e-04   3.552e-05    -3.423    -4.450    -1.026
CaHPO4            7.576e-05   1.181e-04    -4.121    -3.928     0.193
NaHPO4-           6.898e-05   6.871e-05    -4.161    -4.163    -0.002
CaPO4-            5.265e-05   5.244e-05    -4.279    -4.280    -0.002
MgH2PO4+          1.495e-05   1.489e-05    -4.825    -4.827    -0.002
H2PO4-            6.428e-06   3.722e-06    -5.192    -5.429    -0.237
PO4-3             6.226e-07   3.058e-09    -6.206    -8.515    -2.309
CaH2PO4+          5.845e-07   5.822e-07    -6.233    -6.235    -0.002
S(-2)            0.000e+00
HS-               0.000e+00   0.000e+00  -109.461  -109.740    -0.279
H2S               0.000e+00   0.000e+00  -111.319  -111.126     0.193
S-2               0.000e+00   0.000e+00  -113.176  -114.059    -0.883
S(6)             7.111e-02
MgSO4             4.063e-02   6.331e-02    -1.391    -1.199     0.193
SO4-2             1.819e-02   1.994e-03    -1.740    -2.700    -0.960
NaSO4-            1.095e-02   1.091e-02    -1.960    -1.962    -0.002
CaSO4             1.344e-03   2.095e-03    -2.872    -2.679     0.193
HSO4-             1.990e-09   1.982e-09    -8.701    -8.703    -0.002
CaHSO4+           1.094e-10   1.090e-10    -9.961    -9.963    -0.002
------------------------------Saturation indices-----------------------
Phase               SI log IAP  log KT
Anhydrite        -0.58   -5.04   -4.46  CaSO4
Aragonite         1.57   -6.89   -8.45  CaCO3
Calcite           1.70   -6.89   -8.59  CaCO3
CH4(g)         -109.39 -151.18  -41.79  CH4
CO2(g)           -2.68  -20.82  -18.15  CO2
Dolomite          4.97  -12.47  -17.44  CaMg(CO3)2
Gypsum           -0.49   -5.09   -4.60  CaSO4:2H2O
H2(g)           -32.60  -32.60   -0.00  H2
H2O(g)           -1.14   -0.02    1.12  H2O
H2S(g)         -109.96 -149.31  -39.35  H2S
Halite           -1.73   -0.11    1.62  NaCl
Hydroxyapatite   12.29  -29.12  -41.41  Ca5(PO4)3OH
O2(g)          -12.90   65.15   78.05  O2
```

```
Sulfur          -83.06 -116.71  -33.65  S
------------------
End of simulation.
------------------
------------------------------------
Reading input data for simulation 2.
------------------------------------
```

```
-----------
End of run.
-----------
No memory leaks
```


STORRS LAKE 3

```
Database file:  phreeqc.dat
------------------
Reading data base.
------------------
SOLUTION_MASTER_SPECIES
SOLUTION_SPECIES
PHASES
EXCHANGE_MASTER_SPECIES
EXCHANGE_SPECIES
SURFACE_MASTER_SPECIES
SURFACE_SPECIES
RATES
END
------------------------------------
Reading input data for simulation 1.
------------------------------------
TITLE SL10-3WF
SOLUTION 1
pH 8.23
temp 36
pe
density 1.036885
units ppm
Br 98.47
Ca 711.46
C 803 as HCO3
Cl 41265.58
Mg 6643.68
P 130.84
Na 27089.51
S 5392.92 as SO4-2
END
-----
TITLE
-----
 SL10-3WF
----------------------------------------
```

```
Beginning of initial solution calculations.
-----------------------------------------
Initial solution 1.
-----------------------------Solution composition----------------------
Elements           Molality       Moles
Br                1.343e-03   1.343e-03
C                 1.434e-02   1.434e-02
Ca                1.934e-02   1.934e-02
Cl                1.268e+00   1.268e+00
Mg                2.977e-01   2.977e-01
Na                1.284e+00   1.284e+00
P                 4.602e-03   4.602e-03
S                 6.116e-02   6.116e-02
```



```
----------------------------Description of solution--------------------
                                    pH  =   8.230
                                    pe  =   8.230
                       Activity of water  =   0.951
                          Ionic strength  =   1.858e+00
                       Mass of water (kg)  =   1.000e+00
                 Total alkalinity (eq/kg)  =   2.441e-02
                       Total CO2 (mol/kg)  =   1.434e-02
                      Temperature (deg C)  =  36.000
                   Electrical balance (eq)  =   4.971e-01
 Percent error, 100*(Cat-|An|)/(Cat+|An|)  =  15.83
                                Iterations  =   9
                                   Total H  = 1.110262e+02
                                   Total O  = 5.581241e+01
----------------------------Distribution of species--------------------
Log       Log         Log
Species             Molality    Activity  Molality  Activity     Gamma
OH-               6.684e-06   3.549e-06    -5.175    -5.450    -0.275
H+                8.132e-09   5.888e-09    -8.090    -8.230    -0.140
H2O               5.551e+01   9.508e-01    -0.022    -0.022     0.000
Br                1.343e-03
Br-               1.343e-03   6.709e-04    -2.872    -3.173    -0.301
C(-4)             0.000e+00
CH4               0.000e+00   0.000e+00  -113.277  -113.092     0.186
C(4)              1.434e-02
HCO3-             5.319e-03   3.307e-03    -2.274    -2.481    -0.206
MgHCO3+           3.847e-03   3.759e-03    -2.415    -2.425    -0.010
MgCO3             2.147e-03   3.294e-03    -2.668    -2.482     0.186
NaHCO3            1.187e-03   1.820e-03    -2.926    -2.740     0.186
NaCO3-            1.016e-03   9.926e-04    -2.993    -3.003    -0.010
CaHCO3+           3.665e-04   2.278e-04    -3.436    -3.642    -0.206
CaCO3             2.137e-04   3.278e-04    -3.670    -3.484     0.186
CO3-2             2.135e-04   3.189e-05    -3.671    -4.496    -0.826
CO2               2.708e-05   4.154e-05    -4.567    -4.382     0.186
Ca                1.934e-02
Ca+2              1.736e-02   4.727e-03    -1.760    -2.325    -0.565
CaSO4             1.249e-03   1.916e-03    -2.903    -2.718     0.186
CaHCO3+           3.665e-04   2.278e-04    -3.436    -3.642    -0.206
CaCO3             2.137e-04   3.278e-04    -3.670    -3.484     0.186
CaHPO4            8.489e-05   1.302e-04    -4.071    -3.885     0.186
CaPO4-            6.541e-05   6.390e-05    -4.184    -4.194    -0.010
```

```
CaH2PO4+          5.592e-07   5.463e-07    -6.252    -6.263    -0.010
CaOH+             1.296e-07   1.267e-07    -6.887    -6.897    -0.010
CaHSO4+           7.869e-11   7.688e-11   -10.104   -10.114    -0.010
Cl               1.268e+00
Cl-               1.268e+00   7.178e-01     0.103    -0.144    -0.247
H(0)             9.985e-37
H2                4.993e-37   7.658e-37   -36.302   -36.116     0.186
Mg               2.977e-01
Mg+2              2.539e-01   9.143e-02    -0.595    -1.039    -0.444
MgSO4             3.379e-02   5.183e-02    -1.471    -1.285     0.186
MgHCO3+           3.847e-03   3.759e-03    -2.415    -2.425    -0.010
MgHPO4            2.220e-03   3.405e-03    -2.654    -2.468     0.186
MgCO3             2.147e-03   3.294e-03    -2.668    -2.482     0.186
MgPO4-            1.707e-03   1.667e-03    -2.768    -2.778    -0.010
```

```
MgOH+             1.430e-04   1.397e-04    -3.845    -3.855    -0.010
MgH2PO4+          1.377e-05   1.346e-05    -4.861    -4.871    -0.010
Na               1.284e+00
Na+               1.272e+00   9.790e-01     0.104    -0.009    -0.114
NaSO4-            9.884e-03   9.656e-03    -2.005    -2.015    -0.010
NaHCO3            1.187e-03   1.820e-03    -2.926    -2.740     0.186
NaCO3-            1.016e-03   9.926e-04    -2.993    -3.003    -0.010
NaHPO4-           8.053e-05   7.867e-05    -4.094    -4.104    -0.010
NaOH              6.809e-07   1.044e-06    -6.167    -5.981     0.186
O(0)             2.223e-17
O2                1.111e-17   1.705e-17   -16.954   -16.768     0.186
P                4.602e-03
MgHPO4            2.220e-03   3.405e-03    -2.654    -2.468     0.186
MgPO4-            1.707e-03   1.667e-03    -2.768    -2.778    -0.010
HPO4-2            4.233e-04   4.121e-05    -3.373    -4.385    -1.012
CaHPO4            8.489e-05   1.302e-04    -4.071    -3.885     0.186
NaHPO4-           8.053e-05   7.867e-05    -4.094    -4.104    -0.010
CaPO4-            6.541e-05   6.390e-05    -4.184    -4.194    -0.010
MgH2PO4+          1.377e-05   1.346e-05    -4.861    -4.871    -0.010
H2PO4-            6.314e-06   3.683e-06    -5.200    -5.434    -0.234
PO4-3             7.365e-07   3.900e-09    -6.133    -8.409    -2.276
CaH2PO4+          5.592e-07   5.463e-07    -6.252    -6.263    -0.010
S(-2)            0.000e+00
HS-               0.000e+00   0.000e+00  -110.201  -110.476    -0.275
H2S               0.000e+00   0.000e+00  -112.079  -111.893     0.186
S-2               0.000e+00   0.000e+00  -113.977  -114.849    -0.872
S(6)             6.116e-02
MgSO4             3.379e-02   5.183e-02    -1.471    -1.285     0.186
SO4-2             1.624e-02   1.840e-03    -1.789    -2.735    -0.946
NaSO4-            9.884e-03   9.656e-03    -2.005    -2.015    -0.010
CaSO4             1.249e-03   1.916e-03    -2.903    -2.718     0.186
HSO4-             1.385e-09   1.353e-09    -8.859    -8.869    -0.010
CaHSO4+           7.869e-11   7.688e-11   -10.104   -10.114    -0.010
-----------------------------Saturation indices-----------------------
Phase               SI log IAP  log KT
Anhydrite        -0.64   -5.06   -4.42  CaSO4
Aragonite         1.59   -6.82   -8.41  CaCO3
Calcite           1.73   -6.82   -8.55  CaCO3
CH4(g)         -110.14 -152.57  -42.43  CH4
CO2(g)           -2.79  -20.93  -18.14  CO2
```

```
Dolomite          4.98  -12.36  -17.34  CaMg(CO3)2
Gypsum           -0.51   -5.10   -4.59  CaSO4:2H2O
H2(g)           -32.92  -32.92   -0.00  H2
H2O(g)           -1.26   -0.02    1.24  H2O
H2S(g)         -110.78 -150.79  -40.01  H2S
Halite           -1.76   -0.15    1.61  NaCl
Hydroxyapatite   12.48  -28.65  -41.13  Ca5(PO4)3OH
O2(g)           -13.76   65.80   79.56  O2
Sulfur          -83.61 -117.87  -34.26  S
------------------
End of simulation.
------------------
-----------------------------------
Reading input data for simulation 2.
-----------------------------------
```
WEB-PHREEQ: Output for a Single Solution Using Simple Spe...
http://www.ndsu.edu/webphreeq/webphreeq-process.cgi
3 of 4 6/16/11 1:34 PM
```
-----------
End of run.
-----------
No memory leaks
```
WEB-PHREEQ: Output for a Single Solution Using Simple Spe...
http://www.ndsu.edu/webphreeq/webphreeq-process.cgi
4 of 4 6/16/11 1:34 PM

STORRS LAKE 4

```
Database file:  phreeqc.dat
------------------
Reading data base.
------------------
SOLUTION_MASTER_SPECIES
SOLUTION_SPECIES
PHASES
EXCHANGE_MASTER_SPECIES
EXCHANGE_SPECIES
SURFACE_MASTER_SPECIES
SURFACE_SPECIES
RATES
END
-----------------------------------
Reading input data for simulation 1.
-----------------------------------
TITLE SL10-4WF
SOLUTION 1
pH 8.57
temp 41.2
pe
density 1.039966
units ppm
Br 167.35
Ca 716.40
C 803 as HCO3
Cl 48151.65
Mg 6159.74
P 123.79
```

```
Na 26105.27
S 6763.09 as SO4-2
END
-----
TITLE
-----
 SL10-4WF
-------------------------------------------
Beginning of initial solution calculations.
-------------------------------------------
Initial solution 1.
-----------------------------Solution composition----------------------
--------
Elements           Molality       Moles
Br                2.299e-03   2.299e-03
C                 1.445e-02   1.445e-02
Ca                1.962e-02   1.962e-02
Cl                1.491e+00   1.491e+00
Mg                2.781e-01   2.781e-01
Na                1.246e+00   1.246e+00
P                 4.387e-03   4.387e-03
S                 7.728e-02   7.728e-02
```



```
----------------------------Description of solution--------------------
                                    pH  =   8.570
                                    pe  =   8.570
                       Activity of water  =   0.948
                          Ionic strength  =   1.903e+00
                       Mass of water (kg)  =   1.000e+00
                 Total alkalinity (eq/kg)  =   2.850e-02
                       Total CO2 (mol/kg)  =   1.445e-02
                      Temperature (deg C)  =  41.200
                   Electrical balance (eq)  =   1.613e-01
 Percent error, 100*(Cat-|An|)/(Cat+|An|)  =   4.92
                                Iterations  =   8
                                   Total H  = 1.110225e+02
                                   Total O  = 5.587665e+01
----------------------------Distribution of species--------------------
Log       Log         Log
Species            Molality    Activity  Molality  Activity     Gamma
OH-               2.070e-05   1.090e-05    -4.684    -4.963    -0.279
H+                3.730e-09   2.692e-09    -8.428    -8.570    -0.142
H2O               5.551e+01   9.479e-01    -0.023    -0.023     0.000
Br                2.299e-03
Br-               2.299e-03   1.138e-03    -2.638    -2.944    -0.305
C(-4)             0.000e+00
CH4               0.000e+00   0.000e+00  -119.863  -119.673     0.190
C(4)              1.445e-02
HCO3-             4.038e-03   2.496e-03    -2.394    -2.603    -0.209
MgCO3             3.617e-03   5.606e-03    -2.442    -2.251     0.190
MgHCO3+           2.637e-03   2.608e-03    -2.579    -2.584    -0.005
NaCO3-            2.190e-03   2.166e-03    -2.660    -2.664    -0.005
NaHCO3            8.588e-04   1.331e-03    -3.066    -2.876     0.190
CaCO3             4.243e-04   6.575e-04    -3.372    -3.182     0.190
CO3-2             3.869e-04   5.652e-05    -3.412    -4.248    -0.835
```

CaHCO3+	2.852e-04	1.763e-04	-3.545	-3.754	-0.209
CO2	9.022e-06	1.398e-05	-5.045	-4.854	0.190
Ca	1.962e-02				
Ca+2	1.715e-02	4.637e-03	-1.766	-2.334	-0.568
CaSO4	1.601e-03	2.481e-03	-2.796	-2.605	0.190
CaCO3	4.243e-04	6.575e-04	-3.372	-3.182	0.190
CaHCO3+	2.852e-04	1.763e-04	-3.545	-3.754	-0.209
CaPO4-	1.067e-04	1.055e-04	-3.972	-3.977	-0.005
CaHPO4	5.799e-05	8.987e-05	-4.237	-4.046	0.190
CaOH+	2.740e-07	2.710e-07	-6.562	-6.567	-0.005
CaH2PO4+	1.701e-07	1.683e-07	-6.769	-6.774	-0.005
CaHSO4+	4.984e-11	4.930e-11	-10.302	-10.307	-0.005
Cl	1.491e+00				
Cl-	1.491e+00	8.383e-01	0.173	-0.077	-0.250
H(0)	4.114e-38				
H2	2.057e-38	3.188e-38	-37.687	-37.496	0.190
Mg	2.781e-01				
Mg+2	2.253e-01	8.104e-02	-0.647	-1.091	-0.444
MgSO4	4.229e-02	6.555e-02	-1.374	-1.183	0.190
MgCO3	3.617e-03	5.606e-03	-2.442	-2.251	0.190
MgHCO3+	2.637e-03	2.608e-03	-2.579	-2.584	-0.005
MgPO4-	2.515e-03	2.488e-03	-2.599	-2.604	-0.005
MgHPO4	1.370e-03	2.124e-03	-2.863	-2.673	0.190

MgOH+	4.195e-04	4.150e-04	-3.377	-3.382	-0.005
MgH2PO4+	3.785e-06	3.745e-06	-5.422	-5.427	-0.005
Na	1.246e+00				
Na+	1.231e+00	9.482e-01	0.090	-0.023	-0.113
NaSO4-	1.230e-02	1.217e-02	-1.910	-1.915	-0.005
NaCO3-	2.190e-03	2.166e-03	-2.660	-2.664	-0.005
NaHCO3	8.588e-04	1.331e-03	-3.066	-2.876	0.190
NaHPO4-	4.958e-05	4.905e-05	-4.305	-4.309	-0.005
NaOH	1.424e-06	2.206e-06	-5.847	-5.656	0.190
O(0)	4.324e-13				
O2	2.162e-13	3.351e-13	-12.665	-12.475	0.190
P	4.387e-03				
MgPO4-	2.515e-03	2.488e-03	-2.599	-2.604	-0.005
MgHPO4	1.370e-03	2.124e-03	-2.863	-2.673	0.190
HPO4-2	2.806e-04	2.653e-05	-3.552	-4.576	-1.024
CaPO4-	1.067e-04	1.055e-04	-3.972	-3.977	-0.005
CaHPO4	5.799e-05	8.987e-05	-4.237	-4.046	0.190
NaHPO4-	4.958e-05	4.905e-05	-4.305	-4.309	-0.005
MgH2PO4+	3.785e-06	3.745e-06	-5.422	-5.427	-0.005
H2PO4-	1.821e-06	1.055e-06	-5.740	-5.977	-0.237
PO4-3	1.218e-06	6.040e-09	-5.914	-8.219	-2.305
CaH2PO4+	1.701e-07	1.683e-07	-6.769	-6.774	-0.005
S(-2)	0.000e+00				
HS-	0.000e+00	0.000e+00	-116.574	-116.853	-0.279
H2S	0.000e+00	0.000e+00	-118.852	-118.661	0.190
S-2	0.000e+00	0.000e+00	-119.862	-120.744	-0.882
S(6)	7.728e-02				
MgSO4	4.229e-02	6.555e-02	-1.374	-1.183	0.190
SO4-2	2.108e-02	2.323e-03	-1.676	-2.634	-0.958
NaSO4-	1.230e-02	1.217e-02	-1.910	-1.915	-0.005
CaSO4	1.601e-03	2.481e-03	-2.796	-2.605	0.190

```
HSO4-              8.940e-10   8.844e-10    -9.049    -9.053    -0.005
CaHSO4+            4.984e-11   4.930e-11   -10.302   -10.307    -0.005
-----------------------------Saturation indices-----------------------
Phase               SI log IAP  log KT
Anhydrite        -0.50   -4.97   -4.47  CaSO4
Aragonite         1.87   -6.58   -8.46  CaCO3
Calcite           2.01   -6.58   -8.59  CaCO3
CH4(g)         -116.69 -158.44  -41.75  CH4
CO2(g)           -3.22  -21.36  -18.15  CO2
Dolomite          5.53  -11.92  -17.45  CaMg(CO3)2
Gypsum           -0.41   -5.01   -4.60  CaSO4:2H2O
H2(g)           -34.28  -34.28   -0.00  H2
H2O(g)           -1.14   -0.02    1.11  H2O
H2S(g)         -117.49 -156.80  -39.31  H2S
Halite           -1.72   -0.10    1.62  NaCl
Hydroxyapatite   13.65  -27.78  -41.42  Ca5(PO4)3OH
O2(g)            -9.45   68.51   77.96  O2
Sulfur          -88.90 -122.52  -33.62  S
------------------
End of simulation.
------------------
-----------------------------------
Reading input data for simulation 2.
-----------------------------------
```
WEB-PHREEQ: Output for a Single Solution Using Simple Spe...
http://www.ndsu.edu/webphreeq/webphreeq-process.cgi
3 of 4 6/16/11 1:37 PM
```
-----------
End of run.
-----------
No memory leaks
```
WEB-PHREEQ: Output for a Single Solution Using Simple Spe...
http://www.ndsu.edu/webphreeq/webphreeq-process.cgi
4 of 4 6/16/11 1:37 PM

OCEAN WATER

```
Database file:  phreeqc.dat
------------------
Reading data base.
------------------
SOLUTION_MASTER_SPECIES
SOLUTION_SPECIES
PHASES
EXCHANGE_MASTER_SPECIES
EXCHANGE_SPECIES
SURFACE_MASTER_SPECIES
SURFACE_SPECIES
RATES
END
-----------------------------------
Reading input data for simulation 1.
-----------------------------------
TITLE Storrs Lake Sea Water
SOLUTION 1
pH 8.26
temp 28
```

```
pe
density 1.022424
units ppm
Br 66.00
Ca 416.00
C 141 as HCO3
Cl 19345.00
Mg 1295.00
P 124.80
Na 10752.00
S 2701.00 as SO4-2
END
-----
TITLE
-----
 Storrs Lake Sea Water
-------------------------------------------
Beginning of initial solution calculations.
-------------------------------------------
Initial solution 1.
-----------------------------Solution composition----------------------
Elements           Molality       Moles
Br                 8.558e-04   8.558e-04
C                  2.394e-03   2.394e-03
Ca                 1.075e-02   1.075e-02
Cl                 5.653e-01   5.653e-01
Mg                 5.519e-02   5.519e-02
Na                 4.846e-01   4.846e-01
P                  4.175e-03   4.175e-03
S                  2.913e-02   2.913e-02
```



```
-----------------------------Description of solution--------------------
                                    pH  =   8.260
                                    pe  =   8.260
                         Activity of water  =   0.981
                            Ionic strength  =   6.666e-01
                        Mass of water (kg)  =   1.000e+00
                 Total alkalinity (eq/kg)  =   8.035e-03
                        Total CO2 (mol/kg)  =   2.394e-03
                       Temperature (deg C)  =  28.000
                    Electrical balance (eq)  =  -2.022e-02
 Percent error, 100*(Cat-|An|)/(Cat+|An|)  =  -1.69
                                  Iterations  =   8
                                     Total H  = 1.110176e+02
                                     Total O  = 5.564663e+01
----------------------------Distribution of species--------------------
Log       Log         Log
Species            Molality    Activity  Molality  Activity     Gamma
OH-                3.669e-06   2.234e-06    -5.435    -5.651    -0.216
H+                 7.284e-09   5.495e-09    -8.138    -8.260    -0.122
H2O                5.551e+01   9.807e-01    -0.008    -0.008     0.000
Br                 8.558e-04
Br-                8.558e-04   5.022e-04    -3.068    -3.299    -0.232
C(-4)              0.000e+00
CH4                0.000e+00   0.000e+00  -113.097  -113.030     0.067
```

C(4)	2.394e-03				
HCO3-	1.635e-03	1.104e-03	-2.786	-2.957	-0.171
MgHCO3+	2.266e-04	1.689e-04	-3.645	-3.772	-0.128
NaHCO3	1.795e-04	2.093e-04	-3.746	-3.679	0.067
MgCO3	1.103e-04	1.286e-04	-3.957	-3.891	0.067
NaCO3-	9.771e-05	7.281e-05	-4.010	-4.138	-0.128
CaHCO3+	5.018e-05	3.388e-05	-4.299	-4.470	-0.171
CO3-2	4.806e-05	9.983e-06	-4.318	-5.001	-0.683
CaCO3	3.532e-05	4.118e-05	-4.452	-4.385	0.067
CO2	1.152e-05	1.344e-05	-4.938	-4.872	0.067
Ca	1.075e-02				
Ca+2	9.257e-03	2.305e-03	-2.034	-2.637	-0.604
CaSO4	1.072e-03	1.250e-03	-2.970	-2.903	0.067
CaHPO4	1.971e-04	2.298e-04	-3.705	-3.639	0.067
CaPO4-	1.404e-04	1.046e-04	-3.853	-3.980	-0.128
CaHCO3+	5.018e-05	3.388e-05	-4.299	-4.470	-0.171
CaCO3	3.532e-05	4.118e-05	-4.452	-4.385	0.067
CaH2PO4+	1.255e-06	9.352e-07	-5.901	-6.029	-0.128
CaOH+	9.160e-08	6.826e-08	-7.038	-7.166	-0.128
CaHSO4+	5.614e-11	4.183e-11	-10.251	-10.378	-0.128
Cl	5.653e-01				
Cl-	5.653e-01	3.522e-01	-0.248	-0.453	-0.206
H(0)	1.075e-36				
H2	5.377e-37	6.268e-37	-36.269	-36.203	0.067
Mg	5.519e-02				
Mg+2	4.488e-02	1.289e-02	-1.348	-1.890	-0.542
MgSO4	7.399e-03	8.626e-03	-2.131	-2.064	0.067
MgHPO4	1.490e-03	1.738e-03	-2.827	-2.760	0.067
MgPO4-	1.059e-03	7.894e-04	-2.975	-3.103	-0.128
MgHCO3+	2.266e-04	1.689e-04	-3.645	-3.772	-0.128
MgCO3	1.103e-04	1.286e-04	-3.957	-3.891	0.067

MgOH+	1.466e-05	1.092e-05	-4.834	-4.962	-0.128
MgH2PO4+	8.937e-06	6.660e-06	-5.049	-5.177	-0.128
Na	4.846e-01				
Na+	4.780e-01	3.372e-01	-0.321	-0.472	-0.152
NaSO4-	6.112e-03	4.554e-03	-2.214	-2.342	-0.128
NaHCO3	1.795e-04	2.093e-04	-3.746	-3.679	0.067
NaHPO4-	1.518e-04	1.131e-04	-3.819	-3.946	-0.128
NaCO3-	9.771e-05	7.281e-05	-4.010	-4.138	-0.128
NaOH	3.410e-07	3.976e-07	-6.467	-6.401	0.067
O(0)	1.591e-19				
O2	7.955e-20	9.275e-20	-19.099	-19.033	0.067
P	4.175e-03				
MgHPO4	1.490e-03	1.738e-03	-2.827	-2.760	0.067
HPO4-2	1.101e-03	1.720e-04	-2.958	-3.764	-0.806
MgPO4-	1.059e-03	7.894e-04	-2.975	-3.103	-0.128
CaHPO4	1.971e-04	2.298e-04	-3.705	-3.639	0.067
NaHPO4-	1.518e-04	1.131e-04	-3.819	-3.946	-0.128
CaPO4-	1.404e-04	1.046e-04	-3.853	-3.980	-0.128
H2PO4-	2.316e-05	1.498e-05	-4.635	-4.825	-0.189
MgH2PO4+	8.937e-06	6.660e-06	-5.049	-5.177	-0.128
CaH2PO4+	1.255e-06	9.352e-07	-5.901	-6.029	-0.128
PO4-3	9.760e-07	1.498e-08	-6.011	-7.825	-1.814
S(-2)	0.000e+00				

```
HS-               0.000e+00   0.000e+00  -109.537  -109.753    -0.216
H2S               0.000e+00   0.000e+00  -111.176  -111.109     0.067
S-2               0.000e+00   0.000e+00  -113.609  -114.323    -0.714
S(6)              2.913e-02
SO4-2             1.455e-02   2.645e-03    -1.837    -2.578    -0.740
MgSO4             7.399e-03   8.626e-03    -2.131    -2.064     0.067
NaSO4-            6.112e-03   4.554e-03    -2.214    -2.342    -0.128
CaSO4             1.072e-03   1.250e-03    -2.970    -2.903     0.067
HSO4-             2.026e-09   1.510e-09    -8.693    -8.821    -0.128
CaHSO4+           5.614e-11   4.183e-11   -10.251   -10.378    -0.128
-------------------------------Saturation indices-----------------------
Phase               SI log IAP  log KT
Anhydrite        -0.84   -5.22   -4.37  CaSO4
Aragonite         0.72   -7.64   -8.36  CaCO3
Calcite           0.86   -7.64   -8.50  CaCO3
CH4(g)         -110.15 -153.66  -43.51  CH4
CO2(g)           -3.37  -21.51  -18.14  CO2
Dolomite          2.63  -14.53  -17.16  CaMg(CO3)2
Gypsum           -0.65   -5.23   -4.58  CaSO4:2H2O
H2(g)           -33.04  -33.04   -0.00  H2
H2O(g)           -1.44   -0.01    1.43  H2O
H2S(g)         -110.08 -151.22  -41.14  H2S
Halite           -2.51   -0.93    1.59  NaCl
Hydroxyapatite   12.24  -28.41  -40.65  Ca5(PO4)3OH
O2(g)          -16.06   66.06   82.12  O2
Sulfur         -82.88 -118.18  -35.30  S
------------------
End of simulation.
------------------
------------------------------------
Reading input data for simulation 2.
------------------------------------
```

```
-----------
End of run.
-----------
No memory leaks
```